ILMATIETEEN LAITOS
METEOROLOGISKA INSTITUTET
FINNISH METEOROLOGICAL INSTITUTE

125
CONTRIBUTIONS

EFFECTS OF BLACK CARBON AND ICELANDIC DUST ON SNOW ALBEDO, MELT AND DENSITY

OUTI MEINANDER

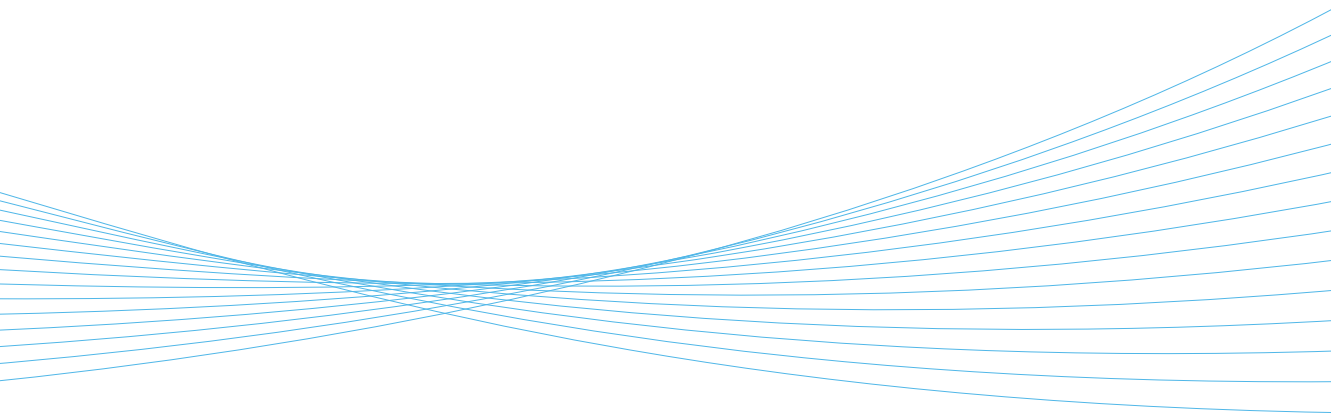

FINNISH METEOROLOGICAL INSTITUTE
CONTRIBUTIONS

No. 125

EFFECTS OF BLACK CARBON AND ICELANDIC DUST ON SNOW ALBEDO, MELT AND DENSITY

OUTI MEINANDER

Finnish Meteorological Institute
Helsinki, Finland

University of Helsinki
The Doctoral Programme in Atmospheric Sciences ATM-DP
Department of Environmental Sciences
Faculty of Biological and Environmental Sciences
Helsinki, Finland

Academic Dissertation in Environmental Sciences

To be presented, with the permission of the Faculty of Biological and Environmental Sciences of the University of Helsinki, for public criticism in Auditorium Brainstorm (Erik Palménin aukio 1) on 18 November, 2016, at 12 o'clock noon.

Helsinki, 2016

Supervisors	Professor Gerrit de Leeuw Climate Research, Finnish Meteorological Institute, Finland Department of Physics, University of Helsinki, Finland
	Professor Pekka Kauppi Department of Environmental Sciences University of Helsinki, Finland
Mentor	Dr. Terhikki Manninen Meteorological Research Finnish Meteorological Institute, Finland
Thesis advisory committee	Professor Ari Laaksonen Climate Research Finnish Meteorological Institute, Finland
	Docent Heikki Lihavainen Atmospheric Composition Research Finnish Meteorological Institute, Finland
	Dr. Pavla Dagsson-Waldhauserova Faculty of Environmental Sciences, Agricultural University of Iceland Institute of Earth Sciences, University of Iceland Faculty of Physical Sciences, University of Iceland, Iceland Faculty of Environmental Sciences, Czech University of Life Sciences, Czech Republic
Pre-examiners	Professor Pauline Stenberg Department of Forest Sciences University of Helsinki, Finland
	Professor Lars Eklundh Department of Physical Geography and Ecosystem Science Lund University, Sweden
Custos	Professor Pekka Kauppi Department of Environmental Sciences University of Helsinki, Finland
Opponent	Professor Tiit Nilson Department of Remote Sensing Tartu Observatory, Estonia

Finnish Meteorological Institute Contributions No. 125
ISBN 978-951-697-895-9 (paperback)
ISSN 0782-6117 Finnish Meteorological Institute Contributions
Erweko
Helsinki 2016

ISBN 978-951-697-896-6 (pdf)
http://ethesis.helsinki.fi
Published also by the University of Helsinki in Unigrafia Oy, Helsinki 2016.

FINNISH METEOROLOGICAL INSTITUTE

Published by Finnish Meteorological Institute
(Erik Palménin aukio 1), P.O. Box 503
FIN-00101 Helsinki, Finland

Series title, number and report code of publication
Finnish Meteorological Institute
Contributions 125, FMI-CONT-125

Author
Outi Meinander

Date
October 2016

Title

Effects of black carbon and Icelandic dust on snow albedo, melt and density

Abstract

Light-absorbing impurities in the cryosphere are of hydrological, environmental and climatic importance. The wet and dry deposition of black carbon (BC), organic carbon (OC), and dust particles affect the optical properties and melt of snow and ice. In the Arctic region, the climatic effects are amplified, and surface albedo feedback is often cited as the main contributor.

The aim of this thesis is to fill in some of the gaps in our knowledge of the effects of BC, OC, and Icelandic dust on snow in the European Arctic through a series of field and laboratory experiments and an analysis of the resulting data, including modeling. The thesis presents a new hypothesis on the snow density effects of light-absorbing impurities, an important quantity for climate modeling and remote sensing. Three processes are suggested to explain the proposed ”BC density effect”. Experimental results show that dirty snow releases melt water quicker than cleaner snow.

The albedo of natural seasonally melting snow in Sodankylä, north of the Arctic Circle, is found to be asymmetric with respect to solar midday, thus indicating a change in the properties of the snow. The radiative transfer modeling results show that the observed solar zenith angle asymmetry results in a 2–4 % daily error for satellite snow albedo estimates. Surface albedo model results indicate that the biggest snow albedo changes due to BC are expected in the ultraviolet (UV) part of the electromagnetic spectrum. The albedo of natural seasonal snow measured in Sodankylä, is found to be lower than expected. Solar UV and visible (VIS) albedo values of 0.6–0.8 in the accumulation period and 0.5–0.7 during melting are observed. The low albedo values are explained to be due to large snow grain sizes up to ∼3 mm in diameter, meltwater surrounding the grains and increasing the effective grain size, and absorption caused by impurities in the natural snow (87 ppb BC and 2894 ppb OC). The BC contents of the surface snow layer at the Sodankylä Arctic Research Center, Finland, is higher than expected. Increased BC in spring time suggests surface accumulation of hydrophobic BC during snow melt. Some of the high BC concentrations are related to anthropogenic soot transported from the Kola Peninsula, Russia. The origin of OC can be anthropogenic or natural, and may include pollen, seeds, lichens, natural litter or microorganisms that reside in snow and ice.

Iceland is the most important Arctic dust source, but a scientific assessment of its impacts on the cryosphere is currently unavailable and scientific results are urgently needed to investigate the role of Icelandic dust in Iceland and elsewhere, in the past, present and future. Experimental results on Icelandic volcanic ash show that a thin layer increases the snow and ice melt but that an ash layer exceeding a certain critical thickness causes insulation.

The Arctic results of this thesis have relevance to the assessment of Arctic climate change, including modeling and satellite applications.

Publishing unit
Finnish Meteorological Institute, Research and Development, Climate Research

Classification (UDC)
502.3/.7, 504, 550.3

Keywords
Arctic, aerosol, black carbon, Iceland, dust, albedo, snow, ice

ISSN and series title
0782-6117 Finnish Meteorological Institute Contributions

ISBN
978-951-697-895-9 (paperback), 978-951-697-896-6 (pdf)

Language
English

Pages
122

ILMATIETEEN LAITOS

Julkaisija	Ilmatieteen laitos (Erik Palménin aukio 1) PL 503, 00101 Helsinki	Julkaisun sarja, numero ja raporttikoodi Finnish Meteorological Institute Contributions 125, FMI-CONT-125
Tekijä Outi Meinander		Julkaisuaika Lokakuu 2016

Nimeke

Mustan hiilen ja Islannin pölyn vaikutukset lumen heijastavuuteen, sulamiseen ja tiheyteen

Tiivistelmä

Valoa absorboivien partikkeleiden kuiva- ja märkälaskeuma lumen tai jään pinnalle vaikuttaa lumipeitteen optisiin ominaisuuksiin ja sulamiseen ja on tärkeä hydrologian, ympäristön ja ilmaston kannalta. Arktisella alueella ilmastovaikutukset korostuvat etenkin lumen heijastavuuden ja sulamisen takaisinkytkentä-mekanismin takia.

Tämän väitöskirjan tavoitteena on mittaus- ja mallitulosten avulla tuottaa uutta tietoa noen (BC) ja orgaanisen hiilen (OC), sekä Islannin vulkaanisen pölyn laskeuman vaikutuksista Arktisen lumen sulamiseen ja optisiin ominaisuuksiin. Työssä esitetään uusi hypoteesi, jonka mukaan valoa absorboivat hiukkaset voivat vähentää sulavan pintalumen tiheyttä, joka on tärkeä ilmastomallien ja lumen satelliittimittausten muuttuja. Tätä selitetään kolmella mahdollisella prosessilla.

Sodankylässä vuotuisen lumipeitteen heijastuskyky (albedo) oli lumen sulamiskaudella alhaisempi kuin kirjallisuuden perusteella osattiin odottaa. Lumen ultraviolettisäteilyn (UV) ja näkyvän valon (VIS) heijastuskyky oli 0.6–0.8 talviaikaan ja 0.5–0.7 sulamiskaudella. Alhaista albedoa selittävät lumen suuri kidekoko ja kidettä ympäröivä sulamisvesi, sekä lumen valoa absorboivat epäpuhtaudet (87 ppb nokea ja 2894 ppb orgaanista hiiltä). Sodankylän Arktisen tutkimuskeskuksen pintalumen mustan hiilen pitoisuudet olivat odotettua (< 60 ppb) suuremmat. Nokea kertyi lumen pintakerrokseen lumen sulaessa. Toinen syy korkeisiin nokipitoisuuksiin oli kaukokulkeuma lähialueilta. Orgaaninen hiili voi olla peräisin orgaanisten yhdisteiden päästöistä tai se voi koostua luonnollisista lumelle kertyneestä tai siinä kasvavasta orgaanisesta materiaalista, kuten neulaset, siitepölyhiukkaset, siemenet, sienirihmat, jäkälät ja levät.

Sulamiskaudella lumen heijastuskyky oli auringon korkeuskulman funktiona epäsymmetrinen, koska lumen fysikaalisten ominaisuuksien muuttuminen päivän mittaan vaikutti albedoon. Säteilynkuljetusmallilaskelmat osoittivat, että tämä epäsymmetria voi aiheuttaa 2–4 % virheen satelliittimittausten perusteella tehtyihin albedoarvoihin. Pinta-albedon mallilaskelmat osoittivat, että noki vähentää lumen heijastuskykyä sitä enemmän mitä lyhyempi säteilyn aallonpituus on kyseessä ja eniten ihmissilmälle näkymättömillä UV-säteilyn aallonpituuksilla.

Arktisella alueella Islannin pöly voi olla merkittävä lumen sekä jään ja jäätiköiden optisten ominaisuuksiin ja sulamiseen vaikuttava tekijä, ja mahdollisesti yhtä suuri tai jopa tärkeämpi kuin noki. Tutkimustuloksia on toistaiseksi hyvin vähän. Tässä työssä havaittiin, että ohut tuhkakerros edisti lumen ja jään sulamista, mutta suurempi määrä toimi eristeenä ja hidasti sulamista.

Väitöskirjan tuloksia voidaan hyödyntää Arktisen alueen ilmastonmuutoksen arvioinnissa, mukaan lukien mallinnus- ja satelliittisovellutukset.

Julkaisijayksikkö

Ilmatieteen laitos, Tutkimus ja menetelmäkehitys, Ilmastotutkimus

Luokitus (UDK)	Asiasanat
502.3/.7, 504, 550.3	Arktinen, aerosoli, Islanti, musta hiili, orgaaninen hiili, lumi, jää, albedo

ISSN ja avainnimike

0782-6117 Finnish Meteorological Institute Contributions

ISBN

978-951-697-895-9 (nid.), 978-951-697-896-6 (pdf)

Kieli	Sivumäärä
englanti	122

Prewords

This thesis work on light-absorbing particles in snow completes my postgraduate Phil.Lic. university degree into PhD, more recognized internationally. However, I am also aware that it is important to avoid using "Dr." when, e.g., booking flight tickets ("Is there a doctor on board this flight?")…the best memories are thanks to many people! I want to thank my co-authors of the original publications included in this thesis, Pavla, Anna, Terhikki, Mona (and her co-authors), Kaisa, Anu, Hanne, Oli, Aki, Antti, Matti, Aku, Jonas, Stelios, Petri, Roux, Michael, Leif, Jean-Louis, Olivier, Lasse, Onni, Rigel, Veijo, Martti, and Gerrit. Special thanks to Gerrit for his support and supervision of my thesis, and Terhikki for kindly mentoring me. I also thank Pekka Kauppi, my supervisor from the University of Helsinki, for his help. I am most grateful for all the supportive people surrounding me, including my family and friends.

Prof. Steven Warren, University of Washington, USA, I thank for his guidance on BC in snow while in Norway, and Dr. Sarah Doherty for the BC analysis of some of my snow samples. In addition to the co-authors, recent collaboration and great discussions and future plans have taken place thanks to many people, especially prof. Olafur Arnalds; prof. Joe Prospero; prof. Zhijun Li; as well as Maria Gritsevich, Jouni Peltoniemi, Timo Nousiainen, and many other colleagues. I also want to acknowledge Liisa Jalkanen, who initially employed me as a summer worker for the FMI Chemistry laboratory, and prof. Juhan Ross I remember for his positive supervision. For many years, my practical work at FMI was part of prof. Esko Kyrö's Antarctic-Arctic research, thank you Esko and thanks to all Marambio collaborators! Timo Vihma I thank for his supervision of my Antarctic Thesis for MetPD (meteorology), and Roberta Pirazzini for sharing her experiences in the Antarctic snow research. The FMI Snow Team of Kirsti Kylhä, the members of COST SNOW ES1404 of Ali Nadir Arslan, our '553research group', and Antti Aarva and Sodankylä personnel, as well as the morning-coffee table (most often Laura, Tiina, Kirsi, Simo and Leif), deserve to be mentioned.

The members of the thesis advisory committee (Pavla, Ari and Heikki), as well as prof. Pauline Stenberg and prof. Lars Eklundh (pre-examiners of this thesis) I gratefully thank for their valuable comments on the thesis draft. Prof. Tiit Nilson I thank for accepting to be my opponent. Finally, I want to thank Dr. Yrjö Viisanen, our R&D director, prof. Jouni Pulliainen, our Sodankylä Arctic Center director, and Dr. Juhani Damski, FMI Director-General, for the excellent working conditions and scientific environment provided at FMI. This thesis was prepared at FMI within the ATM-DP, FCoE ATM and NCoE CRAICC of the University of Helsinki, prof. Markku Kulmala. I am thankful for this support.

Sometimes research work has challenges similar to those faced by the crew onboard the Starship Enterprise (Star Trek series, which belongs to my favorites), but more surprisingly some imagination things from Start Trek have recently become realistic, too: let's consider a food replicator vs 3D-printing, and holodeck vs the Finnish invention of SmogScreen! That makes me wonder: When can we be beamed up and energized? While waiting for that to happen, let's set a course to the Arctic. These are the voyages.

Helsinki, October 2016, Outi Meinander

Contents

List of original publications and author's contribution

This thesis consists of an introductory overview, followed by five research articles. In the introductory part, these papers are cited according to their roman numerals PAPER I–V.

I Meinander, O., Kontu, A., Lakkala, K., Heikkilä, A., Ylianttila, L., and Toikka, M.: Diurnal variations in the UV albedo of Arctic snow, Atmos. Chem. Phys., 8, 6551-6563, doi:10.5194/acp-8-6551-2008, 2008.

II Meinander, O., Kazadzis, S., Arola, A., Riihelä, A., Räisänen, P., Kivi, R., Kontu, A., Kouznetsov, R., Sofiev, M., Svensson, J., Suokanerva, H., Aaltonen, V., Manninen, T., Roujean, J.-L., and Hautecoeur, O.: Spectral albedo of seasonal snow during intensive melt period at Sodankylä, beyond the Arctic Circle, Atmos. Chem. Phys., 13, 3793-3810, doi:10.5194/acp-13-3793-2013, 2013.

III Meinander, O., Kontu, A., Virkkula, A., Arola, A., Backman, L., Dagsson-Waldhauserová, P., Järvinen, O., Manninen, T., Svensson, J., de Leeuw, G., and Leppäranta, M.: Brief communication: Light-absorbing impurities can reduce the density of melting snow, The Cryosphere, 8, 991-995, doi:10.5194/tc-8-991-2014, 2014.

IV Dragosics, M., Meinander, O., Jónsdóttír, T., Dürig, T., De Leeuw, G., Pálsson, F., Dagsson-Waldhauserová, P., and Thorsteinsson, T.: Insulation effects of Icelandic dust and volcanic ash on snow and ice. Arabian Journal of Geosciences, 9, 126, doi: 10.1007/s12517-015-2224-6, 2016.

V Meinander, O., Dagsson-Waldhauserova, P., and Arnalds, O.: Icelandic volcanic dust can have a significant influence on the cryosphere in Greenland and elsewhere. Polar Research, 35, 31313, doi:10.3402/polar.v35.31313, 2016.

O. Meinander was responsible for the PAPER I–III and V. She planned the contents of the PAPER I–II, invited the co-workers needed, and participated in a large part of the work and data-analysis and writing, except the SILAM modeling calculations. In PAPER III, she created the hypothesis; the reasons for the density effects were formulated by all the co-authors as a team. For PAPER IV, O. Meinander was responsible for planning and supervising the work and manuscript writing of PhD student M. Dragosics at the Institute of Earth Sciences, University of Iceland. For PAPER V, she was the initiator of the paper and responsible for planning the contents and arguments presented, with contributions from the other co-authors.

Abbreviations

AMAP	Arctic Monitoring and Assessment Programme
ARC	Arctic Reserach Center
AWS	Automated Weather Station
BB	Broadband
BC	Black Carbon
BHR	Bihemispherical Reflectance
BRDF	Bidirectional Reflectance Distribution Function
BRF	Bidirectional Reflectance Factor
DP	Doctoral Programme
EC	Elemental Carbon
EM	Electromagnetic
ET	Extraterrestrial
FCoE	Finnish Center of Excellence
FMI	Finnish Meteorological Institute
GAW	Global Atmospheric Watch
IPCC	Intergovernmental Panel of Climate Change
IPY	International Polar Year
LAI	Light Absorbing Impurity
LAP	Light Absorbing Particle
LW	Longwave
MAC	Mass Absorption Cross section
MBFR	Multiband Filter Radiometer
MODIS	Moderate Resolution Imaging Spectrometer
NASA	National Aeronautics and Space Administration
NCoE	Nordic Center of Excellence
NIR	Near Infrared
OC	Organic Carbon
PEEX	Pan-Eurasian Experiment
PM	Particulate Matter
RT	Radiative Transfer
SLCF	Short-Lived Climate Forcer
SMEAR	Station for Measuring Ecosystem-Atmosphere relations
SNICAR	Snow, Ice, and Aerosol Radiation -model
SNORTEX	Snow Reflectance Transition Experiment
SW	Short Wave
UV	Ultraviolet
VIS	Visible
WMO	World Meteorological Organization
WOUDC	World Ozone and Ultraviolet Data Center, Canada

1 Introduction

1.1 Background

Atmospheric aerosols are small (3 nm – 100 µm) liquid or solid particles suspended in the atmosphere. These particles originate from various natural and anthropogenic sources. Aerosol species include sulfates, sea salt, nitrates, organic carbon, black carbon, ash, and wind-blown dust. They can be directly emitted into the atmosphere, or formed (from precursor gases) through chemical and physical processes, and they are capable of being long-range transported. The atmospheric residence time of aerosol particles ranges from hours for coarse particles towards days (or weeks) for fine mode particles (< 1 µm). The residence time of fine mode particles is significantly shortened by wet deposition. The properties of the particles can be described based on their shape, size, and chemical composition. A significant feature of aerosol particles is their ability to scatter and absorb atmospheric solar radiation. Light-absorbing aerosol particles include soot (black carbon, BC), ash, dust, and the so called brown-carbon fraction of organic carbon (OC).

In the cryosphere, light-absorbing particles (LAP) are of hydrological, environmental, and climatic importance, depending of their physical and chemical properties. When deposited on snow and ice surfaces, the climatic effects of dark particles are due to reduced albedo and induced melt of darker surfaces, which again lowers the albedo and increases melt via the albedo feedback mechanism (Arrhenius 1896, Warren and Wiscombe 1980, Doherty et al. 2010). In the Arctic region, these climatic effects are amplified, and the surface albedo feedback is often cited as the main contributor to a phenomenon known as Arctic amplification, referring to greater warming in the Arctic compared to the global average (Arrhenius 1896, Serreze and Barry 2011, Pithan and Mauritsen 2014). Currently, Arctic amplification is understood to have a variety of causes on different temporal and spatial scales, including the albedo feedback, retreat of sea ice, changes in atmospheric and oceanic heat fluxes, changes in cloud cover and water vapor content, soot on snow, and heat absorbing BC aerosols in the atmosphere (Serreze and Barry 2011). Darkening and melt effects are most often linked to BC, but OC and dust can have similar effects. In addition to deposited atmospheric particles, cryospheric light-absorbing impurities (LAI) may consist of natural organic litter like needles, pebbles, and various microorganisms that reside in snow and ice.

The sources for BC are mainly incomplete combustion of carbonaceous material, like fossil fuels and biomass. In the Arctic, BC originates from emissions from industrial and biofuel burning, mostly from long-range transported extra-Arctic emissions from Europe, North America, Former Soviet Union and East Asia (Sharma et al. 2013, Jiao et al. 2014). The BC emissions of China and India have been evaluated among the largest of the Asian BC hot-spot region (Wang et al. 2014). Gas flaring can also be a significant source at high

latitudes (Stohl et al. 2013). Koch and Hansen (2005) say that half of biomass-originating BC in the Arctic comes from north of 40^{o}N (North America, Russia, and Europe, each contributing 10–15 %). They also report that Russia, Europe, and south Asia each contribute about 20–25 % of BC to the low-altitude springtime ‘‘Arctic haze”, which consists primarily of anthropogenic particles with high sulfur concentrations and other components such as soot.

BC can affect the Arctic climate through several mechanisms. These include direct heating of the Arctic atmosphere (Ramanathan and Carmichael 2008), darkening and increased melt of Arctic snow and ice (Hansen and Nazarenko 2004, Flanner et al. 2007, Bond et al. 2013), alteration of Arctic cloud shortwave and longwave properties and cloud formation (Koch and Del Genio 2010), and perturbation of the poleward heat flux through forcing exerted outside the Arctic (AMAP 2015). Arctic climate response has been found sensitive to the vertical distribution and deposition efficiency of BC reaching the Arctic (Flanner 2013). The Intergovernmental Panel on Climate Change Fifth Assessment Report (IPCC 2013) assesses the BC on snow/ice to have a global and annual mean direct radiative forcing of 0.40 Wm^{-2}. BC emissions occurring within the Arctic have been found to induce about fivefold greater warming, normalized to the mass of emissions, than emissions from mid-latitudes, because a higher fraction of within-Arctic emissions deposit to snow and sea ice than mid-latitude emissions (Sand et al. 2013). The role of BC in snow and ice has been widely investigated, and detailed scientific assessments have been presented in Bond et al. (2013), IPCC (2013), and AMAP (2015).

Black carbon is a Short-Lived Climate Forcer (SLCF) and it undergoes regional and intercontinental transport from source regions during its short atmospheric lifetime. Atmospheric removal of BC occurs within a few days to weeks via precipitation and contact with surfaces (Bond et al. 2013). The life time of BC can be largely determined by factors that control local deposition rates, e.g., precipitation (Zhang et al. 2015). Wet-scavenging processes (in-cloud and below-cloud scavenging) are a major source of uncertainty in predicting atmospheric BC concentrations over remote regions (Schwarz et al. 2010). When emitted, BC is mostly hydrophobic (Laborde et al. 2013) but can become coated with water-soluble components through atmospheric aging processes, where BC changes from hydrophobic to hydrophilic. Aerosols can also form complex mixtures. For example, soot particles can mix with nitrates and sulfates, or they can coat the surfaces of dust.

The main sources of OC aerosols, co-emitted in the atmosphere with BC, are anthropogenic activities and wildfires (e.g., Hegg et al. 2010). Bond et al. (2013) mention that a large fraction of particulate light absorption in Arctic snow (about 30 to 50 %) is due to non-BC constituents and most of the absorption would be due to light-absorbing OC, called brown carbon. Different types of brown carbon can include coal combustion, biomass burning, organic compounds emitted from local soils, and volatile organic compounds (VOC) emitted by vegetation. France et al. (2012) explained that BC alone could not account for all the absorption seen in the Barrow snowpacks, and an additional absorption by Humic Like Substances (HULIS, part of brown carbon), and other chromophores was necessary to explain the observed variation. Voisin et al. (2012) measured HULIS optical properties and reported them to be consistent with aged biomass burning or a possible marine source. McNeill et al. (2012) discussed the adsorption and

desorption of organic species to and from snow and ice surfaces, and how these processes influence the transport of organic trace gases through the snowpack. A much higher OC to EC ratio (205:1) was reported for snow than in air (10:1), indicating that snow would be additionally influenced by watersoluble gasphase compounds (Hagler et al. 2007). According to AMAP (2015), in case of using the thermo-optical analysis method for OC in snow, pieces of organic material, such as bits of leaf or twig, can contribute significantly to the OC results. Cryoconite (a mixture of dust, pebbles, soot, and microbes) (Tedesco et al. 2015) and color-pigmented algae (Benning et al. 2014, Lutz et al. 2016) have been added in the discussions on snow darkening and melt more recently, especially in Greenland. In the melting of glaciers (glaciar snow melt), the role of BC is considered uncertain, because few measurements of glacial BC content exist, and the impact of natural impurities, such as soil dust and algae, has not sufficiently been accounted for (Bond et al. 2013).

Dust is a major environmental factor in the Earth system with important impacts on global energy and carbon cycles. Atmospheric desert dust particles are soil particles suspended in the atmosphere from regions of dry unvegetated soils with erosion and strong winds. Because of its effects from timescales of minutes (as with dust devils, cloud processes and radiation) to millennia (as with oceanic sediments, and loess sediments formed by the accumulation of wind-blown silt), dust is not only a key environmental player, but also a recorder of environmental change (Knippertz & Stuut 2014). The multiple processes in which dust takes part include dust interaction with continental and marine ecosystems by being a source of micronutrients; when deposited in the cryosphere, dust changes the amount of reflected solar radiation; dust affects the solar radiation in the atmosphere and properties of clouds and thereby also precipitation. Studies show that at low and mid-latitudes, Saharan dust can affect the albedo and long-term mass balance of an Alpine glacier (Di Mauro et al. 2015, Gabbi et al. 2015). Dust from Asian deserts is deposited on Himalayan snow resulting in darkening and increased snow melt (Gautam et al. 2013). Mineral dust from the Colorado Plateau can shorten snow cover duration of the San Juan Mountain range (Painter et al. 2007). Recently, it has been recognized that dust produced in high latitude and cold environments may have regional or global significance (Bullard et al. 2016). Dust is included in the IPCC (2013) report as an anthropogenic source due to the development of agriculture which favors the generation of dust.

In the Arctic region, Iceland is the most active dust source (Arnalds et al. 2016). The dust day frequency in Iceland is similar to that in the major desert areas of the world (Mongolia, Iran, USA, China). Frequent volcanic eruptions with the re-suspension of volcanic materials and dust haze increase the number of dust events fourfold, resulting in 135 dust days in Iceland annually (Dagsson-Waldhauserova et al. 2014). High-latitude dust transport over the North Atlantic with inputs from Icelandic dust storms was described for the first time by Prospero et al. (2012). About 50 % of the annual dust events in the southern part of Iceland take place at sub-zero temperatures, when volcanic dust may be mixed with snow (Dagsson-Waldhauserova et al. 2015). There are over 30 active volcanoes or volcanic systems in Iceland, and seven major dust sources (Arnalds 2010, Arnalds et al. 2016). The properties of ash and dust from these sources show considerable physical and chemical variability. Icelandic volcanic dust properties, origin and transport

have been widely investigated (Arnalds et al. 2016), but fewer investigations are available for dust-cryosphere interaction (Dagsson-Waldhauserova 2015, Arnalds et al. 2016).

Figure 1.1. Dark volcanic dust on the surface of an Icelandic glacier. Light-absorbing aerosols, such as black carbon, organic carbon, ash and dust, originate from various natural and anthropogenic sources. When deposited on snow and ice surfaces they reduce the surface albedo and increase melt via the albedo feedback mechanism. Photo O. Meinander, Solheimajökull, Iceland, in March 2016.

This thesis deals with effects of BC, OC and Icelandic volcanic dust on snow and ice properties in the Arctic region, as discussed in connection with sources of emissions, and transport and deposition. For black carbon, different names are used in the literature. Here BC refers to light-absorbing carbonaceous substances when there is no reference to a specific measurement method. Elemental carbon (EC) is used when results refer to the carbon content specific thermo-optical method. Soot is composed mainly of carbon and produced when organic (carbon-containing) material is burned. An individual hydrophobic soot particle is composed of graphitic layers and has a typical diameter of 45 nm (AMAP 2015). Volcanic dust (Figure 1.1) is defined as any volcanic material which is re-suspended from old deposits of any volcanic material, regardless of age and mode of formation (Dagsson-Waldhauserova et al. 2015). According to AMAP (2015), there is no fixed definition for the Arctic, and the term Arctic is there used for latitudes North of 60°N. More often, the Arctic is defined as the area north of the Polar Circle. In case of Iceland, Arctic dust events have been used to refer to NE Icleand, and Sub-Arctic dust events to S Iceland (Dagsson-Waldhauserova et al. 2014). Here the Arctic results refer mainly to Arctic Finland (PAPER I–III) and Iceland (PAPER III–V), but also to the Arctic

region more broadly (PAPER V). Due to the lack of standardization of reflectance terminology (Shaepman-Strub et al. 2006), this thesis uses notations following Shaepman-Strub et al. (2006). Albedo is defined as bihemispherical reflectance (BHR). For clarity, spectral albedo (BHR_λ) is distinguished from the eryhemally weighted broadband albedo (BHR_{ery}). The term light-absorbing refers to the electromagnetic radiation at 300–2500 nm.

In the next section 1.2, I will identify the scope, research questions and objectives of the thesis. The main gaps of knowledge and open research questions at the time this research was conducted, which this thesis addresses, are also presented in section 1.2. This is followed by describing the outline of the thesis in section 1.3. Thereafter, theory and scientific knowledge of effects of light-absorbing impurities will be introduced in section 2. Then chapters on materials and methods, and overview of results and discussion, will be presented. The thesis is completed with summary and conclusions, and plans for future work.

1.2 Scope, research questions and objectives

The aim of this thesis is to fill in some of the gaps in our knowledge and understanding of the impacts of the light-absorbing aerosols of BC, OC, and Icelandic volcanic dust, on the snow and ice albedo, melt and density, especially in the Arctic. Such effects are of hydrological, environmental and climatic importance via surface darkening and increased snow melt. The thesis contributes with new continuous Arctic measurement data, field campaigns, and laboratory experiments since the International Polar Year (IPY) 2007/2008, for the data-sparse region in the Arctic, in the Northern Europe. The work started with the Sodankylä snow ultraviolet (UV) albedo measurements (initiated during IPY 2007/2008, PAPER I), continued including effects of BC/OC on Sodankylä snow (PAPER II), a hypothesis on BC density effects (PAPER III), effects of Icelandic dust (PAPER IV), and the role of Icelandic dust in the Arctic cryosphere more broadly (PAPER V). The thesis also includes some Arctic-Antarctic aspects, and discusses some of the challenges and possibilities in modeling and satellite approaches.

When the work on Sodankylä snow started with the continuous in situ UV albedo measurements (PAPER I–II), this was the first of its kind in Finland; only the UV irradiance and VIS albedo (at visible wavelengths) were included in the atmospheric radiation measurements of the Finnish Meteorological Institute (FMI). Earlier, UV albedo measurements had been made elsewhere in the Arctic and Antarctic (Smolskaia et al. 1999, Perovich et al, 2002, Pirazzini 2004, Wuttke et al. 2006). The Snow UV albedo is of importance as it amplifies the amount of the surface UV radiation. The stratospheric ozone depletion increases the UV irradiance reaching the ground, too. The UV radiation has many positive and negative impacts. The UV albedo of snow can be the reason behind a painful eye condition known as snow blindness (UNEP 2002). The UV radiation is needed for the vitamin D production and it has a harmful effect on causing DNA damage and skin cancer (WHO 2006), as well as material degradation (Andrady et al. 2015, Heikkilä 2014), and it is important in air chemistry in photolysis reactions. Estimates on the snow UV

albedo were used for satellite UV algorithms in Arola et al. (2003), and Tanskanen and Manninen (2007). The snow UV albedo measurements in Sodankylä were initiated during IPY 2007/2008, and investigated then with the help of ancillary meteorological and snow information (PAPER I). Later (PAPER II-V), the work included snow albedo, melt and density investigations linked to atmospheric particles deposited in snow, which is of particular interest due to the UV absorbing properties of some of the aerosol particles.

The albedo effects of dirty snow were first published by Warren and Wiscombe (1980). Their results are currently in use in the snow albedo model SNICAR (Flanner et al. 2007), acknowledged and used by the IPCC (2013), too. Recently, more than 30 years later, an empirical dataset on impurities in Arctic snow were made available by Doherty et al. (2010). Their investigation updated the 1983–1984 survey of Clarke and Noone (1985). The work of Doherty et al. (2010) covered BC in snow in Alaska, Canada, Greenland, Svalbard, Norway, Russia, and the Arctic Ocean, but no snow samples from Finland were included. Their closest place was Tromso, Norway, which represented the European Arctic. In 2013, Svensson et al., Forsström et al. and PAPER II reported BC concentrations in snow samples collected in the European Arctic snowpacks.

Next, I will identify the contribution of the PAPER I–V to different scientific questions and objectives. The specific research questions, to which answers were searched for in this thesis, were as follows:

Q1: What is the in situ snow UV albedo in Sodankylä, north of the Arctic Circle and why? (= Objective of the PAPER I–II)

Q2: How much BC and OC is there in seasonal snow in Sodankylä and why? (= Objective of the PAPER II)

Q3: Why does dirty snow melt faster than clean snow, i.e., what happens after impurities absorb radiation and snow melt starts? (= Objective of the PAPER III)

Q4: How does Icelandic volcanic dust interact with snow and ice and why, and what are the potential impacts of Icelandic dust? (= Objective of the PAPER IV–V)

Q5: What are the challenges, needs and possibilities in modeling and remote-sensing approaches and in bipolar Arctic-Antarctic research? (= Objectives of the PAPER I, II and V).

In this thesis work, these research questions related to effects of elemental carbon, organic carbon, and Icelandic volcanic dust, on snow and ice optical properties, melt and density have been investigated. Various approaches were used, as will be explained in the Chapter 3.

1.3 Outline of the thesis

The thesis consists of five original papers. These are referred to by roman numbers (PAPER I–V). The contributions of PAPER I–V to the thesis are presented in Table 1.1. The focus of PAPER I–II is on the snow albedo and reflectance, and BC/OC in natural Arctic Sodankylä snow. PAPER III presents a new hypothesis on the snow density

effects. PAPER IV shows experimental data where snow melt increases for smaller amounts of Icelandic dust particles in snow, and insulation can take place in case of thicker dust layers. PAPER V states that the scientific assessment of impacts of Icelandic dust in cryosphere is currently missing, urges for scientific investigation, and hypothesizes that in the Arctic Icelandic dust can have similar or larger albedo and melt effects on the cryosphere than soot.

Table 1.1. The contribution of PAPER I–V to the thesis.

Subject	PAPER I	PAPER II	PAPER III	PAPER IV	PAPER V
Black carbon		X	X		X
Organic carbon		X	X		X
Icelandic dust			X	X	X
Snow /Ice albedo	X	X	X		X
Snow /Ice melt	X	X	X	X	X
Snow density			X		

The structure of the thesis is planned as follows. In the next chapter, the theoretical and scientific literature of light-absorbing impurities and cryosphere is described, with the focus in Arctic. The materials and methods are presented in Chapter 3 and the Chapter 4 contains an overview of the main results and their discussion based on the original papers. The synthesis includes effects of BC, OC, and Icelandic volcanic dust on the snow and ice albedo, melt and density, as well as modeling and remote sensing related aspects. Conclusions and future aspects are included in Chapters 5–6.

2 Light-absorbing particles in the Arctic snow

Light-absorbing atmospheric particles deposited in snow cause changes in the interaction of solar irradiance and snow. According to the law of energy conservation, the incoming solar radiation can be absorbed, reflected or transmitted. A change in any of these components can therefore be used to indicate changes in the properties of the target under investigation. Clean non-melting snow reflects generally 80–90 % of the incident solar radiation (Wiscombe and Warren 1980). Darker, dirty snow absorbs more solar radiation, decreasing snow reflectivity (Warren and Wiscombe 1980). This in turn increases snow melt, which again decreases the reflectance of snow. This is known as the snow albedo feedback mechanism. Hence, in the presence of light-absorbing particles in snow, the key driving force for snow melt is the decrease in snow reflectivity. In addition, for the surface radiation balance, changes in snow surface reflectivity are most critical. As the irradiation that is reflected back to space does not heat the Earth, snow cover cools the climate both locally and globally and is an important factor in the global energy balance. The climatic affects are amplified in the Arctic. In this chapter, we first take a look on the theory to understand what light is (section 2.1), and what controls the solar irradiance at the Earth surface (section 2.2), where after factors affecting the snow bihemispherical reflectance, i.e. albedo, of clean and dirty snow are presented (section 2.3).

2.1 Electromagnetic radiation

Light is electromagnetic radiation, whose main source in the Earth is the Sun. According to the wave model of electromagnetic radiation, the solar spectral irradiance $E(\lambda)$ consists of wavelengths from 100 to 5000 nm (Harris 1987). The term spectral is used when the wavelength dependency is being described. Electromagnetic waves are often categorized by their location within the electromagnetic spectrum. For example, electromagnetic radiation at 300–400 nm is called ultraviolet (UV) radiation, at 400–700 nm visible (VIS) radiation, and at 700–2500 nm near-infrared (NIR) radiation. Light most often refers to light visible to human eye in the wavelength range of 400–700 nm. It should be noted that only thermal IR is directly related to the sensation of heat, while NIR is not. Because of the similarity in the behavior of UV, VIS and NIR regions of the spectrum, they are all incorporated in the field of physical research known as optics. In ecophysiology, agriculture, forestry and oceanography, the waveband between 400–700 nm contains what is known as photosynthetically active radiation (PAR). In addition to the wave model,

electromagnetic radiation is, according to the particle theory, composed of many discrete units called photons or quanta. The wave and quantum models of electromagnetic radiation are related by the equation

$$Q = h\,f = \frac{hc}{\lambda} \tag{2.1}$$

where Q = energy of a quantum [J]; h = Planck's constant, 6.626×10^{-34} [J sec]; f = frequency [s^{-1}]; c = velocity of light, 299792458 [m/s]; and λ = wavelength [m].

Only 2 % of the radiated extraterrestrial (ET) solar energy corresponds to the wavelength range below 220 nm and 3 % above 2700 nm (Agrawal 1986).

2.2 Solar irradiance at the Earth surface

Due to the absorption and scattering properties of the Earth's atmosphere, only part of the ET solar spectral irradiance is passed through the atmosphere. Incident solar radiation, i.e., solar irradiance at the Earth's surface, has both direct (sunlight) and diffuse (skylight) components. The direct solar irradiance $E_{dir}(\lambda)$ reaching the Earth surface is regulated by the product of the extraterrestrial spectral irradiance $E_{ET}(\lambda)$ and a wavelength-dependent effective transmission function T (Bird and Riordan 1986):

$$E_{dir}(\lambda) = E_{ET}(\lambda)\ D\ T(\lambda, \theta, \tau_r, \tau_a, \tau_w, \tau_O, \tau_u) \tag{2.2}$$

where $E_{dir}(\lambda)$ is the direct spectral irradiance on a surface normal to the direction of the Sun at ground level, $E_{ET}(\lambda)$ is the extraterrestrial spectral irradiance at the mean Earth-Sun distance, D is the correction factor for the Earth-Sun distance, θ is the solar zenith angle, and τ_r, τ_a, τ_w, τ_O, τ_u are the transmittance functions of the atmosphere for molecular (Rayleigh) scattering, aerosol attenuation, water vapor absorption, ozone absorption and uniformly mixed gas absorption, respectively.

The direct irradiance on a horizontal surface is obtained by multiplying Eq. (2.2) by $\cos\theta$. The surface albedo is a non-dimensional, unitless quantity that indicates how well a surface reflects solar energy. Albedo values vary between 0 and 1 (0–100 %). The spectral surface albedo is defined as the Bihemispherical Reflectance (BHR_λ), i.e., the ratio of the radiant flux reflected from a unit surface area into the whole hemisphere to the incident radiant flux of hemispherical angular extent as a function of wavelength (Schaepman-Strub et al. 2006):

$$BHR_\lambda = \frac{d\Phi_r(\theta_i, \phi_i, 2\pi, 2\pi, \lambda)}{d\Phi_i(\theta_i, \phi_i, 2\pi, \lambda)} \tag{2.3}$$

where Φ_r is the reflected radiant flux [W/nm], Φ_i is the incident radiant flux [W/nm], and (θ_i,ϕ_i) is the incident solar angle (zenith, azimuth).

In optical remote sensing terms, this definition of the surface albedo is often named as blue-sky albedo. The total diffuse solar irradiance $E_{diff}(\lambda)$ at the Earth surface is a sum (Bird and Riordan 1986) of components of Rayleigh $E_r(\lambda)$ and aerosol scattering $E_a(\lambda)$, and the component $E_g(\lambda)$ that accounts for the multiple reflection of irradiance between the ground and the air:

$$E_{diff}(\lambda) = E_r(\lambda) + E_a(\lambda) + E_g(\lambda) = E_{ET}(\lambda)\ D\ T(\lambda, \theta, \tau_r, \tau_a, \tau_{w,} \tau_{O,} \tau_u)\ k(BHR_\lambda, r_{s\lambda}) \qquad (2.4)$$

where $k = BHR_\lambda r_{s\lambda}/(1–BHR_\lambda r_{s\lambda})$; BHR_λ = bihemispherical spectral surface reflectance; $r_{s\lambda}$ = spectral sky reflectivity.

In some research applications it may be assumed that diffuse radiation is isotropic, i.e. has the same intensity regardless of the direction of measurement. The contribution of direct and diffuse components varies according to the solar elevation and wavelength: the smaller the wavelength and the lower the sun, the larger the diffuse component. Under an overcast fully cloudy sky all light is diffuse sky radiation.

Radiation having wavelength smaller than 100 nm (X-rays and Gamma rays) is absorbed in the ionosphere by oxygen molecules (O_2) and free oxygen atoms (O). The ET ultraviolet radiation range is 100–400 nm, but atmospheric absorption of oxygen molecules (O_2) prevents the most harmful UV-C radiation (100–280 nm) from reaching the surface. UV-B radiation (280–315 nm) is strongly absorbed by stratospheric ozone (O_3) with the absorption bands of Hartley (between 200–300 nm, with a maximum absorption at 255 nm), Huggins (weak absorption between 300–360 nm), and Chappuls (weak between 440–1180 nm) (Liou 2002). Carbon dioxide (CO_2) has absorption bands at 2300 and 4500 nm. Water vapor, $H_2O(g)$, has some absorption between 600 and 2000 nm and at 3000 nm.

In addition to the mechanism of atmospheric absorption, particles in the atmosphere cause atmospheric scattering. In general, if the particle is very much smaller in diameter than the wavelength of radiation, ‘Rayleigh scattering’ dominates. When the diameter of the particle is much larger than the wavelength, geometric ‘nonselective scatter’ prevails. ‘Mie scattering’ takes place when atmospheric diameter of the particle is of the order of the wavelength of the incoming radiation. The Mie scattering theory (Mie 1908) assumes homogenous spheres, none of which is a valid assumption for dust. For the non-spherical particles of dust and ash, Mie assumption is thus an error source in the scattering calculations (Nousiainen and Kandler 2015).

Changes in the values of the parameters in the atmospheric transmission function $T(\lambda)$ can be studied by in situ measurements, or radiative transfer (RT) model calculations, or by using satellite data. In the RT equation, the propagation of the electromagnetic radiation through the atmosphere can be described using a rather complicated equation including all the possible directions of propagation, where solar irradiance loses energy to the atmosphere by absorption, gains energy by atmospheric emission, and redistributes energy by scattering. A detailed description of the RT equation is found in Liou (2002),

for example. Often, a simplified two-stream approximation is used, where two directions (streams) of upward ($E\uparrow$) and downward ($E\downarrow$) irradiance are included. The solution of the RT equation generally yields the directional quantities of diffuse and direct irradiances upward and downward. The ratio of all reflected upward (↑) irradiance to the incident downward (↓) irradiance includes the diffuse and the specular radiation reflected.

2.3 Radiation - snow interaction

The solar electromagnetic radiation at wavelengths < 5000 nm is called shortwave (SW) radiation. At longer thermal wavelengths radiation is emitted. For the snow or ice (glacier) surface radiation balance, the net energy flux E_N is due to differences between downward (↓) and upward (↑) non-thermal shortwave (SW) and thermal longwave (LW) radiative fluxes, and can be expressed as (Garratt 1992):

$$E_N = E_{SW\downarrow} - E_{SW\uparrow} + E_{LW\downarrow} - E_{LW\uparrow} \tag{2.5}$$

where the net shortwave flux depends on the incident solar radiation and on the surface Bihemispherical Reflectance BHR (albedo), and the net longwave flux depends on the downwelling longwave radiation, the Stefan-Boltzmann constant σ ($5.670373\times10{-}8\mathrm{W\ m^{-2}K^{-4}}$), the surface emissivity ε_s, and the temperature of the surface T_s (in Kelvin):

$$E_N = (1 - \mathrm{BHR})\, E_{SW\downarrow} + E_{LW\downarrow} - \{(1 - \varepsilon_s)\, E_{LW\downarrow} + \varepsilon_s\, \sigma\, T_s^4\} \tag{2.6}$$

This shows that E_N is most critically influenced by the surface characteristics of the BHR (albedo) and emissitivity ε_s. Emissivity ε_s (0–1) is a measure of the thermal emittance of a surface, defined as the ratio of radiant heat flux emitted by a material to that emitted by a blackbody radiator at the same temperature, with values usually close to 1, e.g., for water ε_s = 0.97 (Robinson & Davies 1972), and for snow 0.97–1.0. The surface albedo, i.e., the capability of the surface to reflect the incoming irradiance, is a variable that varies highly temporally, spatially and spectrally from 0 to 1, depending on the surface properties. Hence, for the surface radiation balance, changes in albedo values are the most critical.

When snow melt rate is computed, all the variables affecting this heat exchange are required. Snow melt depends on the heat exchange between the snowpack and its environment. The energy balance of the snowpack can be written (Kuusisto 1984):

$$E_m = E_{SWn} + E_{LWn} + E_s + E_l + E_p + E_g - E_t \tag{2.7}$$

where E_m is the energy available for the snow melt, E_{SWn} is the net SW radiation, E_{LWn} is the net LW radiation, E_s is the sensible heat flux, E_l is the latent heat flux, E_p is the heat content of precipitation, E_g is the heat exchange at the ground surface, and E_t is the change of the internal energy of the snow-pack.

According to Kuusisto (1984), the components E_{LWn}, E_s and E_l can be considered to be limited to the snow surface or the uppermost surface layer with a thickness of a few millimeters, and E_m, E_s and E_t can be distribued throughout the snow pack. Intra-pack snowmelt can occur due to solar radiation even if the temperature of the snow surface layer is below zero. In practice snowmelt can start at the snow surface even if the temperature within the snowpack is negative, and the base of the snowpack at very low air temperatures (Kuusisto 1984).

For melting snow, the density of snow increases. Density has been used as a proxy for snow age (Doherty et al. 2016). Density refers to mass per volume, usually specified in [kg/m^3]. Snow density can be given as a ratio [%] to the water density 1000 kg/m^3.

2.3.1 Albedo of clean snow

The SZA dependency for surface albedo (U-shape) can be been expressed as (Briegleb et al. 1986):

$$\mathrm{BHR}(\cos\theta) = \mathrm{BHR}_0 \frac{(1+p)}{1+2p\cos\theta} \tag{2.8}$$

where BHR_0 is the broadband albedo for $\cos\theta = 0.5$ ($\theta = 60^o$) as given in their Table 2, and p is an empirical parameter.

Briegleb et al. (1986) measured various surfaces to determine the value of their empirical parameter p. They report $p = 0.4$ for arable land, grassland and desert, and $p = 0.1$ for all other types. According to these authors, ignoring the SZA dependence by using $\cos\theta = 0.5$ for all SZA, their model gives a 10 % variation of the TOA albedo from SZA of 0^o–60^o, compared to the observed ~30 % TOA albedo variation.

The directional reflectance properties of a target are defined by its spectral Bidirectional Reflectance Distribution Function (BRDF_λ) [sr^{-1}], which can not be directly measured (Schaepman-Strub et al. 2006). When directional reflectance properties of a surface are measured, the procedure usually follows the definition of a spectral reflectance factor BRF_λ [unitless], given by the ratio of the reflected radiant flux Φ_r [W] from the surface area to the reflected radiant flux from an ideal and diffuse surface Φ_r^{id} [W] of the same area, under identical geometry and single direction illumination (Schaepman-Strub et al. 2006):

$$\mathrm{BRF}_\lambda = \frac{\mathrm{d}\phi_r(\theta_i,\phi_i;\theta_r,\phi_r;\lambda)}{\mathrm{d}\phi_r^{id}(\theta_i,\phi_i;\lambda)} \tag{2.9}$$

where $(\theta_i,\phi_\mathrm{i})$ is the incident solar angle and $(\theta_r,\phi_\mathrm{r})$ the reflection angle (zenith, azimuth).

If the surface reflects the incident radiation isotropically, it is called a Lambertian reflector. For the ideal Lambertian surface there is no angular dependency. Both clean and dirty snow represent non-Lambertian surfaces (Peltoniemi et al. 2015). In remote sensing applications, the Lambertian assumption for snow needs to be corrected (Li et al. 2007). When an object has a sharp reflectance maximum in the backward direction, it is called a hot spot. Snow, in turn, is known as typically forward scattering (Peltoniemi et al. 2015).

The geometric manner in which the object reflects energy is also important. This factor is primarily a function of the surface roughness of the object. In specular reflectance the angle of reflection equals the angle of incidence. Rough surfaces can reflect uniformly in all directions and act as diffuse (Lambertian) reflectors. Polarized reflectance, in turn, has been considered to be generated by specular reflection at the surface of reflecting elements, such as leaves, or rocks and sand grains (e.g., Hansen and Hovenier 1974). At the top of the atmosphere, solar radiation is unpolarized, but specular reflection and atmospheric scattering generate polarized radiation.

For snow, the albedo is typically very high compared to other natural objects or surfaces. In the UV and VIS range, the albedo for clean snow is ~0.97–0.99 (Wiscombe and Warren 1980, Grenfell et al. 1994, Hudson et al. 2006). The most important factor to determine the snow albedo is the snow grain size (Wiscombe and Warren 1980, Warren and Wiscombe 1980, Mayer and Kylling 2005, Flanner et al. 2007, Gardner and Sharp 2010). Recent studies have also used the snow specific surface area (SSA) to determine the optical properties of the snow, where SSA is usually defined as the surface area per unit mass (Gallet et al. 2014).

According to the theory (Wiscombe and Warren 1980), snow albedo decreases as the grain size increases. A smaller effective radius increases the probability that an incident photon will scatter out of the snowpack (Gardner and Sharp 2010). Melting snow undergoes a metamorphism process that modifies the spectral albedo (Weller 1972). The liquid water content of snow increases, and wet snow has a lower albedo than dry snow (Blumthaler and Ambach, 1988). When snow ages, with or without melting, snow grain size increases and albedo lowers (Wiscombe and Warren 1980).

More recently, Räisänen et al. (2015) have investigated the single scattering (ω) properties of snow and developed new parametrizations for RT models. The single scattering albedo refers to the ratio of scattering efficiency to total extinction efficiency

$$\omega = \frac{\sigma s}{\sigma s + \sigma a} \tag{2.10}$$

where σs and σa are the scattering and absorption coefficient, respectively.

The single-scattering albedo is unitless, and a value of unity implies that all extinction is due to scattering (a single-scattering albedo of zero implies that all extinction is due to absorption). Räisänen et al. (2015) stated that in many radiative transfer applications single-scattering properties of snow have been based on the assumption of spherical grains due to the convenience of using Mie theory, although snow consists of non-spherical grains of various shapes and sizes. Räisänen et al. (2015) say that often the spectral

albedo of snow can be fitted by radiative transfer calculations under the assumption of spherical snow grains, when the effective snow grain size is considered an adjustable parameter (i.e. determined based on the albedo rather than microphysical measurements). In most (if not all) physically based albedo parameterizations that explicitly link the albedo to snow grain size, spherical snow grains are assumed. The new approach used angular scattering measurements of blowing snow to construct a reference phase function, i.e., the intensity of the scattered light as function of scattering angle, for snow.

The albedo of a glacier, lake or sea ice is influenced by the same factors as in case of snow, with the exception that instead of being governed by grain size, the frequency and location of scattering events (air-ice interfaces) are determined by the size and distribution of air bubbles, brine inclusions and cracks within the ice (Gardner and Sharp 2010).

2.3.2 Albedo of dirty snow

Snow containing light-absorbing impurities has a lower albedo than clean snow (Warren and Wiscombe 1980, Flanner et al. 2007, Gardner and Sharp 2010, Hadley and Kirchstetter 2012). Modeling of the dirty snow albedo is complicated by the fact that the light absorption by particles in the snow depends on the snow and impurity grain sizes and shapes.

Originally, Warren and Wiscombe (1980) stated that light-absorbing particles in snow offer an explanation for the discrepancy they found between the theory of snow albedo (Wiscombe and Warren 1980) and the observed albedo, and which could not be resolved on the basis of near-field scattering or nonsphericity effects. Warren and Wiscombe (1980) refer to the careful measurements in the Arctic and Antarctic that revealed a "grey absorber" (suggesting soot affecting these data rather than red color desert dust), whose imaginary part of the refractive index was nearly constant over the visible spectrum. The refractive index is a complex number of $m = n+i\,\kappa$, where the real part n is the refractive index and the imaginary part κ is the absorption.

Furthermore, small highly absorbing particles, present in concentrations of only 1 part per million by weight (ppmw) or less can lower the snow albedo in the visible by 5–15 % from the high values of pure snow (Warren and Wiscombe 1980).

Small amounts of strongly absorbent impurities like soot, dust and volcanic ash, lower the snow albedo in the spectral region where the absorption by ice is the weakest ($\lambda < 0.9$ μm) (Gardner and Sharp 2010). These authors further explain that at shorter wavelengths, photons generally experience more scattering events and travel a greater distance through snow, increasing the probability that the photon will encounter an absorbing impurity and not re-emerge from the snowpack. As the effective grain radius of snow increases, the average travel path lengthens, further increasing the probability of encountering an absorbing impurity. For wavelengths $\lambda > 0.9$ μm, the already strong absorption by ice leads to short travel paths, and the snow spectral albedo is negligibly influenced by the presence of impurities. Impurities located within ice grains (internal mixture) are 1.4 times more absorbing than impurities located in the air (externally mixed), but impurities concentrated near the surface have a greater impact on the albedo.

More recently, a new approach to isolate the effect of BC on snow albedo through laboratory experiments (to quantify the snow-albedo reduction associated with increasing amounts of BC and as a function of snow grain size) was developed in Hadley and Kirchstetter (2012). These authors also compared their experimental observations with the output of the Snow, Ice and Aerosol Radiation (SNICAR) model of Flanner et al. (2007), as a step towards verifying the predicted climate impacts of BC in snow. Snow was made in the laboratory with BC concentrations ranging from 0 to 1700 ppb. Their laboratory snow grains were spherical (equivalent to those of snowpacks simulated by models) and resembling naturally aged and rounded snow grains better than freshly fallen flakes. They examined different sizes of snow grains characterized by optical effective radii (R_{eff}) of 55, 65 and 110 μm.

Hadley and Kirchtetter (2012) measured decreasing snow albedo with increasing levels of BC contamination, where the radiative perturbation of BC was largest in VIS and became insignificant in NIR, confirming the fundamental assumption of a BC-induced snow-albedo reduction as hypothesized by Warren and Wiscombe (1980). The wide span in the simulated spectral albedo of BC-contaminated snow illustrated sensitivity to the mass absorption cross section (MAC) for BC. The MAC is a measure of how much sunlight BC particles can absorb, often expressed in units of m^2g^{-1} (AMAP 2015). The mass absorption cross-section MAC is the light absorption coefficient (σ_{abs}) divided by the density of the particle material multiplied with the volume of material in the particle (Adler et al. 2009):

$$\mathrm{MAC} = \frac{\sigma_{abs}}{\rho V} \tag{2.11}$$

The upper limit of their simulated spectral albedo corresponded to a BC MAC equal to 7.5 $m^2\ g^{-1}$ (at 550 nm), reasonable for freshly emitted BC. Their lower limit corresponded to snow contaminated with BC that is twice as absorbing (MAC = 15 $m^2\ g^{-1}$), and usable for atmospherically aged BC. Their results show that the albedo of both the pure and the BC-contaminated snow was lower when snow grains are larger. For example, an increase in R_{eff} from 55 to 110 μm causes a decrease of the pure-snow albedo by 0.05 (from 0.82 to 0.77), and an increase of solar absorption in snow by 28 %. Moreover, the radiative perturbation of BC in snow was amplified with increasing snow grain size (as predicted by Warren and Wiscombe 1980). Hadley and Kirchstetter (2012) conclude that their measurements supported the inclusion of a positive feedback in climate models to account for the increased solar energy absorbed by BC in ageing snow. They did not measure melt rate, but state their data to be consistent with an earlier study where enhanced snow-melt rate in BC-contaminated snow were measured.

3 Materials and methods

3.1 Radiometric measurements

Radiometric measurements of incoming and reflected solar radiation, measured with various kinds of passive instruments, are included here. Broadband (BB) radiometers measure an integrated value over a certain wavelength range, while multiband filter radiometers (MBFR) measure simultaneously several integrated wavelength ranges. Spectroradiometers, in turn, separate the radiation into small wavelength bands, with a typical resolution of 1 nm or less. Spectral measurements form the basis to which lower resolution measurements, as well as satellite and model data, can be validated and verified. Data of all these types of BB, MBFR, and spectral radiometers, at wavelengths of UV, VIS and NIR, for incoming and reflected EM radiation, were used for this thesis. It can be noted here that the operational meteorological local albedo is defined to be measured bihemispherically at a standard height of 1–2 m (WMO, 2008, I. 7).

Figure 3.1. Incoming and outgoing solar irradiance data measured by broadband (type SL-501 and CM-14), multifilterband (type NILU-UV) and spectral (type Bentham) radiometers were used in PAPER I–II.

3.1.1 Broadband UV and VIS albedo

The UV albedo measurements were the focus of PAPER I, while in PAPER II these observations were utilized together with the VIS broadband and spectral albedo data. The UV albedo data were obtained from the FMI operational albedo field in Sodankylä, FMI Arctic Research Center (FMI-ARC), to the north of the Arctic Circle. The measurements on the UV albedo of Arctic snow were started in 2007 under prof. Esko Kyrö's bipolar Arctic-Antarctic research project, with the help of FMI-ARC and the FMI Observation Unit (FMI-HAV). I put effort into initiating these measurements, which were included as part of the FMI International Polar Year (IPY 2007–2008) activities. Since 2007, the UV albedo measurements on the FMI operational albedo field have been maintained

continuous during snow time. The data are stored as 1-minute average values in the FMI Climate data base. These data have also been agreed to be included in the WMO GAW data base of the World Ozone and Ultraviolet Radiation Data Center (WOUDC), Canada.

Two UV sensors of SL501 (www.solarlight.com) with similar spectral and cosine responses (Fig. 1 in PAPER I) have been used, one facing upwards and the other downwards, at a height of 2 m from the ground. For the albedo measurements, a fixed device for the setting up and support of the two sensors, including independent leveling possibilities for the upward and downward SL501s, a blower to keep the sensors defrosted, and a data logger system, was planned and constructed at FMI-HAV.

The SL501 spectral response resembles the action spectrum for erythema, wavelengths in the UVB (280–310 nm) being most weighted (Seckmeyer et al. 2005). The erythemally weighted snow UV albedo, BHR_{ery}, is measured as the ratio of upwelling UV irradiance E_{ery} to the downwelling UV irradiance bihemispherically at 2π :

$$BHR_{ery} = \frac{Eery\uparrow}{Eery\downarrow} \tag{3.1}$$

where E_{ery} represents the bihemispherically measured temporal and spectral integral of the convolution of the solar irradiance and the erythemal response function.

The electrical signal (U) of the SL-501 sensor is related to the incoming erythemally weighted UV-B irradiance. The conversion of the raw signal into erythemal irradiance E_{ery} [W/m^2] requires a calibration factor with knowledge of the SZA and O_3 (as formulated by Webb et al. 2006):

$$E_{ery} = (U - U_{offset})\, C\, f_n(\theta, TO_3) * \varepsilon(T) * Coscor(\theta) \tag{3.2}$$

where E_{ery} is erythemal effective irradiance, U is the measured electrical signal from the radiometer, U_{offset} is the electrical offset for dark conditions, C is the calibration coefficient (a constant value determined for specific conditions like $\theta = 40^o$ and $O_3 = 300$ DU), f_n is a function of a calibration matrix normalized at solar zenith angle $\theta = 40^o$ and $O_3 = 300$ DU, $\varepsilon(T)$ is the temperature correction function, Coscor is the cosine correction function.

In practice, the temperature of the sensor is regulated (not corrected), and the calibration is made using a fixed calibration coefficient provided by the Finnish Radiation Safety Authority (STUK). The calibration procedure includes various SZA and O_3 values, but one optimized calibration coefficient value from these is calculated for each sensor. Because of the fixed sensor specific calibration coefficient value (one number per one sensor, valid for the time period following after the calibration until the next calibration), extra consideration has to be paid on the scientific usability of these data.

In our case, the sensors for upward and downward measurements are selected to represent as similar cosine and spectral responses as possible, and the sensor with the better response is used to measure the smaller signal of outgoing reflected radiation. The effect of cosine error is smaller for the upwelling reflected radiation due to the missing

direct component. Therefore under clear sky and high SZA the surface albedo derived from SL501 may be an overestimation of the real surface albedo. Uncertainties and errors decrease with increasing diffuse radiation under the full cloudiness or lower sun.

In PAPER I, an empirical calibration to the data is made, by calibrating one SL501 sensor with another one. Three SL501 were used for this purpose. The irradiance measured by the albedo sensors and one independent SL501 on the roof of the observatory were compared. Due to the SZA dependent uncertainty remaining in the data calibrated this way, the data is also divided into subsets, representative of certain SZA only.

In addition to SL501 UV sensors, field pyranometer broadband surface albedo data from the SNORTEX field campaign were included in PAPER II (Fig. 6 in PAPER II). The sensor is a Kipp & Zonen CM-14 albedometer (www.kippzonen.com) measuring at one non-weighted broadband from 310 to 2800 nm, and whose relative accuracy was estimated at 5–10 %. The general technical data of the CM-11 pyranometer applies to the CM-14 albedometer, and the relative spectral transmittance is largest (> 0.5) at 400–900 nm. The CM-14 instrument was carefully leveled on a tripod and operated without breaks during the field day. The instrument was mounted at a height of 1.5 m, implying an observed area with a radius of 15 m. During postprocessing (post-processed data provided by the co-author AR), the data were corrected for the shadowing effect of the tripod legs and imperfections in cosine response at high solar zenith angle conditions. These pyranometer data were used as an independent data set to give evidence for the measured low surface albedo values.

3.1.2 Multiband measurements on the snow surface albedo

A multichannel radiometer of type NILU-UV (www.nilu.no) was used for PAPER I to provide an independent ancillary data set. Multichannel instruments are like several wide spectral channel broadband instruments within one. The calculation of UV and VIS (or PAR channel) irradiance from the MBFR instruments may be affected, e.g., by SZA, variable ozone and cloudiness, and the fact that UV and VIS/PAR are not measured spectrally. There are at least three MBFR instruments that have been commonly used: type NILU-UV, type GUV (www.biospherical.com, applied in the US National Science Foundation (NSF) UV Radiation Monitoring Network), and type UVMFR (www.yesinc.com). Here one NILU-UV was installed looking downwards in the FMI operational surface albedo field (same place as for the SL501 albedo sensors) of the Sodankylä Arctic Research Center. Another NILU-UV was facing upwards at 30 m distance on the roof of the FMI Sodankylä Observatory.

The UV surface albedo can be calculated as a ratio of downwelling irradiance to upwelling radiation. The NILU-UV has a teflon diffuser, and the incoming radiation is passed through filters for band selection and is received by 5 or 6 silicon detectors placed side by side underneath the diffuser. The total (diffuse and direct) incoming UV irradiance is measured in five channels with center wavelengths at 305 nm, 312 nm, 320 nm, 340 nm, and 380 nm. Each channel bandwidth is about 10 nm. The sixth channel covers the photosynthetically active radiation (PAR, 400–700 nm). A portable lamp unit for relative calibration can be used to check the relative stability. The erythemal irradiance E_{ery} is

calculated using a linear combination of the five channels of the instrument, and utilizing the absolute calibration coefficients (provided by the NILU Corp.):

$$E_{ery} = a(v1) + b(v2) + c(v3) + d(v4) + e(v5) \quad (3.3)$$

where a,b,c,d and e are the absolute calibration coefficients for the raw voltage signal (vi) of each of the five channels of the instrument.

3.1.3 Spectral snow surface albedo

In addition to the SL-501 UV, pyranometer, and multiband-filterradiometer (MBFR) NILU-UV data, Bentham spectrometer data were used for investigating the snow surface albedo in PAPER II. Guidelines for the spectral instruments are found in the WMO GAW report No. 125 and 212 (WMO 2001 and 2014). In practice, the measured specral irradiance $E_M(\lambda)$ varies from the "true" spectral irradiance $E(\lambda)$ due to various errors which may be related with the instrumental characteristics, like the calibration procedures, or the operational procedures.

Due to its big size and weight Bemtham suits best for measuring the surface albedo in one location, as done here. Instrumentation for spectral surface albedo measurement has been improved recently, and good-quality portable field spectrometers with large spectral ranges (300–2500 nm) are available. Here, the Bentham spectrometer was operated by an experienced Bentham specialist (the co-author SK), who provided the corrected data used in PAPER II.

3.2 Snow analysis and measurements

3.2.1 BC/OC in snow

Results of the analysis of BC/OC in snow in Sodankylä are utilized in PAPER II and PAPER III. Snow surface (appr. first 2 cm of snow) samples have been collected during snow covered season from the same location, protected with reindeer fences, in the Sodankylä Arctic Research Center for impurity analysis on a weekly basis since 2009. The sampling has been made by a FMI-ARC technician. Snow BC/OC samples have first been collected and filtered, and then the filters have been sent for analysis to University of Stockholm, Sweden (Prof. Johan Ström). These BC/OC results had not been investigated or published until PAPER II, where BC/OC data of 2009–2011 are utilisized to understand the measured and modeled snow surface albedo. BC results were also used in PAPER II for the long-range transport analysis to study the origin of the BC in snow. For PAPER III, all FMI snow BC/OC analysis data available with simultaneous snow density data were utilized. These consisted mainly of campaign data.

The sampling and analysis for BC/OC in snow follow the general methodology developed by Forsstrom et al. (2009) and Aamaas et al. (2011). Surface snow is collected in a container, then carefully melted in a microwave oven (avoiding evaporation and increased impurity concentration), and filtered through sterilized micro-quartz filters (55 mm diameter) using a pump attached to the filtering system to create a vacuum during filtering. The volume of meltwater is needed for concentration conversions. Dried filters are analyzed with a Thermal/Optical Carbon Aerosol Analyzer (OC/EC) (Sunset Laboratory Inc., Forest Grove, USA) for their elemental carbon (EC) and organic carbon (OC) concentration, following the NIOSH 5040 protocol developed by Birch (2003). The EC is used as a proxy of BC. The thermal–optical method was created by Birch and Cary (1996), where a detailed description of the method is presented. In practice, a piece of the filter (1 cm^2) is punched for the analysis. The thermal-optical carbon aerosol analyzer first heats the filter piece in a helium atmosphere, and organic carbon released from the filter is detected. Then, the filter is heated in an oxygen atmosphere, and EC is released and detected.

For PAPER III, I collected and filtered snow samples within SNORTEX-2010 experiments, using the methods of Prof. Steven Warren (Doherty et al. 2010). Samples were collected to allow a later method comparison between the spectrometer and the Single Particle Soot Photometer (SP2) analysis methods. These filters were sent for analysis to the University of Washington, USA, and analysed by Dr. Sarah Doherty using a spectrometer method, and the duplex samples were stored in a freezer to wait for the SP2 method development.

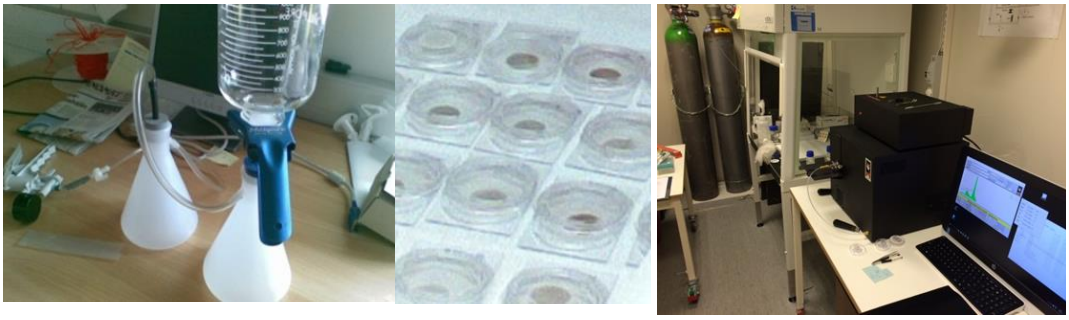

Figure 3.2. Snow EC/OC analysis data are used for PAPER II–III. The collected snow samples are first filtered, then the filters are analyzed using the NIOSH thermo-optical method. The photo on the right shows the EC/OC analyzer currently at FMI. Photos O. Meinander.

3.2.2 Snow density

For PAPER III, snow densities (weight per volume) were measured manually, for either the whole snowpack vertical column (snow tube and balance for SR and SNORTEX experiments), or for separate horizontal snow layers (density cutter and a balance for the SoS experiment to measure the density of the visually dirty surface snow). Combined data

of snow density and BC were collected from all existing Sodankylä campaigns for PAPER III. The hypothesis of snow density effects of impurities existed before any data. After the first promising results were obtained, all possible combined FMI data of density and BC were collected together. The uncertainties related to the BC and density measurements are considered in PAPER III.

3.2.3 Snow fork for snow liquid water content

PAPER II uses the measurements of snow liquid content with the commercially available Snow Fork by Toikka Oy (www.toikkaoy.com). The sensor is a steel fork that is used as a microwave resonator. The Snow Fork measures the electrical parameters of resonant frequency, attenuation, and 3 dB bandwidth. The liquid water content is calculated from these measurements. In addition to the actual snow liquid water content, the snow impurities and grain sizes, hardness and density, etc., may affect the measurement results. As the calculation is based on semi-empirical equations of natural clean snow, the calculation is expected to contain more uncertainties in case of dirty snow.

3.2.4 Meteorological Automatic Weather Station data

The Sodankylä automatic weather station (AWS) measures the state of the atmosphere at a height of 2 m once a minute. From these data, information on, e.g., air temperature, the onset of precipitation, snow depth and cloud cover, can be obtained. The Sodankylä Arctic Research Center measurement program includes a large variety of environmental parameters. Here use was made of the daily minimum and maximum air temperatures and snow depth for PAPER I. In PAPER II, the measured aerosol parameters and total ozone as input values for the RT calculations, and the beginning and amount of rain for SILAM transport model calculations.

3.2.5 Snow grain size and other snow properties

In PAPER I–II, snow grain size is visually estimated using a plate with two grid sizes of 1 mm and 2 mm (Fig. 4 in PAPER I). Snow grain size data were utilized for the surface albedo data analysis in PAPER I. The snow grain size and shape data (provided by the co-author AK) was based on Fierz et al. (2009) for seasonal snow on the ground.

A simple “Snow ball test” is used for PAPER II. The test is in regular use in all Sodankylä snow research. This practical test tells if the properties of snow are such that one succeeds in making a snowball out of the snow on the ground. Snowballs can only be made when snow properties are suitable for making them, i.e., when snow contains water but is not too wet. With the test, for instance the start of snowmelt can be easily detected, as corresponding snow property information would be hard to determine otherwise.

Additional ancillary data of snow grain shape, snow layer thicknesses, and snow temperature are available for PAPER I–II as part of the SNORTEX. Although some of the

data allow investigation of the properties of the snowpack, the focus of the original papers and the thesis summary is on surface snow (not on snowpack properties).

3.2.6 BC and volcanic particles used in the experiments

For the Soot on Snow (SoS) experiment at Sodankylä (PAPER III), BC (soot) and Icelandic volcanic ash and silt particles (Fig. 3.3) were collected. Soot originated from chimneys of residential wood-burning fireplaces, except for one experimental spot with soot from a chimney of an oil burner, and another one with soot from a peat-burning power plant. Volcanic sand in PAPER III was collected from Myrdalssandur, Iceland. The sand was a dark mixture of the volcanic ash of glaciofluvial nature, originating from under the Myrdalsjokull glacier, which may be mixed with the ash of the Eyjafjallajokull eruption in 2010 and the Grimsvotn eruption in 2011. The glaciogenic silt was collected close to the Myrdalssandur and it was lighter in colour than sand, from light-brown to slightly yellowish colour consisting mainly of silt and some coarse clay sized particles, which could be deposited on the local glaciers as well as transported over several hundreds of kilometers towards Europe. These particles were collected from ground as such and were not sieved nor cleaned before the experimental utilization.

For PAPER IV, different Icelandic ash and dust particles were utilized. Icelandic volcanic ash was collected on Eyjafjällajökull just after the eruption ended in late May 2010 (Fig. 1 of PAPER IV). The ash particles were sieved and the grains with sizes 1 ϕ (500 μm) and 3.5 ϕ (90 μm) were used in the experiments in FMI Kumpula. In addition, both particle types were investigated by Scanning Electron Microcopy SEM analysis for their shape, size and surface features. The bulk density for 1 ϕ ash was 2.7 g/cm^3 and for 3.5 ϕ it was 2.5 g/cm^3. The Krumbein phi (ϕ) scale for particle size is defined as:

$$\phi = -log_2 D/D_0 \tag{3.4}$$

where D is the diameter of the particle, D_0 is a reference diameter (equal to 1 mm to make the equation dimensionally consistent).

Icelandic dust samples were collected by collecting snow samples at 16 locations on the surface of Vatnajökull in October 2013. The samples represent dust that was deposited on the glacier surface during one summer. The top 8 cm of the snow surface (about 1–2 kg of snow) was collected from an area of appr. 57 x 10^{-3} m^2. The samples were then melted, evaporated and the mass of the dust was weighted. This information was then used to link the experimental results of PAPER IV to natural conditions in Iceland.

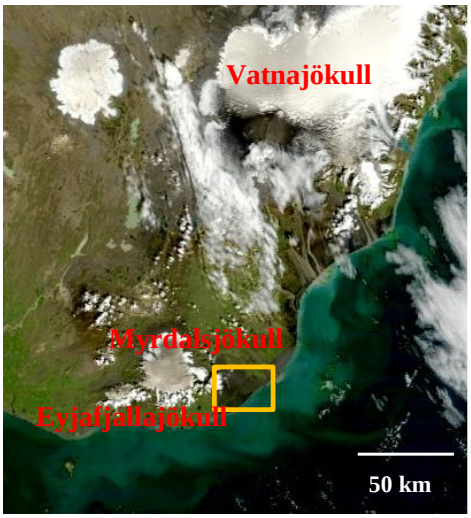

Figure 3.3. The Terra/MODIS satellite image (downloaded from NASA LAADS Web) of Iceland shows the origin of the collected volcanic material from Myrdalsjökull glacier (the yellow rectangle on the southern coast). The origin of volcanic ash mixed with the particles was from volcanoes of the Eyjafjallajökull (west from Myrdalsjökull) and Grimsvötn (under Vatnajökull glacier on the eastern coast). Icelandic dust–cryosphere interaction is a topic included in PAPER III–V. Image courtesy of NASA Level-1 and Atmosphere Archive & Distribution System (LAADS) Distributed Active Archive Center (DAAC), Goddard Space Flight Center, Greenbelt, MD.

3.3 Experiments

Experiments were an essential part of the work included in the original publications of this thesis. Two large-scale experiments were arranged in Sodankylä (67°22’N, 26°39’E, 179 m a.s.l.), Finnish Meteorological - Arctic Research Center (FMI-ARC), which is part of the Pallas/Sodankylä Global Atmospheric Watch (GAW) station of the World Meteorological Organization (WMO). PAPER II is based on results gained during the SNORTEX experiment in Sodankylä (section 3.3.1). Paper IV uses Sodankylä results from SoS experiments (section 3.3.2), as well as from the SnowRadiance (SR), an ESA-funded project aiming at determining snow properties from optical satellite measurements. PAPER IV is based on results gained during indoor and outdoor experiments (section 3.3.3) carried out at FMI HQ at Kumpula Campus, Helsinki, close to the SMEAR III station (Järvi et al. 2009), i.e., Station for Measuring Ecosystem-Atmosphere relations.

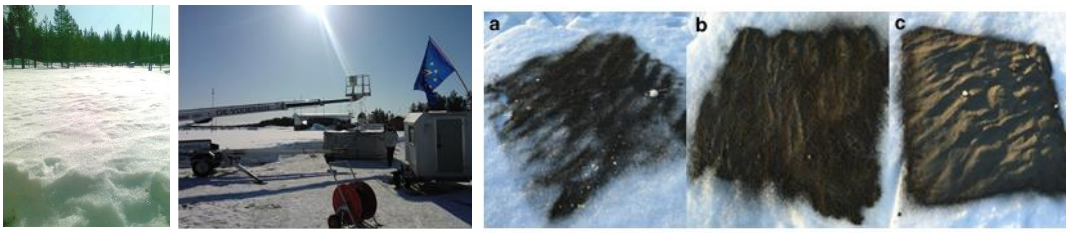

Figure 3.4. The outdoor and indoor experiments were an essential part for PAPER I–IV. SNORTEX (left) and Soot on Snow (middle) Experiments in the Sodankylä Arctic Research Center (67°22’N, 26°39’E, 179 m a.s.l.), North of the Arctic Circle (Photos O.Meinander). Icelandic ash and dust (right; a,b,c) on snow at Kumpula, closeby the SMEAR III station (60°12'N, 24°58'E), picture from **PAPER IV**. © Author(s) 2016, published with open access at Springerlink.com.

3.3.1 SNORTEX

PAPER II is an outcome of the Finnish-French “Snow Reflectance Transition Experiment” (SNORTEX, 2008–2010). SNORTEX aimed at acquiring in situ measurements of snow and forest properties in support of the development of modeling tools, and validating coarse resolution satellite products (Manninen and Roujean 2014). The SNORTEX study area was located in Finnish Lapland beyond the Arctic Circle, and benefitted from existing facilities provided by FMI-ARC. SNORTEX sites consisted of: (1) The Arctic Center at Sodankylä; with temporal daily data series of various parameters collected within SNORTEX, as well as operationally by FMI. (2) SNORTEX experiment sites in the Sodankyla region, representing different types of environment, e.g., open area, forested area, and snow on the lake.

3.3.2 Soot on Snow

PAPER III is based on The Soot on the Snow (SoS-2013) experiment. SoS-2013 was carried out in Sodankylä to study the effects of deposition of BC, Icelandic volcanic sand and glaciogenic silt on the surface albedo, snow properties and melt of the seasonal snow. The experimental area was a large, flat, fenced open space of Sodankylä airport (not in active use), and the gravel ground was not covered with concrete or asphalt. Different amounts of impurities were deposited to snow on different spots with the help of a blower and a tent. Each spot had a diameter of 4 m. Thereafter the spots were monitored until the snow had completely melted. The sites were left to develop naturally, introducing as little disturbance as possible. In addition to PAPER III, the experiment is described in Peltoniemi et al. (2015) and Svensson et al. (2016) (where I am a co-author).

3.3.3 Icelandic dust

For PAPER IV, four outdoor and laboratory experiments were carried out using three setups of: 1. snow (AoS-2015); 2. ice (AoI-2015, Roof 2015); and 3. snow over ice (AiC-2015). Ash of 1 ϕ grain size was used for the AoS-2015, AoI-2015 and AiC-2015 experiments, whereas ash of 1 and 3.5 ϕ was used for the Roof 2015 experiment. Layer thicknesses were measured in dry condition of the ash.

The Ash on Snow (AoS-2015) experiment was an outdoor experiment on the effect of ash on snow in natural conditions in an urban area in Kumpula Campus area closeby the SMEAR III station, in Helsinki. The experiments started on 6 February 2015 using natural snow in a fenced area, i.e., unperturbed by direct human interference. Three different amounts of ash (15 g (166 g m^{-2}); 85 g (944 g m^{-2}); and 425 g (4722 g m^{-2}, 15 mm layer thickness)) with grain size 1 ϕ, were deposited on an area of 0.3×0.3 m^2 on a snow surface. Snow density was 280 kgm^{-3}. Snow depth and temperature were then monitored for 17 days when the snow melted naturally.

A controlled experiment with ash on ice was made both indoors (AoI-2015) and outdoors (Roof-2015), to identify and separate the effects of temperature and solar irradiance. Ash on Ice (AoI-2015) were laboratory experiments to examine the effect of ash layer thickness on ice melting, in a temperature-stabilized environment kept at +24°C. For these experiments, small, transparent plastic boxes were filled with 200 ml of tap water and frozen (surface area 84 cm^2). This resulted in an ice layer with a depth of 25–28 mm. To find the insulating threshold of ash on ice, four different amounts of the 1 ϕ impurity were deposited (3 g (1.3 ml, 366 g m^{-2}), 35 g (15 ml, 4219 g m^{-2}, 1 mm layer thickness), 71 g (30 ml, 8437 g m^{-2}, 3 mm layer thickness) and 283 g (120 ml, 33,749 g m^{-2}, 9–13-mm layer thickness)). After deposition of material, the ice was transferred into white pots with holes in the bottom to measure the meltwater runoff.

The laboratory experiments were repeated outside on the roof of the FMI building in sunny conditions to study effects of solar irradiance in addition to that of temperature above zero. The experiment was repeated with the same volume of impurities, but using two different grain sizes of the Eyjafjallajökull 2010 ash: 1 ϕ (samples A) and 3.5 ϕ (samples B). The concentrations for the 3.5 ϕ B-samples were: 2.46 g (1 ml, 292g m^{-2}); 36.8 g (15 ml, 4385 g m^{-2}, 1 mm layer thickness), 73.7 g (30 ml, 3–5-mm layer thickness, 8772 g m^{-2}) and 294.7 g (120 ml, 35,086 g m^{-2}, 9–13-mm layer thickness). The concentrations for the 1 ϕ ash were the same as used in AoI-2015.

The Ash in Container (AiC) experiment was performed in a cold container of the University of Helsinki snow laboratory, where ash was deposited on snow over ice. The purpose was to investigate how ash insulates and prevents snow melt compared to the outdoor results. The AiC setup was closer to the conditions on the glacier surface, than the ash on snow setup. A big pot, inside a cold container, was filled at the bottom with a thick ice layer and on top of that an 8.5 cm thick layer of snow was added. Two different amounts of impurities were used (the same as in the outdoor experiments): 15 g (166 g m^{-2}) and 425 g (4722 g m^{-2}, 15 mm thickness) of 1 ϕ Eyjafjallajökull ash on a 0.3×0.3 m^2 area. The experiment started at a temperature of −10°C inside the container; then, the cooling system was shut down, and the laboratory adapted to outdoor temperatures up to +4°C. Snow depth and behavior of the ash were monitored.

3.4 Modeling

For the thesis, results from three different types of models were utilized. These include the RT modeling (section 3.4.1), snow surface albedo modeling (section 3.4.2), and long-range transport modeling (section 3.4.3). The RT modeling was needed to show how big error the observed SZA surface albedo asymmetry would cause on the satellite based detection of the surface albedo when the SZA asymmetry is not corrected. The surface albedo modeling was used to investigate if and how the measured surface albedo values could be simulated. Snowpack or snow melt modeling were out of the scope of the current work. Transport modeling results were needed to investigate what could be the source for the unexpectedly high BC concentrations measured in Sodankylä seasonal surface snow.

3.4.1 RT modeling

The RT model LibRadtran (Mayer and Kylling 2005) was utilized for irradiance estimates in PAPER II. For the physical modeling of the solar irradiance, there are several RT models available. These include the Library for radiative transfer LibRadtran (www.libradtran.org); FastRT (http://nadir.nilu.no/~olaeng/fastrt/fastrt.html with a simpler version in http://nadir.nilu.no/~olaeng/fastrt/fastrt-ez.html); the Tropospheric Ultraviolet and Visible (TUV) Radiation Model of the National Center for Atmospheric Research (NCAR, USA); the Santa Barbara DISORT Atmospheric Radiative Transfer (SBDART, http://www.crseo.ucsb.edu/esrg/pauls_dir/); and the SMARTS2 (e.g., http://www.fsec.ucf.edu/en/publications/pdf/FSEC-PF-270-95.pdf). In the model, a radiative transfer equation solver is needed. There are different solvers available, including 1-D and 3-D solvers. Several input parameters are required for the model inputs. These are, e.g., the Extraterrestrial Source Spectra (for which several models exist, rredc.nrel.gov), and standard atmosphere model (providing with vertical profiles of pressure, temperature, water vapor and ozone density and other gases for various climatic conditions like tropical, midlatitude summer, midlatitude winter, subarctic summer, or subarctic winter). Inputs also include a cloud model (the computation of radiative transfer within a cloudy atmosphere requires knowledge of the scattering efficiency, the single scattering albedo, which is the probability that a extinction event scatters rather than absorbs a photon, and the asymmetry factor, which indicates the strength of forward scattering), as well as aerosol models (e.g., the aerosol model by Shettle 1989) and surface models to parameterize the spectral reflectivity of various surface types like ocean water, lake water, vegetation, snow and sand; the spectral reflectivity of a large variety of surface conditions can be approximated by combinations of these basic types.

An action spectrum describes the relative effectiveness of energy at different wavelengths in producing a particular biological response. The response may refer to effects, e.g., at a molecular level (e.g., DNA damage), or at a whole organism level (plant growth). There are several UV action spectra: the erythemal action spectrum given by McKinlay and Diffey (1987), and the DNA damage action spectrum of Setlow (1974), to name a few. By multiplying the erythemal irradiance [W/m^2] by 40, UV-Index scale is gained. Often there is decline in relative response as the wavelength increases indicating

the importance of the UV-B. These responses could be more sensitive to ozone depletion, as especially UV-B irradiance increases with lower ozone levels. With a strong UV-A dependence, the ozone depletion would not have as great an impact. Radiation amplification factors (RAF) give the increase of biologically effective irradiance in response to ozone depletion. Biological weighting functions which are heavily weighted in the UV-B region (e.g., DNA) have RAF > 1, and biological weighting functions weighted outside the UV-B region, like UV-A spectral region, have RAF < 1.

3.4.2 Snow albedo modeling

In PAPER III, the Snow, Ice, and Aerosol Radiation (SNICAR) on-line version (Flanner et al. 2007) was used to obtain simulated data on the snow albedo to compare with the in situ surface albedo data. The measured parameter values of snow depth, snow grain size and elemental carbon (BC) content were used as input values to simulate a clear sky case (day 22 April) and a diffuse sky case (24 April). In SNICAR-online, there are two types of black carbon input parameters: (1) uncoated (mimicking hydrophobic particles), with properties tuned to achieve a mass absorption cross-section of 7.5 m^2g^{-1} at 550 nm (Bond and Bergstrom 2006); and (2) sulfate-coated black carbon (mimicking hydrophilic black carbon), which is composed of a weakly-absorbing shell (sulfate) surrounding BC, resulting in an absorption enhancement (per unit mass of black carbon) of about 1.5 (Bond et al. 2006). Most of the BC in the snow at Sodankylä can be assumed to originate from long-range transport, and therefore the BC in snow can be assumed to become hydrophilic. Yet, with the current snow analysis data we cannot determine that all BC would be hydrophilic. Therefore, in the simulated data, I used both these options separately to compare their effect on the surface albedo. For melting seasonal snow in northern Finland, the averaged snow density values of 329 kg m^{-3} for forest, and 349 kg m^{-3} for open sites, have been reported (Kuusisto 1984). From these the value reported for northern Finland was used. The snow BC concentration can be assumed to be approx. double the EC concentration determined by the thermos-optical method (Chow et al. 2001, Aamaas et al. 2011). The parameter value of the mass absorption coefficient MAC was tuned to produce surface albedo values close to the lowest measured surface albedo of 0.4–0.5 at UV.

3.4.3 Long-range transport modeling

The origin of the detected BC in Sodankylä surface snow samples was investigated in PAPER III by means of transport modeling. The two most commonly applied models to consider were NOAA's HYSPLIT model (REF, http://ready.arl.noaa.gov/HYSPLIT.php) and FMI's SILAM model (Sofiev et al. 2008 and http://silam.fmi.fi). SILAM was tested and found applicable for the purpose. SILAM model calculations were provided by SILAM specialists Dr. RK and MS, co-authors of PAPER III.

For the application of PAPER II, a simple method ("algorithm") was developed to study the origin of BC in snow samples using SILAM transport model calculations (Figure

3.5). First, the measured BC in snow concentrations were divided into two groups of "clean" and "dirty" cases by the day and BC contents. Snow was considered clean if it contained < 20 ppb BC, based on results by Doherty et al. (2010), and dirty if > 30 ppb. Only cases where there was snowfall before 24 h or less prior to the snow sampling were included. The modeling was then performed with SILAM (System for Integrated modeLing of Atmospheric coMposition) version v5.2. The meteorological fields from short-term operational forecasts of the European Centre for Medium-range Weather forecasts (ECMWF) were used as a driver for SILAM. The adjoint simulations were performed with resolution 0.5 × 0.25 degree on a domain 10–60 °E, 55–75 °N with 8 vertical layers of thickness from 30 m at surface to 2000 m, within a height range from surface to 6 km. The footprints were taken for the layer 150–300 m, which were expected to correspond to the height of industrial emissions due to combustion. The observational function of atmospheric concentrations corresponding to measured in-snow concentrations was taken to be uniform with height from the surface to the bottom of a cloud and weighted by snowfall intensity in time, so total sensitivity is unity. The footprints were calculated for each sample separately.

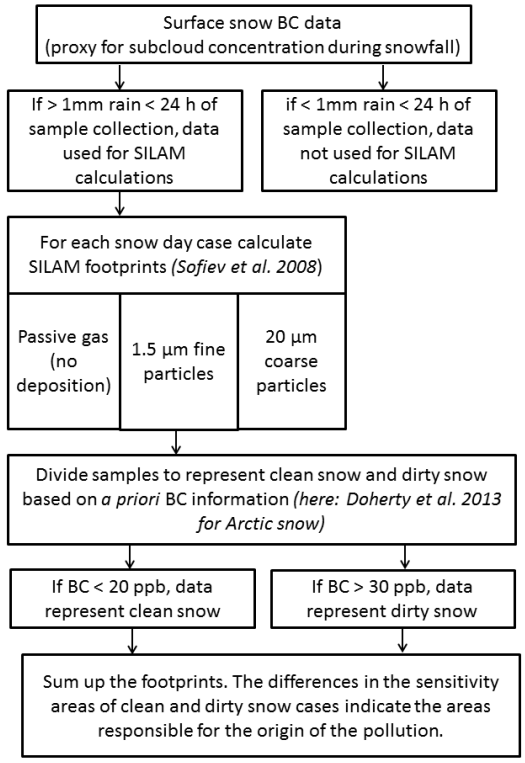

Figure 3.5. An illustration of the algorithm used to investigate the origin of the BC content in surface snow, based on text presented in **PAPER II**.

To minimize the effect of dry deposition and to ensure the consistency between observed and modeled snowfalls, only the cases were selected when snowfall was reported by both the weather station at Sodankylä and the meteorological driver, reporting more than 1 mm snowfall within 24 h before the sample collection and the amount of the precipitation agreeing within a factor of 2 between them. The volumetric content of black carbon was used as a tracer of anthropogenic pollution. With the above criteria, out of 70 snow samples we selected 10 “clean” (< 20 ppb of BC) and 12 “dirty” (> 30 ppb of BC) samples and calculated the average footprint for both classes. Since the size of airborne black carbon is unknown, the footprints were calculated for passive gas with no deposition, for 1.5 μm (fine) particles and for 20 μm (coarse) particles.

4 Overview of results and discussion

4.1 Albedo of seasonally melting snow, north of the Arctic Circle

The role of snow albedo-feedback mechanisms in snow melt is often cited as the main contributor to the Arctic climate change amplification. In Finland, Arctic snow melt related studies on the naturally layered snow have the advantage of seasonal snow melt, despite the northern location. PAPER I investigates the Arctic snow albedo and seasonal snow melt in Sodankylä utilizing both meteorological and cryospheric parameters, such as snow depth, snow grain size, and air temperature. PAPER II proceeds further and utilizes also data on light-absorbing impurities deposited in snow.

In PAPER I, a SZA-dependency (U-shape), as described in Briegleb et al. (1985), in the surface albedo data is evident (Fig. 4.1). It is explained to be possibly partly due to changed spectral response of the sensors. On the basis of the post-calibration measurements, it was calculated that for SZA of 56–60 degrees, the sensor SZA dependency (the U-shape due to difference in the spectral responses of the sensors), caused an error of less than 3 %. PAPER I states that the U-shape might be partly due to the different radiation components the upward and downward radiometers detect; for the downward looking sensor the diffuse and specular reflectance, while for the upward sensor the direct and diffuse radiation. The surface albedo data in PAPER I are then grouped according to cloudiness, as well as according to the status of accumulating or melting snow. For clear sky and fully cloudy days, a diurnal variability in the snow UVB surface albedo is found, possibly indicating changes in the physical properties of snow. PAPER I explains that if this diurnal variation in the surface albedo is due to any shadowing effects, rather than changes in the snow properties, shadowing would be best seen under clear sky conditions, and not in cloudy situations. Since this is not the case, an explanation is searched from changes in snow properties, especially snow grain melt metamorphism (change in snow grain shape and structure), and changes in the liquid water content of the snow. In addition to the U-shape and temporary diurnal variability in the surface albedo, a possible SZA asymmetry in the surface albedo is suggested in some of the data. SZA asymmetry is not studied further in PAPER I, but has been a subject included in PAPER II.

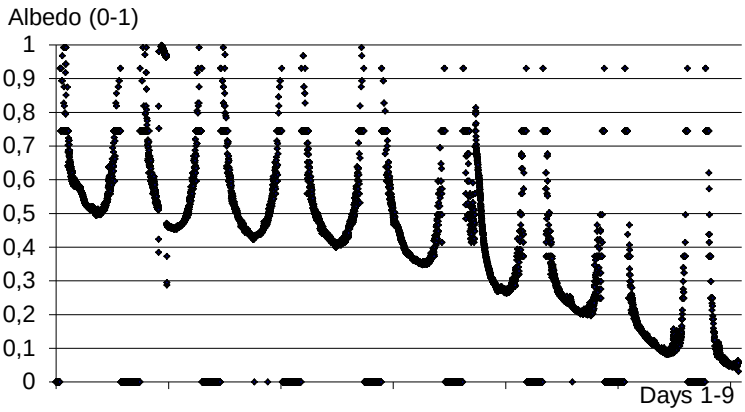

Figure 4.1. The albedo of melting snow shows the diurnal SZA dependency (U-shape, as described in Briegleb et al. 1985), and the temporal decrease in the midday albedo value. The U shape of the albedo is explained to be partly due to differences in spectral responses of the sensors, and partly due to the different radiation components the upward and downward radiometers detect: downward looking sensor detects the diffuse and specular components, while the upward sensor detects the direct and diffuser. The SL501 BRF_{ery} data are for 1-9 May (days 121-129) for SZA > 85^{o}. Redrawn based on Figure 10 of **PAPER I**.

For snow melt, the empirical results of PAPER I from Sodankylä indicate that the change of daily maximum air temperatures from below zero to above zero degrees Celsius is not enough to start the snow melt (on the basis of AWS snow height data). This is explained to indicate the importance of solar irradiance as the starting force for the snow melt. Monotonical snow height decline starts in these data one month later (day 102) than the change of maximum temperature to be above zero degrees Celsius (day 66). It can be noted here that the albedo is possible to decline with and without snow melt as a result of snow metamorphosis and evaporation.

The snow grain size is the key snow property which determines the snow albedo. Yet it is a parameter whose values are among the hardest to obtain. Snow height measurement, on the other hand, are most often available. PAPER I studies whether it is possible to express the grain size in a simple way, with the help of other environmental parameters For the case of seasonally melting snow in Sodankylä, a linear relationship is found for snow grain size as a function of the day of the year, daily maximum air temperature at a height of 2 m, and the height of the snowpack (Eq. 3 of PAPER I).

PAPER II finds diurnal asymmetry in the snow albedo (Fig. 3 and Fig. 6 in PAPER II). This means that instead of the U-shape reported in PAPER I, the albedo signal of intensively melting snow has a feature of a declining line. During each day the albedo decreases on average by 10 %. The albedo is higher in the morning than in the afternoon, i.e., the albedo is asymmetric to SZA. The measurements are made towards the Sun on a relatively flat snow surface, where the forward scattering nature of snow is detected. The diurnally declining albedo has been previously reported in Pirazzini (2004) and Wuttke et al. (2006) using broadband data. The diurnal SZA asymmetry in surface means that the

albedo decline dominates over the SZA-dependent albedo signal. The main driver of the measured albedo is therefore the intensively melting snow. The spectral change in the measured data was greater the shorter the wavelength. This is consistent with the theoretical results of Warren and Wiscombe (1980), which show that the absorption due to impurities in snow increases with the decreasing wavelength.

4.2 Effects of BC/OC on snow albedo, melt and density

Snow containing light-absorbing impurities has a lower albedo than clean snow, and this can affect snow melt via the albedo-feedback mechanism. In PAPER II–V, the snow albedo, melt and density are investigated and discussed in connection to light-absorbing impurities in snow, and BC/OC is included in PAPER II–III.

In PAPER II, the BC contents (Figure 4.2) of the surface snow layer at the Sodankylä Arctic Research Center, Finland, are found to be higher than expected based on literature, and also to increase in spring time (Table 3 of PAPER II). This increase in spring is suggested to be due to accumulation of hydrophobic BC in the surface snow during snow melt, although some of the high BC concentrations are anthropogenic soot from the Kola Peninsula, Russia (more in section 4.4). The origin of OC can be anthropogenic or natural. PAPER II says that at the time of publishing the paper in 2013, the scientific understanding of the snow organic carbon absorption has only started to develop recently. The Sodankylä results from years 2009–2011 suggest some increase of OC in snow toward the late spring (many days with > 2000 ppb in April).

The albedo of natural seasonal snow surface measured in Sodankylä, is found ~0.5–0.7 which is lower than the expected values of ~ 0.97–0.99 for clean snow (Grenfell et al. 1994, Hudson et al. 2006). In PAPER II, the solar UV and VIS albedo values in the range of 0.6–0.8 in the accumulation period, and from 0.5 to 0.7 during melting, are reported. Three independent data sets are used to confirm these observations. The low albedo values are explained to be due to large snow grain sizes of up to ~3 mm in diameter, and meltwater surrounding the grains and increasing the effective grain size, and absorption caused by impurities in snow (87 ppb BC and 2894 ppb OC). This case is further studied with the help of the SNICAR model (Section 4.4).

In addition to the snow-albedo feedback mechanism, a new hypothesis on the snow density effects is suggested in PAPER III. The paper hypothesizes that BC may decrease the liquid water retention capacity of melting snow. PAPER III also presents the first data, where both the snow density and elemental carbon content are measured (Figure 4.3). In an additional laboratory experiment, artificially added light-absorbing impurities cause a decrease in the density of seasonally melting natural snow. No relationship is found in case of natural non-melting snow. Additional laboratory experiments confirm that snow containing impurities releases melt water quicker than cleaner snow. PAPER III suggests three possible processes that might lead to lower snow density. These are: A semi-direct effect of absorbing impurities, where absorbing impurities would cause melt and/or evaporation from the liquid phase and sublimation from the solid phase of the surrounding snow, resulting in air pockets around the impurities, and thus lower snow density; or BC

effect on the adhesion between liquid water and snow grains, where BC reduces adhesion, and the liquid-water holding capacity decreases; or BC effect on the snow grain size, where absorbing impurities increase the melting and metamorphosis processes, resulting in larger snow grains, which lower the water retention capacity.

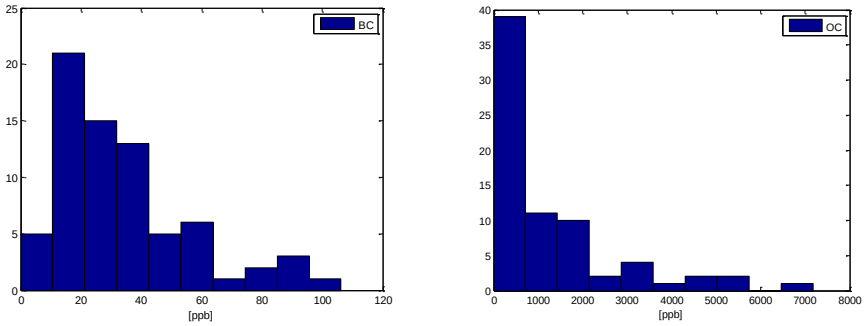

Figure 4.2. Histograms of the BC and OC concentrations [ppb] in the surface snow in Sodankylä during snow time, since the beginning of 2009 until the snow melt in spring 2011. The histograms are based on data presented in Table 3 of **PAPER II**.

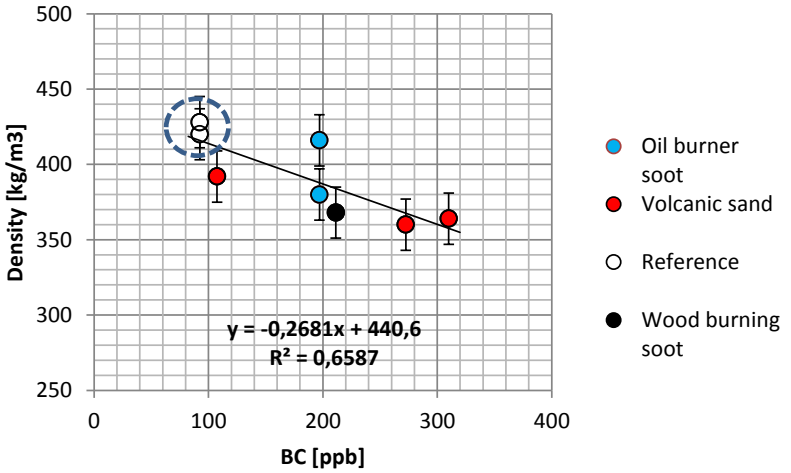

Figure 4.3. The BC content [ppb] vs density [kgm^{-3}] for the naturally melting snow in Sodankylä with and without artificially added impurities. The line is a least square fit through all the points. Redrawn on the basis of Figure 2 of **PAPER III.** © Author(s) 2014. CC Attribution 3.0 License.

4.3 Icelandic dust and cryosphere

In the Arctic region, Iceland is an important source of dust due to glacio-fluvial processes and ash production from volcanic eruptions, combined with frequent high winds. Dust is resuspended from the surface into the atmosphere in dust storms. Iceland faces 135 dust days each year (Arnalds et al. 2016). Icelandic dust and ash particles are dark in color, and due to their light-absorbing properties their impact on the cryosphere can be significant. More scientific results are needed to assess the cryospheric effects of Icelandic dust and ash.

In this thesis, PAPER IV–V deal with effects of Icelandic dust. PAPER III on BC density effects uses also data where Icelandic volcanic particles are artificially deposited in snow. However, PAPER III says that volcanic sand is assumed not to contain BC. The paper refers to Dadic et al. (2013, their Fig. 12a), and FMI's own EC analysis of volcanic sand samples with the thermal–optical method showing hardly any EC.

PAPER IV investigates the melt and insulation effects of Icelandic dust and ash on snow and ice. During volcanic eruptions and dust storms, material is deposited on the glaciers where it influences their energy balance. In PAPER IV, the effects of deposited volcanic ash on ice and snow melt are examined using laboratory and outdoor experiments. These experiments were made in Kumpula, Helsinki, during the snow melt period. Two different ash grain sizes (1 ϕ and 3.5 ϕ) from the Eyjafjallajökull 2010 eruption, collected on the glacier, are used. Different amounts of ash are deposited on snow or ice, after which the snow properties and melt are measured. The results show that a thin ash layer increases the snow and ice melt but an ash layer exceeding a certain critical thickness caused insulation (Table 4.1). The experimental results will be useful for investigating the possible consequences in the natural environment.

Table 4.1. Effective and critical thicknesses for different materials such as tephra, rock debris and dust. The effective thickness is the thickness when the material covered ablation is maximized. According to Brock et al. (2007), the critical thickness is the thickness of the material covering the ice or snow where the ablation rate of the material-covered ice or snow equals that of the clean snow or ice; more material will start to insulate. The results of PAPER IV are in italics. Reproduction of Table 1 of **PAPER IV**. © Author(s) 2016, published with open access at Springerlink.com.

Material	Effective thickness [mm]	Critical thickness [mm]
Mt St Helens (1980) ash	3	24
Hekla (1947) tephra	2	5.5
Rock debris	~10	~15–50
Villarrica tephra	-	< 5
Dust (largely organic matter)	-	1.33
Eyjafjällajökull ash (2010, 1 ϕ)	*1*	*9–15*
Eyjafjällajökull ash (2010, 3.5 ϕ)	*≤ 1–2*	*13*

In PAPER V, the cryospheric role of Icelandic dust is discussed and hypothesized. PAPER V refers first to Benning et al. (2014), where microorganisms, such as the pigmented algae that reside in snow and ice, are argued to possibly cause a substantial reduction in the albedo. Thereafter Dumont et al. (2014) is cited, where the springtime darkening of the Greenland Ice Sheet (GrIS) (observed since 2009) is suggested to be due to an increased load of light-absorbing impurities in snow that consist of soot or dust and, potentially, microorganisms. Tedesco et al. (2015) provide arguments on the reduction of the albedo by cryoconite (a mixture of dust, pebbles, soot, and microbes). The old work of the Finnish explorer Adolf Erik Nordenskiöld (1883) is brought up. Contradiction to these is presented by work on the influence of satellite sensor degradation (Polashenski et al. 2015, more in section 4.4).

PAPER V argues that the assessment of Icelandic dust on snow/ice surface darkening and melt is currently unavailable and therefore scientific research is critically needed. While transport and deposition of light-absorbing Icelandic volcanic dust can have a significant influence on the cryosphere, in Greenland and elsewhere, it is not included when glacier and ice cap melt rates and deglaciation are investigated. The reasoning is based on the following: Iceland is the most important Arctic dust source, and this dust can be transported over the North Atlantic to Europe and Greenland, the dust-storm frequency is large and many dust-storms take place in winter (dust mixes with snow), the fertilising effect of dust can offer an important nutrient source that enables microorganisms to grow, and other living organisms present in Icelandic dust can also be intercontinentally transported. PAPER V also hypothesises that in the Arctic, Icelandic dust may have a comparable or even larger effect on the cryosphere than soot. The particle-cryosphere interaction is controlled also by the particle properties, which vary according to the origin from the seven major Icelandic dust sources (Arnalds et al. 2016). Hydrophobic particles can concentrate on the surface, whereas hydrophilic particles can be washed down with melt water (Doherty et al. 2013) and play a role in creating environmental conditions within snow/ice that favour the existence of microorganisms. Observations and modeling results on Icelandic dust and cryosphere interactions for the past, present, and future are urgently needed is the message of PAPER V.

4.4 Modeling, remote sensing and Arctic-Antarctic aspects

Modeling and remote sensing aspects are included mostly in PAPER II-III (but also PAPER I and V), and Antarctic aspects in PAPER I. To start with, PAPER I studies whether the empirical data show any relationships that could be used for simple parameterizations. A nonlinear regression between reflectivity and snow depth of melting snow in Sodankylä is found (Eq. 4 and Fig. 9 of PAPER I). Previously Arola et al. (2003) also reported a similar simple nonlinear parametrization and used the relationship of snow depth and albedo for estimating the albedo of snow covered surfaces in their satellite method. PAPER I concludes that empirical data as such can be useful for modeling purposes, as earlier Wiscombe and Warren (1980) had said that only a small number of albedo models had been put forward prior to their model, reflecting the lack of high-

quality data against which to check such a model, and the fact that some of the data are contradictory. The BC snow albedo effects are investigated in PAPER II with the help of measured and SNICAR modeled albedo and ancillary data (Fig. 4.4). The SNICAR model user can give the concentration of BC (ppb, or nanograms of BC per gram of ice) as input. The model uses a MAC scaling factor which is experimental. Using MAC = 1, the model uses the value of 7.5 m^2 g^{-1} at 550 nm for uncoated BC (mimicking hydrophobic particles), and 1.5 for sulfate-coated black carbon (mimicking hydrophilic black carbon). Here SNICAR was used to investigate in which conditions the modeled albedo could match the measured albedo. The measured snow albedo values were unexpectedly low, but considered to be good estimates close to the true albedo, as the values were evidenced by three independent measurement data sets. To mactch the measured albedo to the SNICAR modeled albedo required a MAC multifying factor of 10 (Figure 4.4).

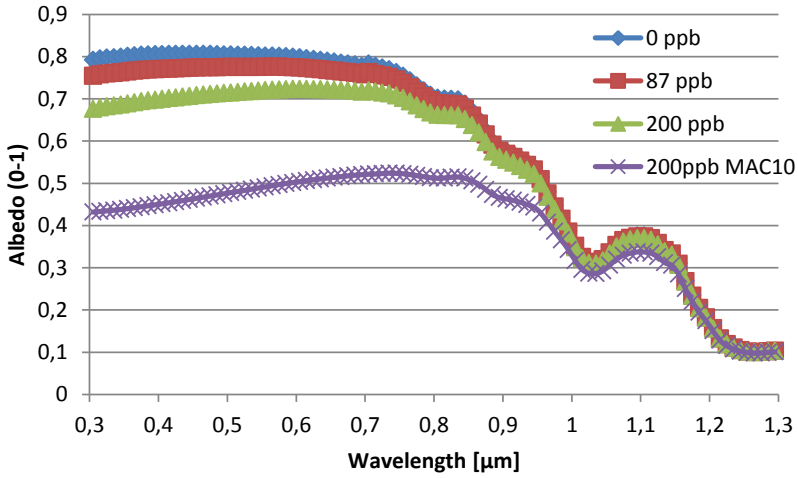

Figure 4.4. The snow albedo spectra at 0.3–1.3 µm simulated for clear sky using the SNICAR model (Flanner et al. 2007). The modeled absorption effects of light-absorbing impurities in snow appear the bigger the shorter the wavelength, and most pronounced at UV. The same spectral absorption feature is also evident for atmospheric absorption of BC (Fig. 9 of Voisin et al. 2012). Realistic parameter values are used as input (SZA = 55 degrees, grain radius 1.5 mm, snow depth 10 cm, snow density 350 kgm^{-3}). The BC and MAC values are then changed to represent the cases of clean snow (blue, 0 ppb), and the EC amount detected using the thermo-optical method (red, 87 ppb). The actual BC concentration in snow, determined by the thermo-optical method, can be assumed (Chow et al. 2001) to be appr. double of the measured EC (green, 200 ppb). To match the measured albedo of ~0.4–0.5 with the modeled, we need a MAC multiplying factor =10 for hydrophobic BC (purple, 200 ppb, MAC 10). Figure 10 of **PAPER II**.

PAPER II states that the diurnal SZA asymmetry in the albedo of melting snow (reported in PAPER I–II) means a potential error in the satellite detected albedo. The RT calculations show that if the 10 % daily melt time asymmetry effect is ignored, an error of

2–4 % in the calculated clear sky downward irradiance is made for one day. This means that if using daily satellite-based albedo data for RT applications, even if the satellite and ground albedo were to match perfectly, there remains an error of the mentioned percentages caused by diurnal snow melting.

Another kind of error source in satellite data is discussed in PAPER V. There the remote sensing results of Polashenski et al. (2015) are cited. They showed that satellite data analysis of Moderate Resolution Imaging Spectrometer (MODIS) surface reflectance from the Terra sensor degradation has important contributions for detecting the Greenland's dry snow zone albedo decline. Polashenski et al. (2015) did not find that enhanced deposition of LAI caused any significant dry snow albedo reduction or melt events, but they acknowledged prior work on GrIS, wherein the impact of MODIS Terra degradation had been concluded as insignificant. Polashenski et al. (2015) agree that part of the dry snow zone albedo decline could be real.

For the SILAM model calculations on the origin of BC in Sodankylä snow in PAPER II, simple rules ("an algorithm") were used to connect the measured BC in snow concentrations to the origins of snow pollution by means of transport modeling. The SILAM footprints were calculated for the "clean" and "dirty" cases (Fig. 9 of PAPER II). The model results show a difference in sensitivity area at Kola Peninsula for clean and dirty footprints. This pattern also agrees with the location of main air pollution sources in the region, mining and refining industries at Kola Peninsula.

Snow density investigated in PAPER III is an important model parameter, because density multiplied by snow depth equals the important climate model parameter of snow water equivalent (SWE).

The Arctic-Antarctic snow albedo aspects are discussed mostly in PAPER I, sections 5.2–5.4. The diurnal decline in albedo and SZA asymmetric albedo of PAPER I, have been found in Antarctic snow by several authors. These SZA asymmetric albedo results are opposite to what is predicted by the theory and have been explained in the Antarctic by changing snow conditions, and diurnal deposition and evaporation of a hoar-frost coating on the snow surface (Pirazzini 2004, Wuttke et al. 2006). Reasons for differences in the Arctic and Antarctic snow albedo are briefly discussed in PAPER I, referring to differences in snow grain sizes, amounts of impurities in snow and air, surface structures, atmospheric moisture, and topography.

5 Summary and conclusions

The Arctic region has warmed more than the global average, a phenomenon known as Arctic amplification. Arrhenius (1896) argued that concentrations of carbon dioxide in the atmosphere could alter the Earth's surface temperature with stronger warming in polar regions due to albedo feedback, i.e., a process where initial warming melts some of the highly reflective snow and ice cover, exposing darker surfaces with stronger absorption of solar energy, leading to further warming and retreat of snow and ice. In reverse, initial cooling leads to increased snow and ice cover, leading to further cooling.

Currently, Arctic amplification is understood to have a variety of causes on different temporal and spatial scales. Albedo feedback is often cited as the main contributor. When dark aerosol particles (BC, OC, dust) are deposited on snow and ice surfaces, the climatic effects are due to reduced albedo and to the induced melt of darker surfaces, which again lowers the albedo and increases melt via the albedo feedback mechanism. In addition to climatic effects, LAI can have, depending on their physical and chemical properties, diverse environmental and hydrological impacts, e.g., in acting as fertilizers or inducing snow and ice melt. The importance of the biological impact on albedo was suggested by Benning et al. (2014), and more recently, on glacier melt by Lutz et al. (2016).

This thesis work has filled in some of the gaps in our knowledge of the effects of LAI on snow in the European Arctic through a series of field and laboratory experiments and analysis of the resulting data, including modeling. The thesis suggests that Icelandic dust in the cryosphere can be one possible cause of Arctic amplification. Icelandic dust is one of the most abundant dust sources in the climate system, and there are about 135 dust events per annum. It has been increasingly recognized that dust produced at high latitude and in cold environments may extend beyond the local source area and have regional or global significance in the Earth system. This thesis states that Iceland is the most important Arctic dust source, but a scientific assessment of its impacts on the cryosphere is currently unavailable, and more scientific results are urgently needed to investigate the role of Icelandic dust in Iceland and elsewhere in the past, present, and future.

As the assessment of the cryospheric role of Icelandic dust is currently missing (referring to PAPER V and Bullard et al. 2016), it also means that until now, Icelandic dust has often been ignored in models and dust effect studies. In the Arctic, Icelandic dust particles can influence both the temperature due to their radiative effects and the albedo feedback effect when deposited.

In terms of radiation budget and climate effects, information on the total shortwave albedo, integrated over the whole solar spectrum and the upper hemisphere, is required. The data acquired within the thesis work on UV and VIS albedo and LAI in snow can be used to calculate the spectral albedo and radiative forcing (i.e., climate impact) of LAI (BC, OC, dust) in snow. The radiative forcing can be inferred from modeling constrained by the in situ data of LAI using the SNICAR and LibRadtran RT models, following the

approach presented in Kaspari et al. (2015), for example. There, the reflected fluxes were calculated for clean and LAI-laden runs integrated over the day to produce all-sky 12 h daily mean radiative forcings.

The atmosphere-cryosphere interactions include a number of processes that are not completely understood. This thesis suggests a "BC density effect" in addition to the "BC albedo effect." To further improve our understanding of the role of LAI in the Arctic feedback processes (positive and negative), we need both long-term observations and modeling. This would require experimental, in situ, and satellite observations of LAI sources, transport, and deposition, and studies on the particle properties and their cryospheric impacts, combined with radiative forcing, long-range transport and climate modeling. In addition, Arctic amplification has inter-connected consequences for the biosphere (e.g., so-called Arctic greening), carbon and hydrogen cycles, and human society. The feedback loops therefore essentially include atmospheric-cryospheric-biosphere-human activities and society interactions.

The results of this thesis contribute to the knowledge on interlinks and feedbacks in light-absorbing impurities and cryosphere interactions. The main findings of this thesis are:

1. Light-absorbing impurities and snow albedo and melt *(the scientific question Q1 of this Thesis):*

- the in situ snow UV and VIS albedo in Sodankylä, north of the Arctic Circle, were in the melting season lower (0.5–0.8) than expected (> 0.9) on the basis of literature (Grenfell et al. 1994).
- the low albedo values, confirmed by three independent measurement set ups, were explained by large snow grain sizes (up to 3 mm in diameter), melt water surrounding the snow grains, and absorption caused by impurities (87 ppb BC and 2894 ppb OC at the time of the albedo measurements)
- diurnal SZA asymmetry in the Arctic snow albedo, during snow melt, was detected opposite to the theory of the SZA dependent U-shape of the albedo signal (Briegleb et al. 1986)
- the SZA asymmetry was explained to be due to changes in the properties of intensively melting snow, where the diurnal albedo decline dominates over the SZA dependency
- spectral change in the measured data was the greater the shorter the wavelength. This is consistent with the theoretical results of Warren and Wiscombe (1980), which show that absorption due to snow impurities increases with decreasing wavelength
- observations on impurities on the surface snow when snow melts (e.g., in case of Icelandic volcanic sand, suggesting hydrophobic particle properties)
- observations on clumping of particles when on melting snow or ice surface
- observations on impurities induced cryoconite holes on melting snow and ice.

2. BC and OC in snow and their origin *(the scientific question Q2 of this Thesis)*

- BC contents of the surface snow layer, sampled weekly during snow time in 2009 - 2011 at Sodankylä, were found higher (up to 106 ppb) than expected (up to 60 ppb during melt, Doherty et al. 2013)

- higher BC concentrations in snow in spring time suggested surface accumulation of hydrophobic BC during snow melt
- some of the high BC concentrations were found to be due to anthropogenic soot transported from the Kola Peninsula, Russia, with industrial activities. This origin was suggested by SILAM footprint calculations utilizing the measured BC in snow data and meteorological data on rainfall, combined with *a priori* threshold values based on literature (Doherty et al. 2010 and 2013), and a rule relating the snow sample collection time with the occurrence of rain events
- the origin of OC (max values > 2000 ppb) can be anthropogenic or natural, and may include pollen, seeds, lichens, natural litter or microorganisms that reside in snow and ice.

3. LAI and snow density *(the scientific question Q3 of this Thesis):*

- a new hypothesis on the snow density effects of light-absorbing impurities, an important quantity for climate modeling and remote sensing, was presented
- three potential processes were suggested to explain the "BC density effect":
    - a semi-direct effect of absorbing impurities, where absorbing impurities would cause melt and/or evaporation from the liquid phase and sublimation from the solid phase of the surrounding snow, resulting in air pockets around the impurities, and thus lower snow density;
    - effect on the adhesion between liquid water and snow grains, where BC reduces adhesion, and the liquid-water holding capacity decreases; or
    - effect on the snow grain size, where absorbing impurities increase the melting and metamorphosis processes, resulting in larger snow grains, which lower the water retention capacity;
- experimental results show that dirty snow release melt water quicker than cleaner snow.

4. Cryospheric effects of Icelandic volcanic dust *(the scientific question Q4 of this Thesis):*

- a scientific assessment of Icelandic dust impacts on the cryosphere is currently unavailable, although Iceland is the most important Arctic dust source, and scientific results are urgently needed to investigate the role of Icelandic dust in Iceland and elsewhere, in the past, present and future
- the experimental results on Icelandic volcanic ash showed that Eyjafjällajökull ash with grain size smaller than 500 μm insulated the ice below at a thickness of 9–15 mm (called as 'critical thickness'). For the 90 μm grain size, the insulation thickness was 13 mm. The maximum melt occurred at thickness of 1mm for the larger particles, and at the thickness of < 1–2 mm for the smaller particles (called as 'effective thickness'). Earlier, similar threshold dust layer thickness values have been given for Mt St Helens (1980) ash, and Hekla (1947) tephra, for example (references given in PAPER IV)
- these results were the first ones reported for the Eyjafjällajökull ash
- in Iceland, the dust layers in the nature can be from mm scale up to tens of meters. These results suggest increased melt in areas with smaller amounts of dust, further away from the eruption, inside Iceland and elsewhere. In literature, long-range transported Icelandic dust has been reported to be found even over the Atlantic (Prospero et al. 2012).

5. Challenges, needs and possibilities in modeling and remote sensing approaches and in bipolar Arctic-Antarctic research (*the scientific question Q5 of this Thesis):*

- the need to understand ground truth processes was shown, as the measured in situ SZA asymmetric albedo was found to result in a 2–4 % daily error for the daily satellite snow albedo estimates
- the snow albedo model results indicated that the biggest snow albedo changes due to BC are expected in the UV part of the EM spectrum, and that the MAC assumptions significantly influence on the simulated spectral albedo values for dirty snow
- clumping mechanism of impurities on snow surface was observed (while, e.g., Schwarz et al. (2013) assume that no BC agglomeration in snow takes place)
- a method to connect the observed BC contents of snow with the origin of pollution for the dirty snow samples using SILAM footprint calculations indicated the areas that were likely to be responsible for the origin of the pollution
- Arctic work can be used for the benefit of the Antartic research. The methods can first be developed and tested in the Arctic, before including them in the Antarctic work, and thereafter the same methods used in bipolar research can give in-depth understanding. The diurnal decline in the albedo and the SZA asymmetric albedo detected in PAPER I, have been found in Antarctic snow and explained in the Antarctic by changing snow conditions, and diurnal deposition and evaporation of a hoar-frost coating on the snow surface (Pirazzini 2004, Wuttke et al. 2006). Reasons for differences in the Arctic and Antarctic snow albedo were discussed in PAPER I, referring to differences in snow grain sizes, amounts of impurities in snow and air, surface structures, atmospheric moisture, and topography.

Warren and Wiscombe (1980) urged high-quality albedo data against which to check the modeled albedo. The need for high-quality in situ data for model and satellite data verification exists. Both the model and the remote sensing approaches require empirical measurement data. Various types of models related to the cryosphere–atmosphere interactions, from the surface albedo to Climate and Earth System Modeling, are under continuous development. Also measurement devices, both ground-based and satellite, continue to improve by their spatial and spectral resolutions and accuracy. A lot of effort is also put on developing algorithms to retrieve various properties of environmentally important parameters, e.g., in satellite aerosol remote sensing (Kokhanovsky and Leeuw 2009). Both the in situ radiometer measurements as well as the radiometers onboard satellites suffer from various errors and uncertainties. PAPER I discussed errors and uncertainties related to the Sodankylä SL501 albedo data, and how these challenges were taken care of. Yet, even data correction for known errors is not always enough. PAPER II showed that a 10 % diurnal SZA asymmetry in the melting snow albedo can cause a 2–4 % error in the satellite albedo estimates, even when satellite data are corrected for their known errors. The observed SZA asymmetry case demonstrates the need for further work on identifying, quantifying and parameterizing ground truth processes, especially when contradicting theory, and these to be implemented in models.

6 Future aspects

6.1 Broader research field and multi-method approaches

The scientific focus of this thesis was on effects of black carbon, organic carbon and Icelandic volcanic dust on Arctic snow and ice optical properties, melt and density, as discussed in connection with sources of emissions, long-range transport and deposition. These atmospheric aerosol particles originate from anthropogenic or natural sources. Further work towards better understanding of the Arctic environment includes various research questions within the atmospheric–cryospheric interactions. The most recent internationally recognized hot topics include at least the role of various light-absorbing impurities in the Arctic amplification, high-latitude dust in the Earth system, biological impacts in the cryosphere, as well as darkening of Greenland.

6.1.1 Experiments and modeling

Future work aiming at improving any aspect related to the SNICAR snow albedo model (Flanner et al. 2007) could benefit also other models where SNICAR is part of, including Climate and Earth System Models.

Such an improvement possibility could exist in the representation of the optical properties of Icelandic dust particles, which depend strongly on source material. This knowledge could be useful for other models, too. Volcanic ash exhibits large optical variability, depending on volcanic mineralogy and type of eruption. According to the SNICAR model documentation, the optical properties of dust are designed to represent "global-mean" characteristics as closely as possible, where a mixture of quartz, limestone, montmorillonite, illite, and hematite is assumed. E.g., in case of dust particles with a large proportion of strongly-absorbing hematite, a larger impact on the snow albedo is expected as compared to the dust in SNICAR. The properties of volcanic ash particles in SNICAR are derived from measurements of ash particles from the Mount St. Helens, Washington, in the Pacific Northwest region of the United States. Therefore, optical characterization of the Icelandic dust particles, i.e., providing data on wavelength dependent refractive indeces, from the seven major dust sources could serve as an improvement for SNICAR.

It could also be worth investigating if the detected changes in the albedo due to LAI (BC, OC, dust) could be further used in regional climate models to compare model runs with and without LAI, to gain an estimate on the LAI albedo impact in the Arctic region. According to Dr. Petri Räsisänen (FMI), The ability for dust emissions to change with changing climate means that they should be made dependent on weather/climate

conditions (e.g., wind and presence of snow on ground) (pers.comm. Dr. Petri Räsisänen, FMI, September 2016).

Organic carbon absorption in the SNICAR modeled snow albedo offers an unsolved question, too. Based on the results presented in PAPER II, I currently assume some moderate or strongly absorbing organic carbon to be present in the snow at the time of the albedo measurements. The organic carbon in the snow can be an important source of absorption. The OC absorption could also partly explain the high MAC value needed for BC to match the measured low albedo values with the SNICAR simulated albedo values. According to Dr. Flanner, the OC that is included in SNICAR is only weakly absorbing, and it is probably too weak to represent the OC that was present in the snow when the low albedo values were measured. Furthermore, it may be difficult to represent OC/brown carbon in the SNICAR model, because the particles exhibit large variability in optical properties, and thus we cannot adequately capture this variability with only one type of OC (Dr. Flanner, pers.comm. 27 May 2016). To derive optical properties for a special version of OC (that is considered representative of the OC in the snow), spectrally-resolved estimates of the "target" MAC would be required. The already existing data could be utilized together with new measurements for the benefit of the SNICAR model development and OC representation in the SNICAR.

The biological impact on the snow and ice albedo and melt has been indicated in Benning et al. (2014) and Lutz et al. (2016). Our Arctic observations and measurements in Sodankylä, Finland, and in Iceland on OC contents in snow also suggest a possibly significant role of organic biological compounds affecting the snow/ice albedo. Our new Icelandic–Finnish co-operative analysis results on BC/OC in snow and glacier ice in Iceland will be the first results for snow and ice in Iceland, as far as we know. The preliminary results suggest very small amounts of BC in snow, and larger OC contents. Also, new understanding on the Sodankylä OC results, i.e., the organic carbon contents in our snow samples, was gained when our recent first microscope investigations on surface snow samples from Sodankylä snow revealed algae and other organic material on the snow surface (Fig. 6.1, photo on the left). In addition, the weekly filter samples were found to contain organic trash (Fig. 6.1, second photo from the left).

Greenland's darkening is currently an unsolved question. Forest fires have also been shown to be an infrequent, but sometimes very large, source of BC deposition to Greenland (e.g. McConnell et al. 2007). To investigate the reasons behind Greenland's darkening, and the albedo feedback (Box et al. 2012), sampling of snow for BC and Icelandic dust particle contents could be undertaken. These results could then be combined with the study of the origin of the impurities in a similar way as presented in PAPER II, using SILAM footprint calculations. Earlier, Greenland Ice Sheet snow was found to have the lowest BC content of the Northern Hemisphere (3 ppb, Doherty et al. 2010). In the percolation zone and the wet-snow zone of the Greenland Ice Sheet, the BC was accumulated in the surface snow due to snow melt, with concentrations of 10–20 ppb (Doherty et al. 2010). According to Warren (2013), the problems of snow thinness and patchiness are nonexistent on the Greenland Ice Sheet, where the snow surface is horizontal, uniform, deep, and unvegetated. The most favorable location for remote sensing would be the wet snow zone of Greenland late in the melting season, when BC has become concentrated at the surface.

The hydrophilic and hydrophobic properties of LAPs, and BC particle size in snow can play a big role in the cryosphere–atmosphere interactions and should be studied more. The SP2 and NIOSH methods are currently in use at FMI, and a comparison data set has been collected for a method comparison. Interesting aspects are also related to the fact that BC is different by its size in the air and snow (Schwarz et al. 2013).

6.1.2 Experiments, modeling and satellite approaches

The need for understanding the basic processes when utilizing satellite data is presented in our recent joint-paper of Peltoniemi et al. (2015) on BRDF changes for contaminated snow. The work shows that the surface of dirty snow remains the darkest when the reflectance is measured at nadir, but at larger zenith angles the surface of the contaminated snow appears almost as white as clean snow. This means that for an observer at the surface, the darkening caused by impurities can be completely invisible, overestimating the albedo, but a nadir-observing satellite sees the darkest points, underestimating the albedo. These observations give reasoning for future investigations on satellite data to compare nadir pixels with non-nadir data, combined with BRDF properties of various impurities on snow and ice surfaces.

The UV part of the EM spectrum can be utilized for detecting LAPs in snow. Painter et al. (2007) observed the most pronounced decrease towards the UV portion of the spectrum due to dust deposition. The spectral absorption properties of soot and Icelandic dust particles alone and on snow are presented in Peltoniemi et al. (2015), too. Current satellite UV algorithms demand better information on the UV albedo, especially for the land when covered by snow (e.g., Arola et al. 2003, Tanskanen and Manninen 2007). The snow albedo changes due to impurities are usually detected at the visible and near-infrared wavelengths, excluding the ultraviolet (UV, $\lambda < 400$ nm). However, as LAPs are often strong UV absorbers, albedo changes could therefore be first detectable in the UV.

Combining UV and BRDF effects for satellite detection of impurities in the cryosphere could serve as an interesting option to be investigated. With a combination of optimal spectral and directional information, it could be tested if a) smaller concentrations than 1000 ppb of BC in snow, referring to Warren (2013), or b) Icelandic volcanic dust in snow, can be detected by remote sensing.

The Sodankylä Arctic snow SL501 albedo data have been compared in international co-operation with the Antarctic albedo data of the Neumeyer station (Meinander et al. 2009), where SZA asymmetry were found in both data sets. The Arctic data can be compared with our Antarctic SL501 albedo data available from Marambio since 2013 (FINNARP 2014). These bipolar irradiance data can also be used for satellite data validation. The first comparison I made for the Marambio NILU-UV data with the OMI satellite overpass data showed a difficulty in seprating clouds from snow in the satellite algorithm (FINNARP 2014). Moreover, Marambio offers a climatically interesting location to investigate the albedo of melting snow and duration of snow free periods, as the Antarctic Peninsula has experienced warming at rates several times the global mean (Trenberth et al. 2007).

For wind-blown Icelandic dust, satellite data can be employed together with AWS data to detect where and when dust events take place, and long-range transport calculations to show where the dust is transported and deposited. For Greenland's darkening, we would also need empirical studies on Icelandic dust and snow/ice interactions to understand the effects of Icelandic dust deposits in Greenland.

6.2 Practical considerations on snow experiments and monitoring

There are many advantages in snow research in Finland. First of all, there are large remote almost untouched areas with clean snow and clean air, and snow melts every year, which enables climate change related experiments and long-term monitoring on naturally melting snow. The topography of Finland is relatively flat, which can make the understanding of processes easier. Finland has five out of the six global snow classes (Sturm et al. 1995), only alpine snow missing. Sodankylä, from where most of the thesis data originated, belongs to the Taiga snow class. For naturally melting snow, effects of snow drift on the albedo results can be assumed smaller compared to places elsewhere with snowdrift affecting results due to non-melting snow and hard winds. Suggestions for practical work related to snow experiments and snow monitoring in Finland and elsewhere include:

1. To identify locally the origin of BC in snow, our findings in PAPER II suggest benefits when using snow sampling and EC/OC analysis combined with the SILAM footprint calculations. This approach can provide relevant information on the origin of the BC in snow complementary to atmospheric BC measurements or other modeling approaches (e.g., Hienola et al. 2013). The SILAM footprint approach (Fig. 3.5 of this thesis) is planned to be applied to investigate BC in Icelandic snow, where the first snow samples have been collected in March 2016.

2. The SL501 snow UV albedo data included in PAPER I–II now offers a 10 year time series, available for validating the SNICAR model. Since 2009, these albedo data are combined with EC/OC in snow. The five years EC/OC data (2009-2013) suggest a spring time snow melt accumulation of the surface layer BC contents similarly to the shorter data set of PAPER II. Combining these EC/OC data with the UV albedo data and SILAM footprint calculations is in preparation, too.

3. To test the hypothesis on the BC density effect presented in PAPER III and to investigate under which circustances this hypothesis is valid, we have collected more materials from Iceland and elsewhere in Finnish–Icelandic–Chinese co-operation, within the "Pan-Eurasian Experiment" (PEEX) of the University of Helsinki.

4. Separating soot and dust effects could be further investigated using the materials of the experiments of PAPER III-IV. The comparisons of effects of soot and dust on snow melt, albedo and density can be investigated based on these materials

5. As a small practical detail of the consequence of the work presented in PAPER II, I suggested to use a sieve away (with known grid size) the biggest trash while filtering Sodankylä snow for impurity analysis. This is the current Sodankylä practice, and this simple improvment could benefit any similar work elsewhere, too.

6. Here use was made from long-term measurements as well as experiments during shorter periods. The radiometers used for lomg-term albedo measurements are applicable in the field, but instrumentation developed especially for field use is available, too. An ASD spectrometer (www.asdi.com) is one instrument often applied in the field (currently in my use at FMI). Its main advantage is the light weight and the quick measurement compared to, e.g., operational albedo sensors, or Bentham with two input optics. A remote cosine response device can be used for measuring BHR. Alternatively, smaller field-of-view reflectance can be computed with measurements from both the unknown material and a reference material, i.e., Spectralon reference panel with approximately 100 % reflectance across the entire spectrum. A contact probe can be attached to an ASD spectrometer to study particle reflectance properties with and without snow (Figure 6.1).

6.3 What is the role of Icelandic dust in the Arctic cryosphere?

Currently, only few studies on effects of Icelandic volcanic dust on the snow and ice albedo and melt have been published (Dagsson-Waldhauserova et al. 2015, Dragosics et al. 2016, Meinander et al. 2016, Svensson et al. 2015, Peltoniemi et al. 2015), although the need for its scientific evidence is high (Myhre et al. 2013). Ecological and climatological significances of volcanic dust events can be variable depending on the properties of the particles; such as their physical properties, chemical composition, and capability to be transported. About half of the annual dust events in the southern part of Iceland take place at sub-zero temperatures, when dust may be mixed with snow (Dagsson-Waldhauserova et al. 2015). Our joint paper (Dagsson-Waldhauserova et al. 2015) shows that the amounts of dust that are transported with wind can't be ignored in Iceland. Icelandic dust is a natural source of LAI, where the dust storm frequency and severerity can be connected to climate change. If more extreme winds would follow as a result of climate change, then more severe Icelandic dust events would take place more often, too.

The glaciers are melting rapidly in Iceland. I recently had the chance to visit a glacier for the first time (Fig. 6.1). The melt of that Solheimajökull-glacier is unbelievable: in 20 years it has shrunk from its southwestern outlet by appr. 900 m (pers.comm. Dr. Dagsson-Waldhauserova 9.6.2016, http://www.ruv.is/frett/hopadi-um-887-metra-en-ekki-240). The assessment of effects of the Icelandic volcanic dust is missing and more research work is urgently needed. Related to Icelandic dust and cryoconite, PAPER V brings out the fact that living organisms present in Icelandic dust (Kelly et al. 2014) can also be intercontinentally transported (Gorbushina et al. 2007, de Leeuw et al. 2014). Hence, the biological impact should be included in the investigations.

For studies of effects of light-absorbing impurities on the Arctic cryosphere, Iceland offers an important hot spot in Europe. The reflectance and albedo properties of snow and various particles (alone and together) can be further connected with their BRDF properties (Aoki et al. 2000, Peltoniemi et al. 2015), as well as SEM analysis on the shape, size and mineral contents of BC, OC, or mineral and volcanic dust particles, not only for Iceland but also elsewhere (e.g., Tirsch et al. 2012), up to Hawaiian volcanic particles or dust particles of the Mars planet.

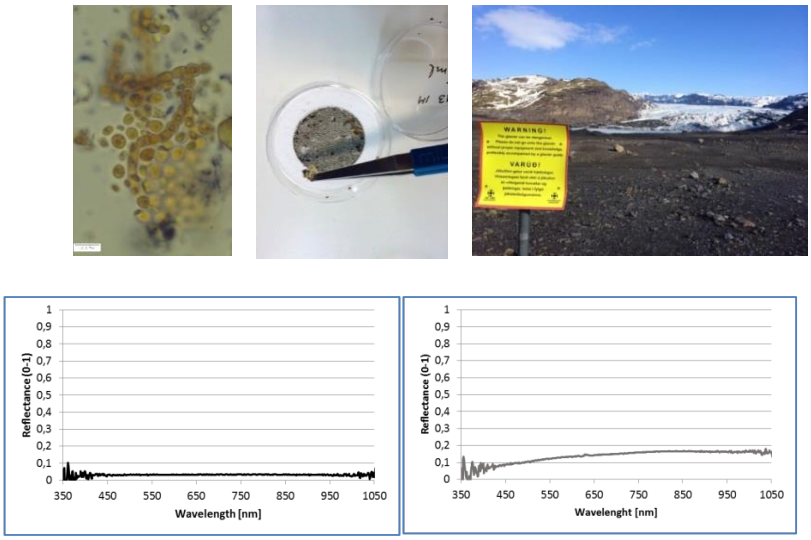

Figure 6.1. The role of organic carbon and Icelandic dust in the Arctic amplification are questions that have received only little scientific attention until now. The OC content in Sodankylä snow samples has been found to be partly due to algae (up left, fist Sodankylä snow microscopic results, photo by Anke Kremp, SYKE, published with the permission of A. Kremp) pollens and other organisms in the snow, as well as trash like needles on the filter (up middle, photo O. Meinander). The mass balance of the glacier Solheimajökull in Iceland is negative and it has been shrinking during the last 20 years by 900 meters from its southwestern corner (up right, photo O.Meinander, March 2016). Spectral reflectance of Icelandic volcanic sand particles (a dark mixture of the volcanic ash of glaciofluvial nature, originating from under the Myrdalsjökull glacier, which was likely mixed with the ash of the Eyjafjallajökull eruption in 2010, and the Grimsvötn eruption in 2011), and Icelandic glaciogenic silt particles collected by the river Mulakvisl, originating from the Myrdalsjökull glacier, possible to be deposited on the local glaciers, as well as long-range transported, measured with a contact probe attached to an ASD spectrometer (O.Meinander).

Acknowledgements

I gratefully acknowledge the Academy of Finland (project "Arctic Absorbing Aerosols and Albedo of Snow" (A^4), decision 254195, and project "Novel Assessment of Black Carbon in the Eurasian Arctic: From Historical Concentrations and Sources to Future Climate Impacts" (NABCEA), decision 296302); the CRAICC Fellowship 2015/2016 of the Nordic Top-level Research Initiative (TRI) project Nordic Centre of Excellence NCoE CRAICC (Cryosphere-atmosphere interactions in a changing Arctic climate); the Finnish Centre on Excellence FCoE ATM in Atmospheric Science funded by the Finnish Academy of Sciences Excellence (project no. 272041); the personal award from the US Alexander Goetz Instrument Support Program (AGISP) for "Arctic Snow Reflectance and Albedo Affected by Black Carbon"; the European Science Foundation ESF Science prize for my poster on Albedo of Arctic Snow; the University of Helsinki Doctoral Programme in Atmospheric Sciences (ATM-DP); the EU COST-STSM-FP0903-10960 for "Reflectance and albedo of snow and vegetation for environmental studies"; and the EU COST-STSM-ES1404 for "Ice and Snow Observations in Iceland: Detecting effects of volcanic dust on snow and ice".

References

Aamaas, B., Bøggild, C. E., Stordal, F., Berntsen, T., Holḿen K. & Strom, J. Elemental carbon deposition to Svalbard snow from Norwegian settlements and long-range transport, Tellus, 63B, 340–351, doi:10.1111/j.1600-0889.2011.00531, 2011.

Adler, G., Riziq, A.A., Erlick, C. & Rudich, Y. Effect of intrinsic organic carbon on the optical properties of fresh diesel soot, PNAS 2010 107,15, 6699-6704, doi:10.1073/pnas.0903311106, 2009.

Agrawal, B.N. Design of geostationary spacegraft, Prentice-Hall, USA, 450 p, 1986.

AMAP. Black carbon and ozone as Arctic climate forcers, Arctic Monitoring and Assessment Programme (AMAP), Oslo, Norway. vii + 116 pp. ISBN – 978-82-7971-092-9, 2015.

Andrady, A. L., Torikai, A., Redhwi, H. H., Pandey, K. K. & Gies, P. Consequences of stratospheric ozone depletion and climate change on the use of materials, Photochemical & Photobiological Sciences, 14, 1, 170-184, 2015.

Aoki, T., Fukabori, M., Hachikubo, A., Tachibana, Y. & Nishio, F. Effects of snow physical parameters on spectral albedo and bidirectional reflectance of snow, J. Geophys. Res.,105, 10219–10236, 2000.

Arnalds, O. Dust sources and deposition of aeolian materials in Iceland, Icel. Agr. Sci., 23, 3–21, 2010.

Arnalds O., Dagsson-Waldhauserova P. & Olafsson H. The Icelandic volcanic aeolian environment: Processes and impacts - A review. Aeolian Research, doi:10.1016/.j.aeolia.2016.01.004, 2016.

Arola, A., Kaurola, J., Koskinen, L., Tanskanen, A., Tikkanen, T., Taalas, P., Herman, J.R., Krotkov, N. & Fioletov V. A new approach to estimating the albedo for snow-covered surfaces in the satellite UV method, J. Geophys. Res., 108, D17, 4531, doi:10.1029/2003JD003492, 2003.

Arrhenius, S. On the influence of carbonic acid in the air upon the temperature of the ground, Philos.Mag.J.Sci. 5, 237-276, 1896.

Benning, L. G., Anesio, A.M., Lutz, S. & Tranter, M. Biological impact on Greenland's albedo, Nature Geoscience 7, 691, 2014.

Birch, M. E. Diesel Particulate Matter (as Elemental carbon) Method 5040, in NIOSH Manual of Analytical Methods, National Institute of Occupational Safety and Health, Cincinnati, Ohio, 2003.

Birch, M. E. & Cary, R. A. Elemental carbon-based method for monitoring occupational exposures to particulate diesel exhaust, Aerosol Sci. Technol., 25, 221–241, 1996.

Bird, R.E. & Riordan, C. Simple solar spectral model for direct and diffuse irradiance on horizontal and tilted planes at the Earth's surface for cloudless atmospheres. J. Clim. Appl. Meteorol. 25, 87-97, 1986.

Blumthaler, M. & Ambach, W. Solar UV Albedo of various surfaces, Photochemistry and Photobiology, 48, 1, 85–88, 1988.

Bond, T. C. & Bergstrom, R.W. Light absorption by carbonaceous particles: An investigative review, Aerosol Sci. Technol., 40, 1, 27-67, doi: 10.1080/02786820500421521, 2006.

Bond, T. C., Habib G. & Bergstrom, R.W. Limitations in the enhancement of visible light absorption due to mixing state, J. Geophys. Res., 111, D20211, doi: 10.1029/2006JD00731, 2006.

Bond, T.C., Doherty, S.J., Fahey, D.W., Forster, P.M., Berntsen, T., DeAngelo, B.J., Flanner, M.G., Ghan, S., Kärcher, B., Koch, D., Kinne, S., Kondo, Y., Quinn, P.K., Sarofim, M.C., Schultz, M.G., Schulz, M., Venkataraman, C., Zhang, H., Zhang, S., Bellouin, N., Guttikunda, S.K., Hopke, Jacobson, P.K., Kaiser, J.W., Klimont, Z., Lohmann, U., Schwarz, J.P., Shindell, D., Storelvmo, T., Warren, S.G. & Zender, C.S. Bounding the role of black carbon in the climate system: A scientific assessment, J. Geophys. Res. Atmos., 118, 11, 5380-5552, doi:10.1002/jgrd.50171, 2013.

Box, J. E., Fettweis, X., Stroeve, J. C., Tedesco, M., Hall, D. K. & Steffen, K. Greenland ice sheet albedo feedback: thermodynamics and atmospheric drivers, The Cryosphere, 6, 821-839, doi:10.5194/tc-6-821-2012, 2012.

Briegleb, B.P., Minnis, P., Ramanathan, V. & Harrison, E. Comparison of Regional Clear Sky Albedos Inferred from satellite Obervations and Model Computations, Journal of Climate and Applied Meteorology, 25, 214-, 1986.

Brock, B., Rivera, A., Casassa, G., Bown, F. & Acuñn, C. The surface energy balance of an active ice-covered volcano: Villarrica volcano, southern Chile, Ann. Glaciol., 45,1, 104–114, 2007.

Bullard, J. E., Baddock, M.,Bradwell, T.,Crusius, J.,Darlington, E. Gaiero, D., Gassó, S.,Gisladottir, G.,Hodgkins, R.,McCulloch, R. McKenna-Neuman, C. Mockford, T., Stewart, H. & Thorsteinsson, T., High-latitude dust in the Earth system, Rev. Geophys., 54, 447–485, doi:10.1002/2016RG000518, 2016.

Chow, J.C., Watson, J.G., Crow, D., Lowenthal, D.H. & Merrifield, T. Comparison of IMPROVE and NIOSH carbon measurements. Aerosol Sci. Technol., 34, 1, 23-34, 2001.

Clarke, A. D. & Noone, K. J. Soot in the Arctic snowpack—a cause for perturbations in radiative-transfer, Atmos. Environ. 19, 2045–2053, 1985.

Dadic, R., Mullen, P. C., Schneebeli, M., Brandt, R. E., and Warren, S. G.: Effects of bubbles, cracks, and volcanic tephra on the spectral albedo of bare ice near the TransantArctic Mountains: Implications for sea glaciers on Snowball Earth, J. Geophys. Res. Earth, 118, 1658–1676, doi: 10.1002/jgrf.20098, 2013.

Dagsson-Waldhauserova, P., Arnalds, O. & Olafsson, H. Long-term variability of dust events in Iceland, Atmos. Chem. Phys., 14, 13411-13422, doi:10.5194/acp-14-13411-2014, 2014.

Dagsson-Waldhauserova, P., Arnalds, O., Olafsson, H., Skrabalova, L., Sigurdardottir, G.M., Branis, M., Hladil, J., Skala, R., Navratil, T., Chadimova, L., von Lowis of Menar, S., Thorsteinsson, T., Carlsen, H.K. & Jonsdottir, I. Physical properties of suspended dust during moist and low-wind conditions in Iceland, Icelandic Agricultural Sciences 27, 25-39, 2014.

Dagsson-Waldhauserova, P., Arnalds, O., Olafsson, H., Hladil, J., Skala, R., Navratil, T., Chadimova, L. & Meinander, O. Snow-Dust Storm: Unique case study from Iceland, March 6-7, 2013, Aeolian Research, doi: 10.1016/j.aeolia.2014.11.001, 2015.

de Leeuw G., Guieu, C., Arneth, A., Bellouin, N., Bopp, L., Boyd, P.W., Denier van der Gon, H.A.C., Desboeufs, K.V., Dulac, F., Facchini, M.C., Gantt, B., Langmann, B., Mahowald, N.M., Maranón, E., O'Dowd, C., Olgun, N., Pulido-Villena, E., Rinaldi, M., Stephanou, E.G. & Wagener, T. Chapter Ocean-Atmosphere Interactions of Gases and Particles, In Liss, P.S. & Johnson, M.T. (eds), Ocean–Atmosphere Interactions of Particles, Part of the series Springer Earth System Sciences, pp. 171-246, ISBN 978-3-642-25642-4, doi:10.1007/978-3-642-25643-1, 2014.

Di Mauro, B., Fava, F., Ferrero, L., Garzonio, R., Baccolo, G., Delmonte, B. & Colombo, R. Mineral dust impact on snow radiative properties in the European Alps combining ground, UAV, and satellite observations, J. Geophys. Res. Atmos., 120, 6080–6097. doi: 10.1002/2015JD023287, 2015.

Doherty, S. J., Warren, S. G., Grenfell, T. C., Clarke, A. D. & Brandt, R. E. Light-absorbing impurities in Arctic snow, Atmos. Chem. Phys., 10, 11647-11680, doi:10.5194/acp-10-11647-2010, 2010.

Doherty, S. J., Grenfell, T.C., Forsström, S., Hegg, D.L., Brandt, R.E. & Warren, S.G. Observed vertical redistribution of black carbon and other insoluble light-absorbing particles in melting snow, J. Geophys. Res.Atmos.,118, doi:10.1002/jgrd.50235, 2013.

Doherty, S. J., Hegg, D.A., Johnson, J.E. , Quinn, P.K., Schwarz, J.P., Dang, C. & Warren, S.G. Causes of variability in light absorption by particles in snow at sites in Idaho and Utah, J. Geophys. Res. Atmos., 121, doi:10.1002/2015JD024375, 2016.

Dumont, M., Brun, E., Picard, G., Michou, M., Libois, Q., Petit, J.-R., Geyer, M., Morin, S. & Josse, B. Contribution of light-absorbing impurities in snow to Greenland's darkening since2009, Nat. Geosci., 7, 509–512, doi:10.1038/ngeo2180, 2014.

Fierz, C., Armstrong, R. L., Durand, Y., Etchevers, P., Greene, E., McClung, D. M., Nishimura, K., Satyawali, P. K. & Sokratov, S. A. The International Classification for Seasonal Snow on the Ground. IHP-VII Technical Documents in Hydrology, no. 83, IACS Contribution no. 1, UNESCO-IHP, Paris,http://unesdoc.unesco.org/images/0018/001864/186462e.pdf, 2009.

FINNARP. Science and support in Antarctica, ISBN 978-951-697-841-6, 2014.

Flanner, M. G., Zender, C. S., Randerson, J. T. & Rasch, P. T. Present day climate forcing and response from black carbon in snow, J. Geophys. Res., 112, D11202, doi:10.1029/2006JD008003, 2007.

Flanner, M. G. Arctic climate sensitivity to local black carbon, J. Geophys. Res., 118, 1840-1851, doi:10.1002/jgrd.50176, 2013.

Forsström, S., Ström J., Pedersen, C.A., Isaksson, E. & Gerland, S. Elemental carbon distribution in Svalbard snow, J. Geophys. Res., 114, D19112, doi:10.1029/2008JD011480, 2009.

Forsström, S., Isaksson, E., Skeie, R.B., Ström, J., Pedersen, C.A., Hudson, S.R., Berntsen, T.K., Lihavainen, H., Godtliebsen, F. & Gerland, S. Elemental carbon measurements in European Arctic snow packs, J. Geophys. Res. Atmos., 118, 13,614–13, 627, doi:10.1002/2013JD019886.2013, 2013.

France, J. L., Reay, H. J., King, M. D., Voisin, D., Jacobi, H., Beine, H. J., Anastasio, C., MacArthur, A. & Lee-Taylor, J. Hydroxylradical and NOx production rates, black carbon concentrations and light-absorbing impurities in snow from field measurements of light penetration and nadir reflectivity of on-shore and offshore coastal Alaskan snow, J. Geophys. Res., 117, D00R12, doi:10.1029/2011JD016639, 2012.

Gabbi, J., Huss, M., Bauder, A., Cao, F. & Schwikowski, M. The impact of Saharan dust and black carbon on albedo and long-term mass balance of an Alpine glacier, The Cryosphere, 9, 1385-1400, doi:10.5194/tc-9-1385-2015, 2015.

Gallet, J.-C., Domine, F. & Dumont, M. Measuring the specific surface area of wet snow using 1310 nm reflectance, The Cryosphere, 8, 1139-1148, doi:10.5194/tc-8-1139-2014, 2014.

Gardner, A. S. & Sharp, M.J. A review of snow and ice albedo and the development of a new physically based broadband albedo parameterization, J. Geophys. Res. 115, F01009, doi:10.1029/2009JF001444, 2010.

Garratt J.R. The atmospheric boundary layer, Cambridge University Press, 1992. Pp. 316, ISBN 0 521 38052 9, 1992.

Gautam, R., Hsu N.C., Lau, W.K-M. & Yasunari T.J. Satellite observations of desert dust-induced Himalayan snow darkening, Geophys. Res. Lett., 40, 988–993, doi:10.1002/grl.50226, 2013.

Gorbushina, A.A., Kort, R., Schulte, A., Lazarus, D., Schnetger, B., Brumsack, H.-J., Broughton, W.J. & Favet, J. Life in Darwin's dust: intercontinental transport and survival of microbes in the nineteenth century, Environ. Microbiol., 9,12, 2911–2922, 2007.

Grenfell, T. C., Warren, S. G. & Mullen, P. C. Reflection of solar radiation by the Antarctic snow surface at ultraviolet, visible, and near-infrared wavelengths, J. Geophys. Res., 99,D9,18 669–18 684, 1994.

Hadley, O. & Kirchstetter, T. Black-carbon reduction of snow albedo, Nature Climate Change 2, 437–440, doi:10.1038/nclimate1433, 2012.

Hagler, G. S. W., Bergin, M. H., Smith, E. A. & Dibb, J.E. A summer time series of particulate carbon in the air and snow at Summit, Greenland, J. Geophys. Res., 112, D21309, doi:10.1029/2007JD008993, 2007.

Hansen, J.E. & Hovenier, J.W. Interpretation of the polarization of Venus, J. Atmos. Sci., 31, 1137-1160, doi:10.1175/1520-0469, 1974.

Hansen, J. & Nazarenko, L. Soot climate forcing via snow and ice albedos, Proc. Natl. Acad. Sci., 101, 423–428, doi:10.1073/pnas.2237157100, 2004.

Harris, R. Satellite remote Sensing, An Introduction, Routledge & Kegan Paul, London and New York, ISBN 0-7102-0305-5, 220 p, 1987.

Hegg, D. A., Warren, S. G., Grenfell, T. C., Doherty, S. J. & Clarke, A. D. Sources of light-absorbing aerosol in Arctic snow and their seasonal variation, Atmos. Chem. Phys., 10, 10923–10938, doi:10.5194/acp-10-10923-2010, 2010.

Heikkilä, A. Methods for assessing degrading effects of UV radiation on materials, PhD Thesis. FMI Contributions No 111, ISBN 978-951-697-844-7, 2014.

Hienola, A. I., Pietikäinen, J.-P., Jacob, D., Pozdun, R., Petäjä, T., Hyvärinen, A.-P., Sogacheva, L., Kerminen, V.-M., Kulmala, M. & Laaksonen, A. Black carbon concentration and deposition estimations in Finland by the regional aerosol–climate model REMO-HAM, Atmos. Chem. Phys., 13, 4033-4055, doi:10.5194/acp-13-4033-2013, 2013.

Hudson, S. R., Warren, S.G., Brandt, R.E., Grenfell, T.C. & Six, D. Spectral bidirectional reflectance of Antarctic snow: Measurements and parameterization, J. Geophys. Res.,111, D18106, doi:10.1029/2006JD007290, 2006.

IPCC the Fifth Assessment Report of the Intergovernmental Panel on Climate Change [Stocker, T.F., D. Qin, G.-K. Plattner, M. Tignor, S.K. Allen, J. Boschung, A. Nauels, Y. Xia, V. Bex and P.M. Midgley (eds.)]. Cambridge University Press, Cambridge, United Kingdom and New York, NY, USA, 2013.

Jiao, C., Flanner, M.G., Balkanski, Y., Bauer, S.E., Bellouin, N., Berntsen, T.K., Bian, H., Carslaw, K.S., Chin, M., De Luca, N., Diehl, T., Ghan, S.J., Iversen, T., Kirkevåg, A., Koch, D., Liu, X., Mann, G.W., Penner, J.E., Pitari, G., Schulz, M., Seland, Ø., Skeie, R.B., Steenrod, S.D., Stier, P. , Takemura, T.. Tsigaridis, K., van Noije, T., Yun, Y. & Zhang, K. An AeroCom assessment of black carbon in Arctic snow and sea ice, Atmos. Chem. Phys., 14, 2399-2417, doi:10.5194/acp-14-2399-2014, 2014.

Järvi, J., Hannuniemi, H., Hussein, T., Junninen, H, Aalto, P. P., Hillamo R., Mäkelä T., Keronen P., Iivola E., Vesala T. & Kulmala M. The urban measurement station smear iii: continuous monitoring of air pollution and surface–atmosphere interactions in Helsinki, Finland, Boreal Env. Res., 14 (suppl. a): 86–109, 2009.

Kaspari, S., McKenzie Skiles, S., Delaney, I., Dixon, D. & Painter, T.H. Accelerated glacier melt on Snow Dome, Mount Olympus, Washington, USA, due to deposition of black carbon and mineral dust fromwildfire, J. Geophys. Res. Atmos., 120, 2793–2807, doi:10.1002/ 2014JD022676, 2015.

Kelly, L.C., Cockell, C.S., Thorsteinsson, T., Marteinsson, V. & Stevenson, J. Pioneer Microbial Communities of the Fimmvörðuháls Lava Flow, Eyjafjallajökull, Iceland, Microbial Ecology 1-15, doi:10.1007/s00248-014-0432-3, 2014.

Knippertz, P. & Stuut, J.-P. (eds.). Mineral Dust – a key player in the Earth System, Springer, ISBN 978-94-017-8978-3, doi:10.1007/978-94-017-8978-3, 2014.

Koch, D. & Del Genio, A. D., Black carbon semi-direct effects on cloud cover: review and synthesis, Atmos. Chem. Phys., 10, 7685-7696, doi:10.5194/acp-10-7685-2010, 2010.

Koch, D. & Hansen, J. Distant origins of Arctic black carbon, A Goddard Institute for Space Studies ModelEexperiment, J. Geophys. Res.,110, D04204, doi:10.1029/2004JD005296, 2005.

Kokhanovsky, A.A. & Leeuw, G. (eds). Satellite Aerosol Remote Sensing Over Land. Springer, ISBN 978-3-540-69396-3, 2009.

Kuusisto, E. Snow accumulation and snowmelt in Finland.Helsinki, Publications of the water Research Institute 55, ISBN 951-46-7494-4, 149 p., 1984.

Laborde, M., Crippa, M., Tritscher, T., Jurányi, Z., Decarlo, P. F.,Temime-Roussel, B., Marchand, N., Eckhardt, S., Stohl, A., Baltensperger, U., Prévôt, A. S. H., Weingartner, E. & Gysel, M., Black carbon physical properties and mixing state in the European megacity Paris, Atmos. Chem. Phys., 13, 5831–5856, doi:10.5194/acp-13-5831-2013, 2013.

Li, W., Stamnes, K., Eide, H. & Spurr, R. Bidirectional reflectance distribution function of snow: Corrections for the Lambertian assumption in remote sensing applications, Optical Engineering 46(6), doi:10.1117/1.2746334, 2007.

Liou, K.N. An Introduction to Atmospheric Radiation, Academic Press; 583 p., 2002.

Lutz, S., Anesio, A.M., Raiswell, R., Edwards, A., Newton, R.J., Gill, F. & Benning, L.G.The biogeography of red snow microbiomes and their role in melting arctic glaciers, Nature Communications, 7:11968 doi: 10.1038/ncomms11968, 2016.

Manninen, T. & Roujean, J-L. SNORTEX, Snow Reflectance Transition Experiment, https://helda.helsinki.fi/bitstream/handle/10138/135970/2014nro7.pdf?sequence=1978-951-697-835-5, ISBN 978-951-697-835-5, Unigrafia Helsinki 2014.

Mayer, B. & Kylling, A. Technical note: The libRadtran software package for radiative transfer calculations – description and examples of use, Atmos. Chem. Phys., 5, 1855–1877, doi:10.5194/acp-5-1855-2005, 2005.

McConnell, J.R., Edwards, R., Kok, G.L., Flanner, M.G., Zender, C.S., Saltzman, E.S., Banta, J.R., Pasteris, D.R., Carter, M.M. & Kahl, J.D.W. 20th century industrial black carbon emissions altered Arctic climate forcing, Science, August 9, 2007, doi: 10.1126/science.1144856, 2007.

McKinlay, A. F. & Diffey, B. L. A reference action spectrum for ultraviolet induced erythemal in human skin. Human Exposure to Ultraviolet Radiation: Risks and Regulations, W. R. Passchler & B. F. M. Bosnajakovic, Eds., Elsevier, 83–87, 1987.

McNeill, V. F., Grannas, A. M., Abbatt, J. P. D., Ammann, M., Ariya, P., Bartels-Rausch, T., Domine, F., Donaldson, D. J., Guzman, M. I., Heger, D., Kahan, T. F., Klan, P., Masclin, S., Toubin,C. & Voisin, D. Organics in environmental ices: sources, chemistry, and impacts, Atmos. Chem. Phys., 12, 9653–9678, doi:10.5194/acp-12-9653-2012, 2012.

Meinander, O., Wuttke, S., Seckmeyer, G., Kazadzis, S., Lindfors, A. & Kyrö, E. Solar Zenith Angle Asymmetry Cases in Polar Snow UV Albedo, Geophysica, 45, 1–2, 183–198, 2009.

Mie, G. Beiträge zur Optik trüber Medien, speziell kolloidaler Metallösungen.Annalen der Physik, 330, 3,377–445, ISSN 1521-3889, doi:10.1002/andp.19083300302, 1908.

Myhre, G., Shindell, D., Bréon, F.-M., Collins, W., Fuglestvedt, J., Huang, J., Koch, D.,. Lamarque, J.-F , Lee, D., Mendoza, B. , Nakajima, T., Robock, A., Stephens, G., Takemura, T. & Zhang, H., Anthropogenic and Natural Radiative Forcing. In: Climate Change 2013: The Physical Science Basis. Contribution of Working Group I to the Fifth Assessment Report of the Intergovernmental Panel on Climate Change [Stocker, T.F., D. Qin, G.-K. Plattner, M. Tignor, S.K. Allen, J. Boschung, A. Nauels, Y. Xia, V. Bex and P.M. Midgley (eds.)]. Cambridge University Press, Cambridge, United Kingdom and New York, NY, USA, 2013.

Nordenskiöld, A.E. Nordenskiöld on the inland ice of Greenland, Science, 2, 44, 732-738, doi: 10.1126/science.ns-2.44.732, 1883.

Nousiainen, T. & Kandler, K. Light scattering by atmospheric mineral dust particles, in: Light Scattering Reviews 9, edited by: Kokhanovsky, A. A., Springer Praxis Books, Springer, Berlin, 2015. Heidelberg, 3–52, doi:10.1007/978-3-642-37985-7, 2015.

Painter, T. H., Barrett, A. P., Landry, C. C., Neff, J. C., Cassidy, M. P., Lawrence, C. R., McBride, K. E. & Farmer, G. L. Impact of disturbed desert soils on duration of mountain snow cover, Geophys. Res. Lett., 34, L12502, doi:10.1029/2007GL030284, 2007.

Peltoniemi, J. I., Gritsevich, M., Hakala, T., Dagsson-Waldhauserová, P., Arnalds, Ó., Anttila, K., Hannula, H.-R., Kivekäs, N., Lihavainen, H., Meinander, O., Svensson, J., Virkkula, A. & de Leeuw, G. Soot on Snow experiment: bidirectional reflectance factor measurements of contaminated snow, The Cryosphere, 9, 2323-2337, doi:10.5194/tc-9-2323-2015, 2015.

Perovich, D. K., Grenfell, T. C., Light, B. & Hobbs, P. V. Seasonal evolution of the albedo of multiyear Arctic sea ice, J. Geophys. Res., 107,C10, 8044, doi:10.1029/2000JC000438, 2002.

Pirazzini, R. Surface albedo measurements over Antarctic sites in summer, J. Geophys. Res., 109, D20118, doi:10.1029/2004JD004617, 2004.

Pithan, F. & Mauritsen, T. Arctic amplification dominated by temperature feedbacks in contemporary climate models, Nature Geosci., 7, 181–184, doi:10.1038/ngeo2071, 2014.

Polashenski, C.M., Dibb, J.E., Flanner, M.G., Chen, J.Y., Courville, Z.R., Lai, A.M., Schauer, J.J., Shafer M.M. & Bergin, M. Neither dust nor black carbon causing apparent albedo decline in Greenland's dry snow zone; implications for MODIS C5 surface reflectance, Geophys. Res. Lett., 42, 9319–9327, doi: 10.1002/2015GL065912, 2015.

Prospero, J.M., Bullard, J.E. & Hodgkins, R. High-Latitude Dust Over the North Atlantic: Inputs from Icelandic Proglacial Dust Storms, Science, 335, 1078, doi: 10.1126/Science.13217447, 2012.

Ramanathan, V. & Carmichael, G. Global and regional climate changes due to black carbon, Nature Geoscience 1, 221 – 227, doi:10.1038/ngeo156, 2008.

Robinson, P.J. & Davies, J.A. Laboratory Determinations of Water Surface Emissivity, Journal of Applied Meteorology, 11,8,1391-1392, doi: 10.1175/1520-0450(1972)011<1391:LDOWSE>2.0.CO;2, 1972.

Räisänen, P., Kokhanovsky, A., Guyot, G., Jourdan, O. & Nousiainen, T. Parameterization of single-scattering properties of snow, The Cryosphere, 9, 1277-1301, doi:10.5194/tc-9-1277-2015, 2015.

Sand, M., Berntsen, T., Kay, J.E., Lamarque, J.F., Seland O. & Kirkevag, A. The Arctic response to remote and local forcing of black carbon, Atmos. Chem. Phys., 13, 211-224, 2013.

Schaepman-Strub, G., Schaepman, M.E., Painter, T.H., Dangel, S. & Martonchik, J.V. Reflectance quantities in optical remote sensing—definitions and case studies, Remote Sensing of Environment 103, 27-42, 2006.

Schwarz, J.P., Spackman, J.R., Gao, R.S., Watts, L., Stier, P., Schulz, M., Davis, S.M., Wofsy S.C. & Fahey, D.W. Global-scale black carbon profiles observed in the remote atmosphere and compared to model, Geophys. Res. Lett., 37:L18812, doi:10.1029/2010gl044372, 2010.

Schwarz, J. P., Gao, R. S., Perring, A. E., Spackman, J. R. & Fahey, D. W. Black carbon aerosol size in snow, Scientific Reports, doi:10.1038/srep01356, 2013.

Seckmeyer, G., Bais, A., Bernhard, G., Blumthaler, M., Booth, R.S., Lantz, K. & McKenzie, R. L. Instruments to measure solar ultraviolet radiation, part II: Broadband instruments measuring erythemally weighted solar irradiance, WOM-GAW report, 2005.

Serreze, M. C. & Barry, R. G. Processes and impacts of Arctic amplification: A research synthesis, Global and Planetary Change 77, 85-96, doi:10.1016/j.gloplacha.2011.03.004, 2011.

Setlow, R.B. The wavelengths in sunlight effective in producing skin cancer: a theoretical analysis, Proc. Nat. Acad. Sci., USA, 71, No. 9, 3363-3366, 1974.

Sharma, S., Ishizawa, M., Chan, D., Lavoué, D., Andrews, E., Eleftheriadis, K. & Maksyutov, S. 16-year simulation of Arctic black carbon: transport, source contribution, and sensitivity analysis on deposition, J. Geophys. Res., 118, 1-22. doi:10.1029/2012JD017774, 2013.

Shettle, E. P. Models of aerosols, clouds and precipitation for atmospheric propagation studies, paper presented at Conference on Atmospheric Propagation in the UV, Visible, IR and MM-Region and Related System Aspects, NATO Adv. Group for Aerosp. Res. and Dev., Copenhagen, 1989.

Smolskaia, I., Nunez, M. & Kelvin, M. Measurements of Erythemal Irradiance near Davis Station, Antarctica: Effect of. Inhomegeneous Surface Albedo, Geophys. Res. Lett., 26, 1381–1384, 1999.

Sofiev, M., Galperin, M. & Genikhovich, E. Construction and evaluation of Eulerian dynamic core for the air quality and emergency modeling system SILAM, in: NATO Science for piece and security Serties C: Environmental Security, Air pollution modelling and its application, XIX, edited by: Borrego, C. and Miranda, A. I., Springer, 699–701, 2008.

Stohl, A., Klimont, Z., Eckhardt, S., Kupiainen, K., Shevchenko, V.P., Kopeikin, V.M. & Novigatsky, A.N. Black carbon in the Arctic: the underestimated role of gas flaring and residential combustion emissions, Atmos. Chem. Phys., 13, 8833-8855, 2013.

Sturm, M., Holmgren, J. & Liston, G. E. A seasonal snow cover classification system for local to global applications, J. Clim., 8, 1261–1283, 1995.

Svensson, J., Ström, J., Hansson, M., Lihavainen, H. & Kerminen, V.-M. Observed metre scale horizontal variability of elemental carbon in surface snow, Environmetal research Letters, 8, doi:10.1088/1748-9326/8/3/034012, 2013.

Svensson, J., Virkkula, A., Meinander, O., Kivekäs, N., Hannula, H.-R., Järvinen, O., Peltoniemi, J., Gritsevich, M., Heikkilä, A., Kontu, A., Neitola, K., Brus, D., Dagsson-Waldhauserova, P., Anttila, K., Vehkamäki, M., Hienola, A., Leeuw, G. & Lihavainen, H. Soot-doped natural snow and its albedo — results from field experiments, Boreal Env. Res., 21, 481–503, 2016.

Tanskanen, A. & Manninen, T. Effective UV surface albedo of seasonally snow-covered lands, Atmos. Chem. Phys., 7, 2759–2764, 2007.

Tedesco, M., Doherty, S., Warren, S., Tranter, M., Stroeve, J., Fettweis, X. & Alexander, P. What darkens the Greenland Ice Sheet?, Eos, 96, doi:10.1029/2015EO035773,2015.

Tirsch, D., Craddock, R. A., Platz, T., Maturilli, A., Helbert, J. & Jaumann, R. Spectral and petrologic analyses of basaltic sands in Ka'u Desert (Hawaii) – implications for the dark dunes on Mars, Earth Surf. Process. Landforms, 37, 434–448, doi: 10.1002/esp.2266, 2012.

Trenberth, K.E., Jones, P.D., Ambenje, P., Bojariu, R., Easterling, D., Tank, A.K., Parker, D., Rahimzadeh, F., Renwick, J.A., Rusticucci, M., Soden, B. & Zhai, P. Observations: surface and atmospheric climate change. In Climate Change 2007: The Physical Science Basis, edited by S. Solomon, D. Qin, M. Manning, Z. Chen, M. Marquis, K. B. Averyt, M.Tignor & H. L. Miller. Cambridge, United Kingdom and New York, N.Y., USA: Cambridge University Press, 2007.

UNEP.Environmental Effects of Ozone Depletion: 2002, Assessment, United Nations Environment Programme. ISBN 92-807-2312-X, http://www.unep.org/OZONE/pdf/eeap-report2002.pdf, 2002.

Voisin, D., Jaffrezo, J.-L., Houdier, S., Barret, M., Cozic, J., King, M. D., France, J. L., Reay, H. J., Grannas, A., Kos, G., Ariya, P. A., Beine, H. J. & Domine, F. Carbonaceous species and HUmic LIke Substances (HULIS) in Arctic snowpack during OASIS field campaign in Barrow, J. Geophys. Res., 117, D00R19, doi:10.1029/2011JD016612, 2012.

Wang, R., Tao, S., Balkanski, Y., Ciais, P., Boucher, O., Liu, J., Piao, S., Shen, H., Raffaella Vuolo, M., Valari, M., Chen, H., Chen, Y., Cozic, A., Huang, Y., Li, B., Li, W., Shen, G., Wang B. & Zhang, Y. Exposure to ambient black carbon derived from a unique inventory and high-resolution model, PNAS, vol. 111 no. 7, 2459–2463, doi: 10.1073/pnas.1318763111, 2014.

Warren, S. G. Can black carbon in snow be detected by remote sensing?, J. Geophys. Res. Atmos., 118, 779–786, doi:10.1029/2012JD018476,2013.

Warren, S. & Wiscombe, W. A Model for the Spectral Albedo of Snow. II: Snow Containing Atmospheric Aerosols, Journal of the Atmospheric Sciences, 37, 12, 2734-2745, doi: http://dx.doi.org/10.1175/1520-0469(1980)037<2734:AMFTSA>2.0.CO;2, 1980.

Webb, A., Grobner, J. & Blumthaler, M. A practical guide to operating broadband instruments measuring erythemally weighted irradiance, WMO SAG UV, COST-726, ISBN 92-898-0032-1, 2006.

Weller, G. The tundra microclimate during snow-melt at Barrow, Alaska, Arctic, 25, 291–299, 1972.

WHO. Solar ultraviolet radiation: global burden of disease from solar ultraviolet radiation, Environmental burden of disease series, No. 13. World Health Organization.ISBN 92 4 159440 3, 2006.

Wiscombe, W. J. & Warren, S. G. A model for the spectral albedo of snow. I: Pure snow, J. Atmos. Sci., 37, 2712–2733, 1980.

Wuttke, S., Seckmeyer, G. & Ḱonig-Langlo, G. Measurements of spectral snow albedo at Neumayer, Antarctica, Ann. Geophys., 24, 7–21, 2006.

WMO. Instruments to Measure Solar Ultraviolet Radiation, Part 1: Spectral Instruments (lead author G. Seckmeyer) (WMO TD No. 1066), 2001.

WMO. Guide to Meteorological Instruments and methods of Observation, WMO-No. 8 (Seventh Edition,6 August 2008), http://www.wmo.int/pages/prog/www/IMOP/publications/CIMO-Guide/CIMO Guide-7th Edition-2008.html, 2008.

WMO. GAW Report No. 212, Standard Operating Procedures (SOPs) for Spectral Instruments Measuring Spectral Solar Ultraviolet Irradiance, http://www.wmo.int/pages/prog/arep/gaw/documents/Final_GAW_212.pdf, 2014.

Zhang, J., Liu, J., Tao, S. & Ban-Weiss, G. A. Long-range transport of black carbon to the Pacific Ocean and its dependence on aging timescale, Atmos. Chem. Phys., 15, 11521-11535, doi:10.5194/acp-15-11521-2015, 2015.

I

Reprinted from
Atmospheric Chemistry and Physics, 8, 6551– 6563,
doi:10.5194/acp-8-6551-2008

Atmos. Chem. Phys., 8, 6551–6563, 2008
www.atmos-chem-phys.net/8/6551/2008/

Atmospheric Chemistry and Physics

Diurnal variations in the UV albedo of arctic snow

O. Meinander[1], **A. Kontu**[1], **K. Lakkala**[1], **A. Heikkilä**[1], **L. Ylianttila**[2], **and M. Toikka**[3]

[1]Finnish Meteorological Institute, P.O. BOX 503, 00101 Helsinki, Finland
[2]Radiation and Nuclear Safety Authority, P.O. Box 14, 00881 Helsinki, Finland
[3]Toikka Engineering Ltd., Hannuntie 18, 02360 Espoo, Finland

Received: 3 January 2008 – Published in Atmos. Chem. Phys. Discuss.: 29 February 2008
Revised: 2 September 2008 – Accepted: 23 September 2008 – Published: 14 November 2008

Abstract. The relevance of snow for climate studies is based on its physical properties, such as high surface reflectivity. Surface ultraviolet (UV) albedo is an essential parameter for various applications based on radiative transfer modeling. Here, new continuous measurements of the local UV albedo of natural Arctic snow were made at Sodankylä (67°22′N, 26°39′E, 179 m a.s.l.) during the spring of 2007. The data were logged at 1-min intervals. The accumulation of snow was up to 68 cm. The surface layer thickness varied from 0.5 to 35 cm with the snow grain size between 0.2 and 2.5 mm. The midday erythemally weighted UV albedo ranged from 0.6 to 0.8 in the accumulation period, and from 0.5 to 0.7 during melting. During the snow melt period, under cases of an almost clear sky and variable cloudiness, an unexpected diurnal decrease of 0.05 in albedo soon after midday, and recovery thereafter, was detected. This diurnal decrease in albedo was found to be asymmetric with respect to solar midday, thus indicating a change in the properties of the snow. Independent UV albedo results with two different types of instruments confirm these findings. The measured temperature of the snow surface was below 0°C on the following mornings. Hence, the reversible diurnal change, evident for ∼1–2 h, could be explained by the daily metamorphosis of the surface of the snowpack, in which the temperature of the surface increases, melting some of the snow to liquid water, after which the surface freezes again.

Correspondence to: O. Meinander
(outi.meinander@fmi.fi)

1 Introduction

The relevance of snow for climate variability and change is based on its physical properties, such as high surface reflectivity, i.e., albedo (IPCC, 2007). High albedo has an important influence on the surface energy budget and on Earth's radiative balance (Forster et al., 2007, e.g.). Snow albedo varies with wavelength, and therefore the strength of the feedback depends on a number of factors, such as the depth and age of the snow cover, and the amount of incoming solar radiation and cloud cover. The albedo of snow may decrease because of anthropogenic soot (Wiscombe and Warren, 1980; Warren and Wiscombe, 1980) and aging and melting (Wiscombe and Warren, 1980; Blumthaler and Ambach, 1988; Wuttke et al., 2006). In the melting process, often initiated in springtime by the increase of shortwave irradiance, the snow grains are filled with liquid water and the density of the snow may increase, e.g., in the open sites of Arctic Finland, to 350 kg/m^3 (Kuusisto, 1984). When the albedo decreases, more radiation is absorbed, and the melting of the snow may increase due to this albedo feedback mechanism (e.g., Bony et al., 2006). In addition to its climate connections, ultraviolet radiation (UV) reflected from snow and ice may cause unprotected eyes the painful condition of snow blindness (UNEP, 2002). The UV albedo for a surface with snow is high, and also due to multiple reflections affects downwelling radiation (Bais and Lubin, 2007). Snow cover can increase erythemal irradiance by up to 60% compared to a snow-free case (Weatherhead et al., 2005, e.g.). Moreover, surface UV albedo is an essential parameter for various applications based on radiative transfer (RT) modeling, including various satellite retrieval algorithms. For example, current satellite UV algorithms demand better information on UV albedo, especially for land when covered by snow (e.g., Arola et al., 2003, Tanskanen and Manninen, 2007).

Published by Copernicus Publications on behalf of the European Geosciences Union.

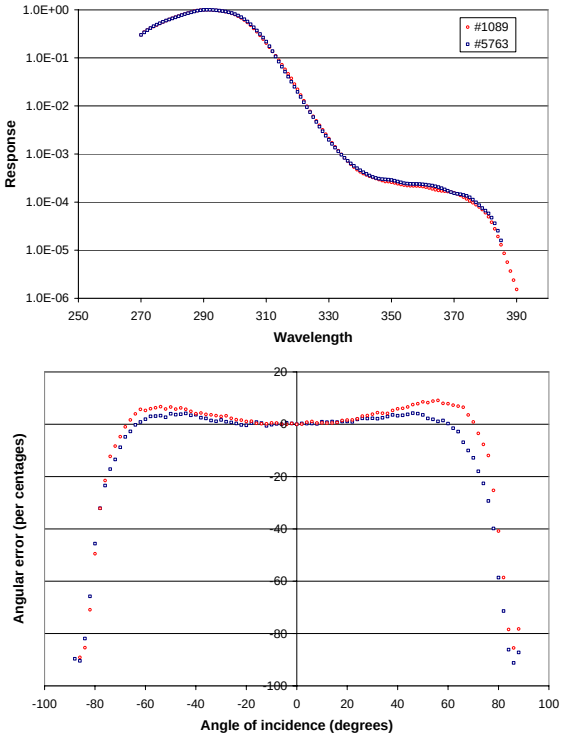

Fig. 1. Spectral (above) and cosine (below) responses of the SL501 sensors. Spectral responses are in logaritmic scale showing the maximal differences. The responses of the upward and downward sensors need to be considered when albedo results are interpreted.

Accurate ground-based long-term albedo measurements of snow are somewhat sparse due to the harsh conditions with snow. Broadband albedo, measured with pyranometers, has been more widely studied (Pirazzini, 2004; Pirazzini et al., 2006; Wuttke et al., 2006), and spectral studies are less (Perovich et al., 2002; Wuttke et al., 2006). Only a few studies on UV albedo of snow have been published, some of them for Antarctic (e.g., Smolskaia et al, 1999; Wuttke, et al., 2006) and few for Arctic snow (e.g., Perovich et al, 2002), and moreover, most of them are campaigns, not continuous high temporal resolution measurements. As far as albedo is concerned, Arctic and Antarctic snow differ from each other especially in two ways: Antarctic snow has smaller snow grain sizes, and has more pure snow unaffected by impurities. Grain sizes of up to approx. 3 mm have been reported for the Arctic snow (Pirazzini et al., 2006). For these reasons, a lower albedo is expected for Arctic snow.

On the basis of earlier studies by others, it was our hypothesis that snow melt will decrease the UV albedo of Arctic snow. Moreover, it was our goal to study, using continuous high temporal resolution 1-min measurements over the whole melt season, how the decrease actually happens: in a single dramatic change, step-by-step or decreasing more or less linearly, little by little. Also, our aim was to study how the temperature of the air and ground, grain size of the snow, and amount of snow, as well as incoming irradiance and cloudiness possibly affect the albedo. To avoid misinterpretation of the experimental data, the error sources have to be considered. A detailed analysis of the uncertainties in UV measurements is available in Bernhard and Seckmeyer (1999), and azimuthal errors in spectral UV data have been explained in Meinander et al. (2006). The effects of instrumental uncertainties, such as calibration and cosine error, atmospheric parameters, solar zenith angle, and geometric aspects, like slopes and shadows, are considered in Sects. 2 and 4, and discussed further in Sect. 5.

2 Materials and methods

2.1 UVB albedo measurements

New polar Arctic measurements on the local UV albedo of snow were planned and carried out in 2007 at Sodankylä, (67°22′N, 26°39′E, 179 m a.s.l.), Finland. For UV albedo measurements, two sensors of the UV Biometer Model 501 from Solar Light Co. (SL501) with similar spectral and cosine responses (Figs. 1 and 2) were used, one facing upwards and the other downwards at a height of 2 m. The SL501 spectral response resembles the action spectrum for erythema, wavelengths in the UVB (280–310 nm) being most weighted. For the albedo measurements, a fixed device for the setting-up and support of the two sensors, including independent leveling possibilities for the upward and downward SL501s, a blower to keep the sensors defrosted, and a data logger system, was planned and constructed at FMI (Fig. 2). Data were logged into the data base from 25 February (day 56) till 15 May (day 135) 2007 at 1-min-intervals. This period included various phases, including both the accumulation and melting of snow. The albedo of snow (A) was calculated from the ratio of downwelling UV irradiance on to upwelling irradiance ($\mathrm{UV_{ery}}\uparrow/\mathrm{UV_{ery}}\downarrow$) measured at 2π.

2.2 Multiband data

In order to gain wavelength-dependent snow albedo information, the reflected irradiance was also measured at 1-min intervals with an multibandfilter radiometer (MBFR, NILU-UV type), placed facing downwards close (3 m) to the SL501 albedo sensors. These multichannel measurements were made from 6 February (day 37) till end of May, 2007. In addition, one NILU-UV radiometer facing upwards was situated close by (30 m), on the roof of the Sodankylä Observatory. The NILU-UV radiometer measures UV in five channels with central wavelengths around 305, 312, 320, 340 and 380 nm, and bandwidths of around 10 nm at FWHM. A sixth channel measures photosynthetically active radiation (PAR) in the range of 400–700 nm. With these channels,

Table 1. The midday SZA values [degrees] (at accuracy of one degree) at Sodankylä (67°22′N, 26°39′E) in 2007, and the time for solar noon [UTC] (at accuracy of ten minutes).

Month	February		March		April		May
Date	1	15	1	15	1	15	1
Solar noon	10.30	10.30	10.30	10.20	10.20	10.20	10.10
SZA	85	80	75	70	63	58	53

UVA and UVB, and erythemally-weighted UV albedo can be calculated from the ratio of downwelling irradiance to upwelling irradiance, UVA↑/UVA↓, UVB↑/UVB↓, and UV_{ery}↑/UV_{ery}↓, measured at 2π. The characteristics of the instruments are described more in detail in Hoiskar et al. (2003).

2.3 Empirical calibration

The aim of this work was to have an understanding of this valuable empirical data set on albedo, measured under the hard conditions of Arctic snow, without introducing any additional uncertainties or errors to the data due to imperfect correction procedures, nor to let the uncertainties and errors in the original data to affect the final results.

During the winter months, the sun does not rise at all at Sodankylä. Even at the beginning of the measurement period in February, the sun is still very low. On 15 March (day 74) the midday SZA falls less than 70.0 degrees for the first time (Table 1). With an SZA larger than 70 degrees, the cosine error increases dramatically (Fig. 1), but as most of the irradiance is then diffuse (at 300 nm more than 90%, e.g. Madronich, 1993), this has only little impact on the measurement results. However, the amount of radiation reaching the Earth is then minimal (UVI<1), increasing the uncertainties in the measurements. On the other hand, during the measurement period, the midday SZA significantly decreases (SZA<55°, UVI>3) as the length of the day grows. To avoid misinterpretation of data, knowledge of the SZA is thus essential.

The optimum calibration of the raw signal requires calibration matrix with SZA and ozone (Webb et al., 2006):

$$E_{\mathrm{CIE}} = (U - U_{\mathrm{offset}}) \times C \times f_n(\mathrm{SZA}, \mathrm{TO_3}) \times \varepsilon(T) \times \mathrm{Coscor} \quad (1)$$

where E_{CIE} is the erythemal effective irradiance, U is the measured electrical signal from the radiometer, U_{offset} is the electrical offset for dark conditions, C is the calibration coefficient (a constant value determined for specific conditions like SZA=40° and O_3=300 DU), f_n is a function that can be expressed as a calibration matrix normalized at, e.g., SZA=40° and O_3=300 DU, $\varepsilon(T)$ is the temperature correction function, and Coscor is the cosine correction function.

The use of Eq. (1) will be discussed more in Sect. 5. Here, the calibration factors (C) of the sensors had been determined by the Finnish Radiation and Nucleation Safety Authority (STUK), before the albedo measurements (in 2005 and 2006), as an average for conditions with 38<SZA<60 degrees. The ratio of the calibration coefficients of the sensors was then C1/C2=1.13. After the albedo measurements, the calibration was carried out again, giving C1/C2=1.19. The sensor with the originally better response was installed to measure the upwelling reflected radiation.

Fig. 2. The holders designed for the albedo measurements.

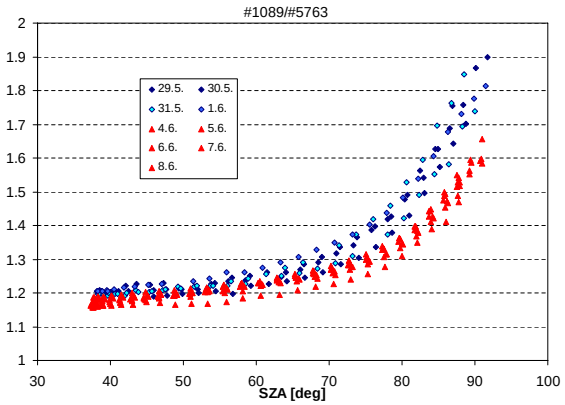

Fig. 3. Results of the post-calibration measurements of the SL501s in 2007.

Keeping in mind that i) the spectral responses of the sensors were measured to be similar (Fig. 1), and ii) the differences in the cosine responses were relatively small (Fig. 1), and iii) we are only interested in the relative signals of these two sensors, the calibration coefficients C1 and C2 might be sufficient for comparison of data representing a narrow SZA range, e.g., within 2–4 degrees. We also know that the upwelling irradiance measured by the SL501 is not as much affected by the cosine error, due to the missing direct component. The albedo derived from the SL501 data may therefore be an overestimation of the real albedo under a clear sky and high solar elevation angles, and uncertainties and errors minimize with increasing diffuse radiation under full cloudiness or lower sun.

However, due to the very low sun (SZA>60°), the use of the laboratory calibration as such was considered unsatisfactory. Several solutions existed: 1) New empirical calibration coefficients (c1 and c2) for the prevailing SZA conditions were produced on 27 March (day 86) by turning both of the sensors upwards and calibrating them against each other; both of them were also calibrated against an SL501 placed on the roof of the observatory. The sensors were again similarly calibrated on 2 May (day 122), and on 11 May (day 131) after snow melt. 2) The data of the prior and subsequent calibrations as a function of SZA were available. These data could be used to produce a simple SZA correction. 3) It would be possible to use a radiative transfer model to calculate the calibration as in Eq. (1).

Here, the empirical calibration approach was used. The aim was to produce empirically calibrated data with error estimates for the prevailing SZAs, without introducing any additional uncertainty or error in the data, due to a simplified SZA correction, as will be discussed more detailed in Sect. 5.

The empirical calibration factors were determined independently using two different SL501 sensors as references. First, the roof SL501 was used as a reference for both of the two albedo measurement sensors. Then, one of the albedo sensors was used as a reference for the other. In addition, empirical calibration procedures were carried out in May after the snow melt.

The empirical calibration factors c1 and c2 were calculated on the basis of the measurements (c1=1.09, c2=0.71 for March; c1=1.29, c2=0.96 for both cases in May). The ratio of the calibration factors in March was c1/c2=1.54 (SZA 67–69°). The ratio of the coefficients was the same whether the independent roof SL501 was used as a reference for both the sensors independently, or one of the two albedo SL501 sensors was used as a reference for the other. In May, the ratio was c1/c2=1.34 (SZA 56–60°). It seems that the ratio c1/c2 could possibly decline with the decline of SZA. The same fall in c1/c2 was evident when studying the data of the solar measurements made in 2007 by STUK for calibrating the same sensors (Fig. 3). It is possible, e.g., that the spectral response of one or both of the sensors had changed since its determination, as will be discussed more in Sect. 5. In any case, we can conclude that we have an SZA dependent-uncertainty in the data.

We can minimize or eliminate the SZA dependency effect by i) picking the corresponding SZA moments for each day, or ii) dividing albedo results into temporal subgroups based on SZA and snow conditions within which the daily variations are similar, and using the same empirical correction coefficient within the shorter period. Both of these approaches were used here, but the first was considered the better of the two, and was used for the more detailed studies for calculation of the empirically calibrated albedo A for SZA 56–60°:

$$A = \frac{c2\mathrm{UV}_{\mathrm{ery}}\uparrow}{c1\mathrm{UV}_{\mathrm{ery}}\downarrow} \quad (2)$$

where $c1$ and $c2$ are the empirically determined calibration factors for the SZA 56–60°, and $\mathrm{UV}_{\mathrm{ery}}\uparrow$ and $\mathrm{UV}_{\mathrm{ery}}\downarrow$ are the simultaneously measured upwelling and downwelling erythemally weighted irradiances.

The first occasion in 2007 on which a midday SZA<60° was achieved, for a period of at least one hour, was on 10 April (day 100). Hence, a continuous temporal data set including data measured with 56<SZA<60 degrees was obtained from 10 April until snow melting. These data were used as the core material for the current study.

The other subgroups used here for temporal data series, were based on SZA and snow, as follows: a) albedo during accumulation of snow in March and at the beginning of April with midday SZA>60° using the March empirical coefficients; b) albedo during the melting period from mid-April until snow melt and end of albedo measurements on 9 May (day 129) with midday SZA<60°. The difference caused by these subgroup calibration differences was also estimated by combining the data sets produced with different calibration coefficients. This comparison reveals the error which had been in the data, if there had been one empirical calibration

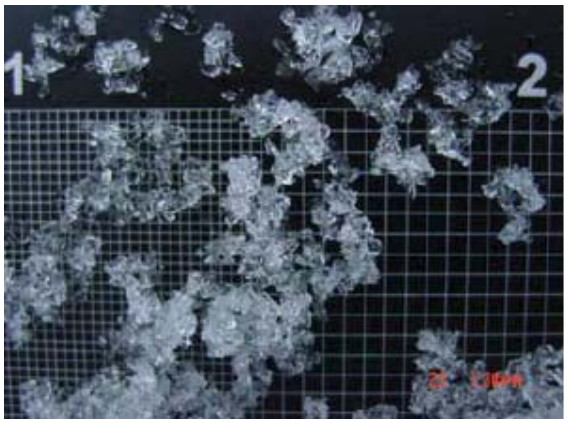

Fig. 4. The grids used for the snow grain size measurements. Numbers 1 and 2 in the figure indicate the corresponding grid sizes of 1 mm and 2 mm.

only, under too large SZA. These data were not used more in-depth studies but rather to understand the long-term variation of the albedo.

2.4 Ancillary data

At Sodankylä, the state of the atmosphere at a height of 2 m is measured once a minute by an automatic weather station (AWS). From these data, information on the beginning of rain, snow depth and cloud cover, e.g., can be gained.

Snow depth (h_s) and grain size (D) were measured at Sodankylä by one of the co-authors (A. Kontu) from November 2006 until 14 May 2007 (day 134), covering the whole albedo measurement period. The grain sizes of all the layers of snow were estimated visually regularly, approx. twice a week, by taking samples of snow on a screen with a mm-grid (Fig. 4). The sampling site was not exactly the same as that of the albedo measurements, but at a distance of 300 m under conditions that can be assumed to be similar. All other activities very close to the albedo measurement were forbidden; the diffusers were, however, cleaned if needed with as little disturbance to the surroundings as possible.

3 Ancillary results

3.1 Snow depth

In 2007, the maximum snow depth at Sodankylä was 68 cm, on 21 March (day 80) (Fig. 6). The second highest value of 67 cm occurred on the day before and the day after, but also on 12 April (day 102). After 12 April, the snow depth decreased monotonically until totally melted.

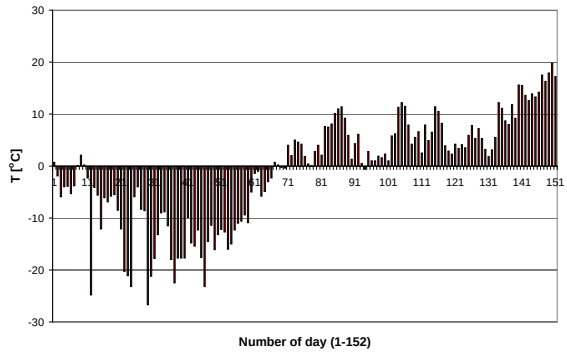

Fig. 5. The maximum air temperature $T_{\max}$ [°C] in 2007 showing the big jump, the "springthaw".

3.2 Temperature

On 7 March (day 66), the daily maximum air temperatures (Fig. 5) indicated a rapid jump, referred here as "a springthaw", from values below zero°C to values above zero. Neither the daily minimum temperatures nor the minimum temperature of the ground showed any similar rapid change.

Between 1 March–15 May (days 60–135), the measured minimum temperature of the ground at 06:00 UTC rose above 0°C on only six days. Otherwise the temperature remained below zero. From this it follows that, apart from these few cases, the snow surface was always frozen in the evening, night and early morning hours, lacking solar warming. On the other hand, the "springthaw" was not enough to start the snow melt alone, thus indicating the importance of radiation as the starting force for the snow melt.

3.3 Snow grain size

In the UV range of wavelengths, the reflected signal comes from the very surface, and only the surface layer grain size data were used here.

In 2007, the measured thickness of the surface layer varied from 0.5 to 35 cm. The surface layer snow grain size results can be divided into two groups: before and after 16 April (day 106) (Fig. 6). Before this date, the snow grain sizes were most often <0.5 mm. Thereafter, the grain size was most often from 1.0 to 2.5 mm, indicating the beginning of the actual snow melt period. However, there are no grain size results available between 10–16 April (days 100–106), and so the snow metamorphosis, with increasing grain size, began sometime within that period.

Grain size data was then studied to determine whether grain size had a relationship to temperature, snow depth and time (the day of the year). Such a relationship would mean that an albedo model could possibly predict Arctic snow UV albedo as a function of time (the day of the year) and temperature, rather than of grain diameter. Using the three variables

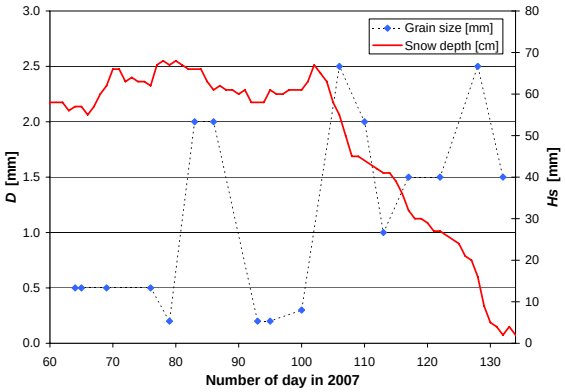

Fig. 6. Snow grain size D [mm] (dashed line with blue squares) and snow depth h_s [cm] (red solid line) in spring 2007.

Table 2. The correlation coefficient (r) of snow grain size and other measured parameters. The number of cases was n=17 between the days of 64–132.

Parameter	r
Minimum ground temperature	0.37
Daily maximum temperature	0.79
Grain size and time (number of day)	0.55
Depth of total snow pack	0.47
Depth of the surface layer	0.22

with the highest linear correlations (Table 2), the empirical relationship, giving an 82% explanation (r^2=0.82) for the Arctic snow grain size during the melting period was:

$$D = -0.04t + 0.19T\,\mathrm{max} - 0.03hs + 4.98 \quad (3)$$

where D is grain diameter, t is time (the day of the year) and Tmax is the daily maximum air temperature at a height of 2 m [°C] and hs is the height of the snowpack. The relationship between snow height and albedo is given in Eq. 4.

Even before the beginning of monotonical decrease in snow depth on 11 April (day 101), there were occasionally days with maximum air temperatures Tmax>0°C. On such days, e.g. on 26 and 29 March (days 85 and 88), the snow grain size was measured to be 2 mm.

4 UV albedo of snow

In addition to SZA information, the results were grouped according to cloudiness, as well as accumulation and melting of snow. We studied first the almost clear sky cases for SZA<60°, followed by cases of variable cloudiness, thereafter cases prior and after melt period, as well as averaged daily albedo during melting. Finally, long term variation in albedo was studied. The most important results were findings of an unexpected diurnal change in albedo during melting.

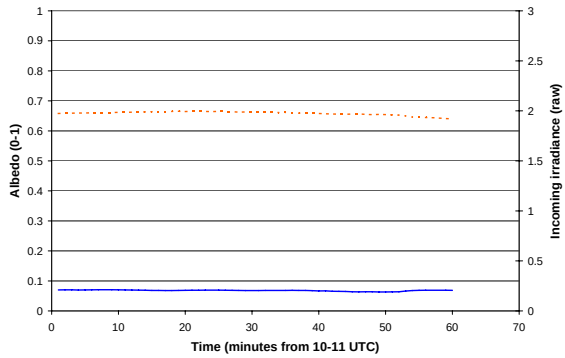

Fig. 7. Flat albedo signal (solid blue line) of a clear sky case (dashed orange line), 10 April (day 100) during the accumulation period.

An overview of the albedo results for SZA<60° in April is shown in Table 3. These results represent all cases of cloudiness. The minimum and maximum of the daily SL501 mean albedo, for SZA 56–60°, are included, indicating the diurnal changes. In some cases the results also suggested an asymmetric albedo, i.e. albedo decreasing from morning to afternoon. The results of the NILU-UV albedo are not included in Table 3, due to their use as complementary data for the current study.

4.1 UV albedo under almost cloudless sky

The signal of the upward sensor was used to study the cloudiness of the sky at exactly the same location and moment at which the albedo measurements were performed. For 56°<SZA<60°, i.e., from 10 April (day 100) onward, the almost-clear or clear-sky cases in April were: the 10, 15, 18, and 22 April (days 100, 105, 108, 112) (Table 3). Of these four cases, the first one occurred at the end of the snow accumulation period, and the last three during the melting season.

4.1.1 Stable albedo during accumulation period

The first case, 10 April (day 100), was an almost clear day during the snow accumulation period. The snow UVB albedo at midday was from 0.64 to 0.66 (Fig. 7), slightly increasing as the sun reached its highest elevation. The slight variation in the incoming irradiance had no effect on the albedo. Similarily, the NILU-UV albedo showed stable UVA and UVB reflectance. The surface layer snow grain size was small, 0.3 mm. The air temperature varied between –19.8 and 2.3°C. At 06:00 UTC the temperature on the surface of the snowpack was –22.9°C. Next, the clear sky cases of the melt season were studied.

Table 3. SL501 UV albedo of Arctic snow at Sodankylä for midday SZA<60° in April 2007. Both the date and number of the day are given. The column of diurnal decline in albedo refers to temporary decline soon after midday (approx. duration), whereas asymmetric decline suggests a decline from morning towards afternoon.

Date	Snow conditions	Cloudiness	Albedo minimum and maximum	Albedo average	Diurnal decline
10.4. (100)	Accumulation period	Almost clear	0.64–0.67 (stable, slightly highest at midday)	0.66	NO
11.4. (101)	Accumulation period	Almost overcast	0.72–0.81 (stable, temporary high values due to snow fall)	0.74	NO
12.4 (102)	Snow melt period starts	Variable	0.66–0.70 (stable, slight indication of diurnal decline)	0.69	NO
13.4. (103)	Melt	Variable	0.66–0.68	0.67	NO
14.4. (104)	Melt	Variable	0.61–0.65 (slight indication of diurnal decline)	0.63	NO
15.4. (105)	Melt	Almost clear	0.55–0.60	0.59	YES (60 min)
16.4. (106)	Rapid melt	Variable	0.56–0.60	0.58	YES (20 min)
17.4. (107)	Rapid melt	Variable	0.54–0.60	0.57	YES (60 min)
18.4. (108)	Rapid melt	Almost clear	0.54–0.60	0.58	YES (100 min)
19.4. (109)	Rapid melt	Variable	0.56–0.63	0.60	YES (60 min)
20.4. (110)	Rapid melt	Variable	0.56–0.62	0.59	YES (60 min)
21.4. (111)	Melt	Variable	0.58–0.61 (stable or slightly lowest at midday)	0.59	NO
22.4. (112)	Melt	Almost clear	0.55–0.60	0.56	YES (100 min)
23.4. (113)	Melt	Almost overcast	0.57–0.61	0.58	NO
24.4. (114)	Melt	Variable	0.51–0.58 (suggesting asymmetric decline)	0.55	YES (80 min)
25.4. (115)	Melt	Variable	0.50–0.54	0.52	YES (80 min)
26.4. (116)	Melt	Variable	0.51–0.52	0.51	NO
27.4. (117)	Melt	Variable	0.46–0.49 (suggesting asymmetric decline)	0.47	NO
28.4. (118)	Melt	Variable	0.46–0.50 (stable or slightly lowest at midday)	0.47	NO
29.4. (119)	Melt	Variable	0.44–0.5 (stable or slightly lowest at midday)	0.47	NO
30.4. (120)	Melt	Variable	0.44–0.46	0.45	NO

4.1.2 Diurnal change in albedo during melting

The second, almost clear sky case of 15 April (day 105) occurred at the very beginning of the snow melt period. During the measurements from 09:00 to 12:00 UTC with SZA 56–60°, the albedo of the snow unexpectedly decreased by 0.05 from 0.6 to 0.55, and then recovered (Fig. 8). The drop in albedo happened soon after solar midday.

The next two almost clear sky cases came in the middle of the melting season, when almost 1/3 of the accumulated snow had melted. On 18 April (day 108), a similar behaviour in snow albedo occurred: a clear change from 0.6 to 0.55 and a recovery back to 0.6. On 22 April (day 112), the same occurred again, but this time the albedo varied at a slightly lower level, changing from 0.58 to 0.53.

Hence, in all three cases at the snow melt period a slight drop in the general albedo level (Fig. 8), asymmetrical to the solar zenith angle, was observed to be superimposed on the general albedo level.

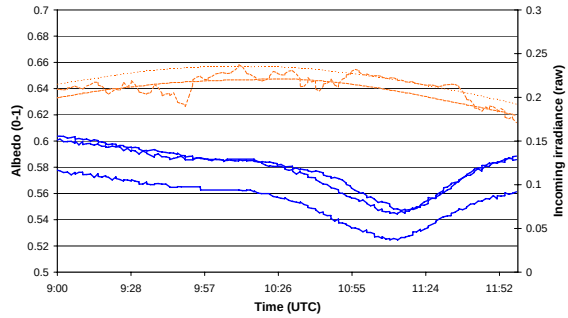

Fig. 8. Diurnal decrease of albedo under clear sky cases of 15, 18 and 22 April (days 105, 108, 112), marked with the solid blue lines. The incoming irradiances are marked with the dashed orange lines.

For a more detailed study, data on temperature, incoming irradiance, and multichannel NILU-UV albedo in the UVA and UVB channels were available:

- 15 April (day 105): the snow depth was 58 cm, and the measured air temperatures were between 2.2–12.2°C. At 06:00 UTC Tmin on the ground was close to zero (0.5°C), and in the next morning it was below the zero (–4.1°C); during that next day the snow depth decreased by 3 cm, with a very thick surface layer (35 cm) and large snow grain size (2.5 mm), indicating a major snow metamorphosis. In the NILU-UV data, both the UVA and UVB albedo decreased, similarily to SL501 albedo.
- 18 April (day 108): air temperature was from –7.8 to 4.2°C, and the snow depth was 45 cm. The next morning, Tmin on of the ground was –4.9°C. In the NILU-UV albedo data, both the UVA and UVB decreased, too. Two days later, a snow grain size of 2.0 mm was measured, while the surface layer depth was 17 cm, both indicating snow metamorphosis and melting continuing intensively.
- 22 April (day 112): air temperatures ranged from –9.9 to 7.9°C, and snow depth was 42 cm. In the NILU-UV data, both UVA and UVB albedo decreased again.

Therefore, we know that the temperature on the snow surface was below zero in the next morning at 06:00 UTC in two cases, but in the first case did temperature remain slightly above zero (0.5°C). The largest grain size of 2.5 mm was measured in this case, too. In all cases, the NILU-UV data confirmed the unexpected discovery using SL501 data: a diurnal change of UV albedo asymmetrically to solar midday was detected using two independent measurement devices.

4.2 UV albedo under variable cloudiness

4.2.1 Stable albedo during accumulating snow

The smallest grain sizes of 0.2–0.3 mm, indicating new snow or snow below-zero conditions during the period of accumulating snow, were observed on four days. Those days were: 20 March; 3, 5, and 10 April (days 79, 93, 95, and 100). The most reliable calibration is for 10 April, which was presented with the clear sky results. The next most reliable cases were on the 3 April: a midday, and stable, albedo of 0.68. On the 5 April the albedo was 0.72, and stable. These cases thus confirm the clear sky case: during the snow accumulation period, the albedo remains stable, increasing slightly, if at all, increasing in the midday period.

4.2.2 Diurnal albedo of melting snow under variable cloudiness

There were two days on which the maximum snow grain size of 2.5 mm in the surface layer, i.e., 16 April and 8 May (days 106 and 128), was measured. On 17 April (day 107) the grain size was measured to be 2 mm, with a 17 cm top layer.

On the basis of the AWS snow depth measurement, the snow pack decreased monotonically since 12 April (day 102). We therefore assume the period of rapid melting, with the largest grain sizes, to have taken place during, at least, the days of 16–20 April (days 106–110). 8 May (day 128) is at the end of the measurement period with the snow partly melted, revealing the ground, too. For this reason these data were not included the cases presented here:

- 16 April (day 106): the thickness of the surface layer was 35 cm, whereas during the three earlier measurements, during the whole accumulation period, it had varied from 1 to 6 cm. Hence, a major change in the snow, with a deep metamorphosized and homogenized surface layer, took place on that day. The cloudiness was highly variable, yet a drop in the SL501 albedo after midday from 0.6 to 0.55 took place.
- 17 April (day107): the snow depth was 50 cm at 06:00 UTC, and 46 cm at 18:00 UTC. The next day it was 45 cm. From this we can conclude that conditions similar to those on the clear sky day of 15 April (day 105), continued on days 106 and 107, despite the variable cloudiness. The SL501 albedo dropped from 0.6 to 0.55 after midday, and then recovered.
- 19 April (day 109): the results showed a similar diurnal decrease in albedo, too.
- 20 April (day 110): the cloudiness was highly variable, but the SL501 albedo decreased from approx. 0.6 to 0.55, as had been found in the clear sky cases earlier presented.

Hence, these cases with variable cloudiness confirm the clear sky SL501 cases during the melting season: an albedo slightly decreasing by 0.05 soon after midday, and then recovering after that.

4.3 Albedo before and after the period of diurnal change

The period of variable albedo began on the 15 April, and ended on 25 April (days 105–115). The cases before and after these dates show a flat albedo signal (Table 3). Prior to the diurnal albedo change, a flat signal of $A>0.6$ was detected. On the basis of the snow depth data, this was the period before the snow melt. Following the variable diurnal albedo, there was a diurnally-stable midday albedo, of $A<0.5$. These results would suggest that, after a drop in the albedo to a level of 0.5, the diurnal change in the albedo disappears, possibly signaling the end of some stage in the melting process.

4.4 Average daily UV albedo of melting snow

The midday erythemally weighted UV albedo ranged from 0.6 to 0.8 in the accumulation period, and from 0.5 to 0.7

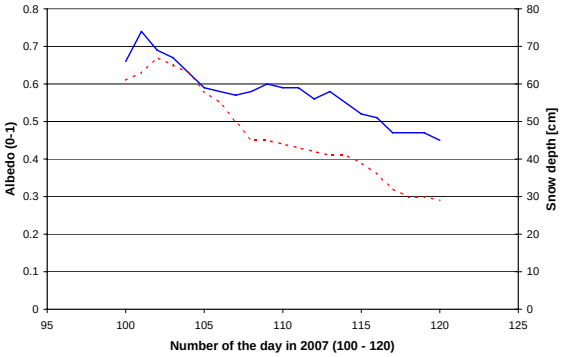

Fig. 9. The measured snow depth (dashed red line) and the measured albedo (solid blue line). Average of snow UV albedo for midday and snow depth for each day during melt season from 10 to 30 April (days 100–120) in spring 2007.

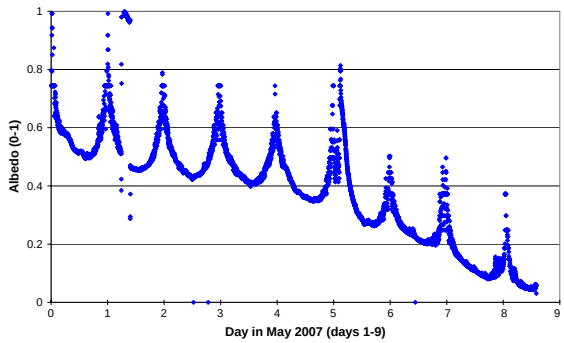

Fig. 10. May albedo data with the U-shape appearing each day. Only cases SZA<85° for each day from 1 to 9 May (days 121–129) shown here.

during melting. The averaged daily UV albedo of snow for 56<SZA<60 degrees during the melt was a second-order polynomial as a function of snow height:

$$A = -6\mathrm{E} - 05h_s^2 + 0.0114h_s + 0.1809 \quad (4)$$

where h_s is the snow height [cm]. This formulation, with r^2=0.86, is adjusted for the melt period only (data of days 100–120, Fig. 9).

4.5 Long term variation in SL501 UV albedo

Studying the time series of the continuous 1-minute albedo data, the SZA-dependency (U-dependency) of the differences between the responses of the sensors is evident (Fig. 10), as well as the occurrence of evening and night-time with no incoming irradiance. On closer inspection, when the midday data with SZA 56–60° are used, the albedo signal is quite flat (e.g., Fig. 7).

An increase in albedo from 0.72 to 0.81 was detected on 11 April (day 101), possibly due to new snow (as evidenced from the AWS data for the same time), but further study is beyond the scope of the present work. More detailed study would require a detailed analysis focusing on the AWS rain data.

The SL501 midday albedo results for Arctic snow, can be divided into two groups: an albedo of 0.6–0.8 between 22 March–14 April (days 81–104) (the accumulation period), and an albedo of 0.4–0.6 between 15 April–3 May (days 105–123) (snow melt). These data were calibrated by using different empirical calibration factors for cases SZA<60° and for SZA>60°. In studying the hypothetical effect of using the March coefficients (midday SZA>60°) for May data, an error<6% was caluculated for 09:00–12:00 UTC. The use of different coefficients for the prevailing SZA conditions, as presented earlier, reduced this error in the long term data.

The albedo of snow was recorded to lower little by little as the snow melted (Fig. 10). The results would also suggest a possible SZA asymmetry in snow albedo (Table 3). The calibration procedures presented in this study have no effect on this finding, as it is a question of asymmetry according to noon: a SZA correction would produce SZA symmetric data if the prevailing conditions had not changed between noon and afternoon. Yet, to study this SZA asymmetry further would require knowledge on the factors affecting the SZA correction in the data (such as the ratio of direct-to-diffuse irradiance). After the beginning of May, the albedo results were characterized more by the amount of ground visible, than by the actual albedo properties of the snow.

5 Discussion

5.1 About errors and uncertainties

Here, use was made of erythemal UV albedo measurements by broadband SL501 radiometers with similar spectral responses, thus resulting in errors of less than 1% due to differences in the sensors (WMO, 1996). According to Hülsen and Gröbner (2007), the typical total uncertainty for SL501 instruments is from 1.7 to 4.3 %. The calibration of the sensors was made before (in 2005 and 2006) and after (2007) the albedo measurements. Prior to the albedo measurements, the spectral and cosine responses of the sensors had been determined to be similar, as presented in Figs. 1 and 2. In the albedo data, the SZA-dependency (U-shape) became evident. We suspected this to be due to changed spectral response. This was confirmed in the post-calibration measurements (Fig. 4). On the basis of our experience, the spectral responses of SL501 sensors may change in time, and therefore the responses should be determined on a regular basis, preferably every year or every second year.

Basically, a drift in a sensor response might be nonlinear, either momentary or lasting, or even occasionally due

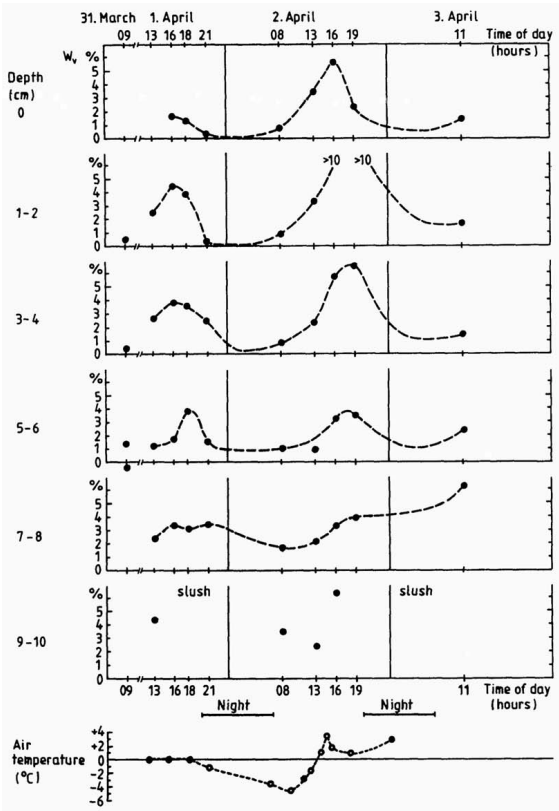

Fig. 11. Measured diurnal variation of liquid water content at different depth levels of snow pack.

to environmental conditions, such as the internal humidity of the sensor, temperature, total ozone, etc. Here, the problem was solved by empirical calibrations, as described, and by using only the data within a SZA-range of 56–60 degrees for the analysis. Thereafter, the error in the data due to the sensors can be determined on the basis of the post-calibration measurements (Fig. 3): within an SZA of 56–60°, the SZA dependency, i.e., the U-shape due to difference in the spectral responses of the sensors, caused an error of less than 3%. The U-shape in the results might also be partly due to the different components the upward and downward radiometers see (for downward looking sensor the diffuse and specular, while for the upward sensor the direct and diffuse). Even if both had identical spectral and angular responses, the errors induced by the combination of imperfect response functions and radiance distributions may be different for the two radiometer orientation. Also, the different orientations of the radiometers might possibly alter the internal temperature and thus affect the responsitivity.

With these empirically calibrated data, any possible dependency of albedo on solar zenith angle could only be compared for similar conditions of cloudiness and solar zenith angles. The empirical calibration provides a direct comparison of the two radiometer readings but then only a smaller SZA range is utilized and the SZA influence on the albedo remains unresolved. On the other hand, any albedo asymmetry close to midday could be reliably studied for SZA 56–60° without introducing any additional uncertainty or error in the data due to a simplified SZA correction. For example, a SZA and ozone dependent calibration factor can not correct the data unless a proper spectral reponse funtion of the sensor is used. An example of such an error (an outlier) possibly introduced by a simple SZA correction in the albedo data is presented in Wuttke et al. (2006). On the basis of our experience, an optimal 1-min SZA correction, for both the upward and downward broadband sensor independently, would require knowledge on the spectral and cosine response functions, temperature correction functions, and 1-minute data on the radiation distribution, and the ratio of the diffuse-to-direct irradiance affected by clouds, ozone, aerosols, albedo and SZA. Hence, the general measurement equation requires a thorough characterization of the two radiometers but may then remove the most SZA dependent artefacts. How ever, the problem of changed spectral response remains. According to our experience, if applying this equation, the spectral responses are to be determined prior and after the measurements.

5.2 Diurnal variations in the albedo

An unexpected diurnal change in UV albedo, measured by the SL501 sensors, was detected during the melt period at SZA $<60°$. The albedo decreased by approx. 0.05 soon after midday and then recovered to the same, or almost the same, level. If this diurnal variation in albedo were to be due to any shadowing effects, rather than the properties of snow, the shadowing would be best seen under clear sky conditions, and not in cloudy situations. Here the diurnal change was evident for all states of sky. Furthermore, as the sensor facing upward was at the same height as the sensor measuring reflected radiation, any shadowing would necessarily be evident in the signal of the incoming irradiance at some time during the day (although not necessarily at the exactly same time as the downward sensor recorded the reflected radiation from the shadowed surface). The incoming irradiance did not indicate any such shadowing (Fig. 8). Also, when the site for the albedo measurements was chosen, the horizon towards the South was selected to be without shadowing. The pole and the frame supporting the sensors were also placed to the North to avoid shadows. Finally, the same diurnal decrease was evident in the data of the NILU-UV radiometer measuring the upwelling radiation close to the SL501.

Our findings on UV albedo of natural melting snow are in accordance with the speculations presented by Wiscombe

and Warren (1980). They explain that snow albedo decrease due to liquid water content increase follows from the fact that liquid water replaces air between ice grains. As the refractive index of liquid water is close to ice for wl<5000 nm, the replacement of air by liquid water between ice grains could increase the effective grain size.

Furthermore, the results of diurnal variation of liquid water content at various snow layers (Fig. 11) by one of the authors (M. Toikka) suggest that the temperature rise increases the liquid water content first on the surface layer of the snowpack. Then, as the temperature drops toward evening and night, the liquid water falls into deeper layers. Thus, liquid water on the snow surface, as well as the effective grain size due to liquid water, would increase only temporarily. When the temperatures drop, most of the liquid water is no longer in the surface layer, but in the layers below. Thus, these diurnal results of the liquid water in snow anticorrelate with the diurnal albedo results, offering empirical explanation to our albedo observations. Earlier, Kuusisto (1984) has also stated that the thick snow cover in northern Finland starts to release water from surface layers through percolation channels, while the deeper layers of the cover are still relatively unmetamorphosized. Opposite to this, in southern Finland, the thin snow cover is quickly metamorphosized all the way to the ground surface.

Similar results on diurnal decline of albedo were observed by Pirazzini in the Antarctica (personal communication, 2007), although not reported in the article by Pirazzini (2004). The same diurnal decline was observed by them in Arctic conditions, too (Pirazzini et al., 2006). In the Antarctic conditions, their observation for the diurnal decline was later in the afternoon. Earlier, a minimum albedo has been detected by McGuffie and Henderson-Sellers (1985) in Canada, too. They suggested the albedo decrease to be due to snow grain metamorphosis caused by heating of the surface.

According to Grenfell et al. (1994) the albedo of snow depends on its physical properties, and varies according to wavelength. Here, the spectral distribution of the snow albedo between UVA and UVB could be studied on the basis of a multiband filterradiometer facing downwards, and another upward MBFR radiometer nearby. These complementary results confirmed the findings of diurnal variability in the UVB albedo.

5.3 Asymmetric albedo

In the current study some indication on the asymmetric UV albedo was observed, too (Table 4). Also, McGuffie and Henderson-Sellers (1985) have reported of diurnal hysteresis of snow albedo, i.e. that the albedo is different for the same solar elevation angle at different times of day. They suggest the variation should be attributed to the diurnal deposition and evaporation of a hoar-frost coating on the snow surface. Pirazzini (2004) and Wuttke et al. (2006) have recorded more recently albedo results in the Antarctic sites with several instruments, which are opposite to the ones predeicted by theory. They both found a decline of albedo for increasing SZA. A possible levelling error was not consired the source for this observed diurnal cycle. Wuttke et al. (2006) speculate the reason for this opposite dependence of albedo on SZA to be rather due to changing snow conditions due to the steady solar insolation. Pirazzini et al. (2006) found similar results in Arctic conditions, too. Earlier, McKenzie et al. (1996) speculated that their UV albedo measurements of long grass (no snow) showing slightly higher albedos in the afternoon than in the morning might be due to either various error sources (e.g., leveling, angledependent reflections) or real changes in the surface, (e.g., morning dew evaporating or light dependent plant physiology). Hence, it is essential to understand and separate all the factors affaecting the albedo results.

5.4 Polar snow and albedo

When Arctic and Antarctic albedo are compared, the reasons to differences might be several, in addition to snow grain size and amount of impurities; e.g., Hansen and Nazarenko (2004) have studied soot climate forcing in the Arctic via snow and ice albedos. If we consider other possible contributors to differences in albedo, these might be due to, e.g., snow grain shape and topography. Differences in precipitation snow grain shapes might, in principle, be due to differences, e.g., in the atmospheric moisture (Antarctic air is known to be dryer than the Arctic atmosphere), temperature (Antarctic atmosphere is colder than Arctic, and sometimes stratospheric air masses reach down into the troposphere there), and aerosol amounts (cleaner Antarctic air). Also, although the measurement area is quite flat, the local albedo may be affected by the topography.The irradiance ratios are influenced not only by the local snow albedo underneath the radiometers, but also the combination of low-albedo and high-albedo surfaces within a larger radius. E.g., Kylling et al. (2000) have studied the effect of inhomogeneous surfaces on the effective albedo. However, although the local albedo is affected by the regional albedo, our measurements at a height of 2 m may be considered to represent local albedo. Furthermore, a term “effective local albedo”, for instance, could be more descriptive for the albedo quantity derived in our study. The critical question is whether the downwelling radiation field on the snow surrounding the observation point (i.e., in the area where the observed $F(\uparrow)$ originates), differs systematically from $F(\downarrow)$ at the observation point. If not, $F(\uparrow/\downarrow)$ should be an accurate estimate of the local albedo. Additionally the snow albedo may have a specular component (Mie scattering), giving rise to a SZA dependent variation. At high SZAs, the Mie scattered photons scattered forward into the snowpack have a greater chance of escaping the snow and still reach the downward-looking sensor. This could partly explain the diurnal U-shape of the albedo. Hence, the specular component may have an important role.

During the winter of 2006/2007, permanent snow fell in Sodankylä in the middle of October, but almost all the snow melted at the end of November (Kontu et al., 2007). Snow density during the winter months was determined to be from 0.18 to 0.21 g/cm^3 (Kontu et al., 2007). In addition to the temperature, other environmental factors, like rainfall, wind, humidity, cloudiness, as well as the properties of the snow and the ground under the snow, affect the process of snow melt. On the basis of AWS data on snow depth, 12 April (day 102) was the date after which the snow amount only decreased from one day to the next. Hence, these data are in accordance with the start of diurnal albedo change detected from 15 until 25 April (days 105–115). The prior and subsequent albedo was stable.

6 Conclusions

For snow the grain size has been reported to vary generally by less than 50% on the topmost 10–20 cm of snow (Warren and Wiscombe, 1980). We found that in the Arctic conditions of Sodankylä, belonging to the global snow class of Taiga snow (Sturm et al., 1995), the grain sizes of the top layer varied from 0.2 to 2.5 mm, containing variation by 125%. Thus the variability in grain size of the Arctic snow in Finland, and the maximum grain sizes were found to be extreme.

In a literature review presented in Warren and Wiscombe (1980) for their albedo model, it was found that some papers reported the albedo to increase with solar zenith angle. We found a slight increase at midday during the accumulation period with small grain size. This could possibly be physically explained by an increase in the specular component at midday compared to morning or afternoon. The midday increase would then be the bigger the smaller the grain size.

In summary, our results suggest:

- a high and stable midday albedo for SZA 56–60° during the snow accumulation period; albedo maximum in solar midday during accumulation period in clear sky and under variable cloudiness
- possibly UV albedo asymmetric to solar zenith angles
- a diurnal change of 0.05 in albedo during the melt period, in cases of clear sky and variable cloudiness with SZA 56–60°
- a little by little decrease in the general abedo level with the melting of snow
- a stable lower albedo at the end of the melt period.

With the help of ancillary data on temperature, grain size and snow depth, these are explained by a high albedo induced by a small grain size during accumulation time, and a diurnal change in albedo by snow grain metamorphosis caused by heating of the surface, melting some of the snow to liquid water, and the metamorphosis ceasing by the end of the melt period. These findings were made possible only by continuous high temporal resolution measurements, and would not have been found by measurement campaigns.

The advantages of snow albedo measurements in Finland are the facts that here i) the snow cover melts every year, and ii) we have five out of the six global snow classes (Sturm et al., 1995), only the alpine snow missing, and iii) the topography in Finland is flat, thus favorable to albedo studies, iv) clean snow can be found in the remote areas of the Finnish Lapland, vi) the snow grain size of the top layer varies greatly from small to extremely big grain sizes of 2.5 mm. In the future, we intend to continue ground-based UV albedo measurements under these conditions in Finland, and comparisons are planned to extend to Arctic-Antarctic, and between UV and broadband albedo. The liquid water content of the top layer of the snow from midday for two hours forward at intervals of approx. half an hour or even less should be measured in the melt period together with continuous high temporal resolution (1-min) albedo measurements and the ancillary data as presented here. Possibly some other parameters may also be included (including spectral albedo), or the temporal resolution of the parameters may be improved to study the diurnal decrease and the possible asymmetry. Wiscombe and Warren (1980) have reported that only a small number of albedo models had been put forward prior to their model, reflecting the lack of high-quality data against which to check such a model, and the fact that some of the data are contradictory. The albedo model introduced in their paper is in use in the commonly-applied radiative transfer (RT) model Libradtran (Mayer and Kylling, 2005), and currently highly referred to. Using our empirical data, a UV albedo parametrization for Arctic snow during accumulation and melt time periods could be elaborated, and the existing albedo models verified.

Acknowledgements. The authors are grateful to A. Aarva, H. Suokanerva, S. Suopajärvi, V. Postila, and P. Koivula for their help with operation of the SL501 sensors. The Academy of Finland has given financial support for this work (FARPOCC-project).

Edited by: M. Blumthaler

References

Arola, A., Kaurola, J., Koskinen, L., Tanskanen, A., Tikkanen, T., Taalas, P., Herman, J.R., Krotkov, N., and Fioletov, V.: A new approach to estimating the albedo for snow-covered surfaces in the satellite UV method, J. Geophys. Res., 108(D17), 4531, doi:10.1029/2003JD003492, 2003.

Bais, A. F. and Dan Lubin, D.: Chapter 7: Surface Ultraviolet Radiation: Past, Present, and Future, In: WMO: Scientific Assessment of Ozone Depletion: 2006, World Meteorological Organization Global Ozone Research and Monitoring Project-Report No. 50, Final Release: February, 2007.

Bernhard, G. and Seckmeyer, G.: Uncertainty of measurements of spectral solar UV irradiance, J. Geophys. Res. 104(D12), 14 321–14 345, 1999.

Blumthaler, M. and Ambach, W.: Solar UVAlbedo of various surfaces, Photochemistry and Photobiology, 48(1), 85–88, 1988.

Bony, S. Colman, T., Kattsov, V. M., Allan, R. P. Bretherton, C. S., Dufresne, J.-L., Hall, A., Hallegatte, S., Holland, M. M., Ingram, W., Randall, D. A., Soden, B. J., Tselioudis, G., and Webb, M. J.: REVIEW ARTICLE, How Well Do We Understand and Evaluate Climate Change Feedback Processes?, J. Climate, 19, 3445–3482, 2006.

Forster, P., Ramaswamy, V., Artaxo, P., Berntsen, T., Betts, R., Fahey, D. W., Haywood, J., Lean, J., Lowe, D. C., Myhre, G., Nganga, J., Prinn, R., Raga, G., Schulz, M., and Dorland, J. V.: Changes in Atmospheric Constituents and in Radiative Forcing, in: Climate Change 2007: The Physical Science Basis. Contribution of Working Group I to the Fourth Assessment Report of the Intergovernmental Panel on Climate Change edited by: Solomon, S., Qin, D., Manning, M., Chen, Z., Marquis, M., Averyt, K. B., Tignor, M., and Miller, H. L., Cambridge University Press, Cambridge, United Kingdom and New York, NY, USA, 2007.

Grenfell, T. C., Warren, S. G., and Mullen, P. C.: Reflection of solar radiation by the Antarctic snow surface at ultraviolet, visible, and near-infrared wavelengths, J. Geophys. Res., 99(D9), 18 669–18 684, 1994.

Hansen, J. and Nazarenko, L.: Soot climate forcing via snow and ice albedos, Proc. Natl. Acad. Sci., 101, 423–428, doi:10.1073/pnas.2237157100, 2004.

Hoiskar, B. K., Haugen, R., Danielsen, T., Kylling, A., Edvardsen, K., Dahlback, A., Johnsen, B., Blumthaler, M., and Schreder, J.: Multichannel Moderate-Bandwidth Filter Instrument For Measurement Of The Ozone-Column Amount, Cloud Transmittance, And Ultraviolet Dose Rates, Appl. Optics, 42, 3472–3479, 2003.

Hülsen, G. and Gröbner, J.: Characterization and calibration of ultraviolet broadband radiometers measuring erythemally weighted irradiance, Appl. Optics, 46(23), 5877–5886, 2007.

IPCC: Climate Change 2007 – The Physical Science Basis, Contribution of Working Group I to the Fourth Assessment Report of the IPCC, (ISBN 978 0521 88009-1 Hardback; 978 0521 70596-7 Paperback), http://www.ipcc.ch/ipccreports/ar4-wg1.htm, 2007.

Kontu, A., Pulliainen, J., Heikkinen, P., Suokanerva H., and Takala, M.: Validation of Microwave Emission Models by Simulating AMSR-E Brightness Temperature Data from Ground-based Observations, Proc. 2007 IGARSS, Barcelona, Spain, 2007.

Kuusisto, E.: Snow accumulation and snowmelt in Finland. Helsinki, Publications of the water Research Institute 55, ISBN 951-46-7494-4, 149 p., 1984.

Kylling, A., Persen, T., Mayer, B., and Svenøe, T.: Determination of an effective spectral surface albedo from ground-based global and direct UV irradiance measurements, J. Geophys. Res., 105(D4), 4949–4959, 2000.

Madronich, S.: Environmental UV Photobiology, Chap. 1, The Atmosphere and UVB Radiation at Ground level. Plenum Press, New York, 1993.

Mayer, B. and Kylling, A.: Technical note: The libRadtran software package for radiative transfer calculations – description and examples of use, Atmos. Chem. Phys., 5, 1855–1877, 2005, http://www.atmos-chem-phys.net/5/1855/2005/.

McGuffie, K. and Henderson-Sellers, A.: The diurnal hysteresis of snow albedo, J. Glaciol., 31(108), 188–189, 1985.

McKenzie, R. L., Kotcamp, M., and Ireland, W.: Upwelling UV spectral irradiances and surface albedo measurements at Lauder, New Zealand, Geophys. Res. Lett., 23(14), 1757–1760, 1996.

Meinander, O., Kazadzis, S., Blumthaler, M., Ylianttila, L., Johnsen, B., Lakkala, K., Koskela, T., and Josefsson, W.: Diurnal discrepancies in spectral solar UV radiation measurements, Appl. Opt. 45, 5346–5357, 2006.

Perovich, D. K., Grenfell, T. C., Light, B., and Hobbs, P. V.: Seasonal evolution of the albedo of multiyear Arctic sea ice, J. Geophys. Res., 107(C10), 8044, doi:10.1029/2000JC000438, 2002.

Pirazzini, R.: Surface albedo measurements over Antarctic sites in summer, J. Geophys. Res., 109, D20118, doi:10.1029/2004JD004617, 2004.

Pirazzini, R., Vihma, T., Granskog, M., and Cheng, B.: Surface albedo measurements over sea ice in the Baltic Sea during the spring snowmelt period, Ann. Glaciol., 44, 7–14, 2006.

Smolskaia, I., Nunez, M., and Kelvin, M.: Measurements of Erythemal Irradiance near Davis Station, Antarctica: Effect of. Inhomegeneous Surface Albedo, Geophys. Res. Lett., 26, 1381–1384, 1999.

Sturm, M., Holmgren, J., and Liston, G. E.: A seasonal snow cover classification system for local to global applications, J. Clim., 8, 1261–1283, 1995.

Tanskanen, A. and Manninen, T.: Effective UV surface albedo of seasonally snow-covered lands, Atmos. Chem. Phys., 7, 2759–2764, 2007, http://www.atmos-chem-phys.net/7/2759/2007/.

UNEP: Environmental Effects of Ozone Depletion: 2002, Assessment, United Nations Environment Programme. ISBN 92-807-2312-X, http://www.unep.org/OZONE/pdf/eeap-report2002.pdf, 2002,

Warren, S. G. and Wiscombe, W. J.: A model for the spectral albedo of snow. II: Snow containing atmospheric aerosols, J. Atmos. Sci., 37, 2734–2745, 1980.

Weatherhead, B., Tanskanen, A., Stevermer, A., Andersen, S., Arola, A., Austin, J., Bernhard, G., Browman, H., Fioletov, V., Grewe, V., Herman, J., Josefsson, W., Kylling, A., Kyrö, E., Lindfors, A., Shindell, D., Taalas, P., and Tarasick, D.: Chapter 5: Ozone and Ultraviolet Radiation. ACIA 2005. Arctic Climate Impact Assessment. Cambridge University Press, 1042, 151–182, 2005.

Webb, A., Gröbner, J., and Blumthaler, M.: A practical guide to operating broadband instruments measuring erythemally weighted irradiance, WMO SAG UV, COST-726, ISBN 92-898-0032-1, 2006.

Wiscombe, W. J. and Warren, S. G.: A model for the spectral albedo of snow. I: Pure snow, J. Atmos. Sci., 37, 2712–2733, 1980.

WMO: WMO GAW report 120. WMO-UMAP Workshop on Broad-Band UV Radiometers, Garmisch-Partenkirchen, Germany, 22–23 April 1996, WMO TD No. 894, 1996.

Wuttke, S., Seckmeyer, G., and König-Langlo, G.: Measurements of spectral snow albedo at Neumayer, Antarctica, Ann. Geophys., 24, 7–21, 2006

Reprinted from
Atmospheric Chemistry and Physics, 13, 3793–3810,
doi:10.5194/acp-13-3793-2013

II

Atmos. Chem. Phys., 13, 3793–3810, 2013
www.atmos-chem-phys.net/13/3793/2013/
doi:10.5194/acp-13-3793-2013

Atmospheric Chemistry and Physics Open Access

Spectral albedo of seasonal snow during intensive melt period at Sodankylä, beyond the Arctic Circle

O. Meinander[1], S. Kazadzis[2], A. Arola[3], A. Riihelä[1], P. Räisänen[1], R. Kivi[4], A. Kontu[4], R. Kouznetsov[1], M. Sofiev[1], J. Svensson[1], H. Suokanerva[4], V. Aaltonen[1], T. Manninen[1], J.-L. Roujean[5], and O. Hautecoeur[5]

[1]Finnish Meteorological Institute, P.O. Box 503, 00101 Helsinki, Finland
[2]Institute for Environmental Research and Sustainable Development, National Observatory of Athens, Greece
[3]Finnish Meteorological Institute, Kuopio Unit, P.O. Box 1627, 70211 Kuopio, Finland
[4]Finnish Meteorological Institute, Arctic Research Centre, Tähteläntie 62, 99600 Sodankylä, Finland
[5]Meteo-France/Centre National de la Recherche Scientifique (CNRS), Toulouse, France

Correspondence to: O. Meinander (outi.meinander@fmi.fi)

Received: 17 August 2010 – Published in Atmos. Chem. Phys. Discuss.: 9 November 2010
Revised: 13 March 2013 – Accepted: 13 March 2013 – Published: 10 April 2013

Abstract. We have measured spectral albedo, as well as ancillary parameters, of seasonal European Arctic snow at Sodankylä, Finland (67°22′ N, 26°39′ E). The springtime intensive melt period was observed during the Snow Reflectance Transition Experiment (SNORTEX) in April 2009. The upwelling and downwelling spectral irradiance, measured at 290–550 nm with a double monochromator spectroradiometer, revealed albedo values of ∼0.5–0.7 for the ultraviolet and visible range, both under clear sky and variable cloudiness. During the most intensive snowmelt period of four days, albedo decreased from 0.65 to 0.45 at 330 nm, and from 0.72 to 0.53 at 450 nm. In the literature, the UV and VIS albedo for clean snow are ∼0.97–0.99, consistent with the extremely small absorption coefficient of ice in this spectral region. Our low albedo values were supported by two independent simultaneous broadband albedo measurements, and simulated albedo data. We explain the low albedo values to be due to (i) large snow grain sizes up to ∼3 mm in diameter; (ii) meltwater surrounding the grains and increasing the effective grain size; (iii) absorption caused by impurities in the snow, with concentration of elemental carbon (black carbon) in snow of 87 ppb, and organic carbon 2894 ppb, at the time of albedo measurements. The high concentrations of carbon, detected by the thermal–optical method, were due to air masses originating from the Kola Peninsula, Russia, where mining and refining industries are located.

1 Introduction

Snow albedo is a key issue for climate change studies in radiative transfer (RT) calculations and satellite applications. The albedo of a surface results from the target's capability to wavelength-dependently reflect the direct and diffuse irradiance. For snow, the albedo is typically very high compared to other natural objects or surfaces. In the ultraviolet (UV) and visible range (VIS), the albedo for clean snow is ∼0.97–0.99 (Grenfell et al., 1994; Hudson et al., 2006), consistent with the extremely small absorption coefficient of ice in this spectral region (Wiscombe and Warren, 1980; Warren et al., 2006; Warren and Brandt, 2008). As the wavelength increases, ice absorption increases and masks the absorbing effect of impurities in snow, like black carbon (BC) (Hadley and Kirschtetter, 2012).

The measured albedo is determined by the target's basic properties and the overall environment around the target. According to the literature (Wiscombe and Warren, 1980; Warren and Wiscombe, 1980) and RT models (Flanner et al., 2007; Gardner and Sharp, 2010; Mayer and Kylling, 2005), the effective snow grain size, i.e., grain size and shape distributions, or specific surface area (Domine et al., 2007), is the most important factor to determine snow albedo. According to theory (Wiscombe and Warren, 1980), snow albedo decreases as the grain size increases, as a smaller effective radius increases the probability that an incident photon will scatter out of the snowpack (Gardner and Sharp, 2010). Other

important snow properties include the liquid water content, the concentration of absorbing inorganic and organic impurities in the snow, as well as their vertical distribution in the snowpack together with snow depth and albedo of the underlying ground. During melt, snow undergoes a metamorphosis process that modifies the spectral albedo (e.g., Weller, 1972). The liquid water content of snow increases, and wet snow has a lower albedo than dry snow (e.g., Blumthaler and Ambach, 1988). Also, as snow ages, with or without melting, the grain size increases and therefore albedo lowers (Wiscombe and Warren, 1980).

In turn, the key environmental factor is the solar illumination (direct and diffuse irradiance), depending on the solar zenith angle (SZA), cloud cover, and atmospheric composition (Flanner et al., 2007; Mayer and Kylling, 2005). Albedo increases as the solar elevation decreases, i.e., albedo is SZA dependent (e.g., Fig. 4 of Gardner and Sharp, 2010), because at higher angles of incidence a photon will, on average, travel a path that is closer to the surface, increasing its probability of experiencing a scattering event that will send it out of the snowpack. In addition, albedo is a scale-dependent variable, but can be measured at any selected height. The operational meteorological local albedo is defined to be measured at a standard height of 1–2 m (WMO, 2008, I. 7). Albedo measurements are influenced not only by the local snow albedo underneath the measuring radiometers, but also the combination of low-albedo and high-albedo surfaces within a larger radius. Therefore, an effective albedo is often defined to describe the net effect of the albedo, as derived by comparison with a model (Kylling et al., 2000; Bernhard et al., 2007). Finally, the ability to accurately detect the albedo of a surface depends on the measurement uncertainties and errors introduced by the measuring systems (e.g., Bernhard and Seckmeyer, 1999).

In this work, the main aim was to catch the short period of the most intensive snowmelt with the highly accurate Bentham spectrometer setup, and study snow albedo together with key parameters of seasonally melting snow beyond the Arctic Circle. The snow albedo measurements were made at Sodankylä, Finland (67°22′ N, 26°39′ E), belonging to the northern boreal forest zone with the snow type of taiga. Our main focus was on spectral albedo, combined with broadband up-welling and down-welling radiation measurements, various ancillary environmental data, and with the modeling of diffuse and direct spectral irradiance and snow albedo. In RT calculations, the aim was to study how big effect (error) would a measured realistic change in diurnal albedo values cause on the modeled irradiance, if the observed diurnal albedo change of melting snow were ignored. In addition, RT calculations were performed to get an estimate of the edge effect (forest surrounding an open field) on the detected albedo. In albedo simulations, our aim was to study if the simulated data agreed with the measured albedo when the known big snow grain sizes of melting snow and measured Sodankylä snow impurity concentrations of elemental and organic carbon were applied. For the purpose of this study, elemental carbon is used synonymously with black carbon due to their measurement technique dependence in snow impurity studies. Our aim was also to show why our snow impurity concentrations, analyzed with the thermal–optical method, were higher than expected when compared to Doherty et al. (2010).

2 Materials and methods

For the albedo measurements, a Bentham-spectrometer setup with two entrance optics, as well as broadband UV SL-501 radiometers and CM-14 albedometers, performed irradiance measurements during the Snow Reflectance Transition Experiment SNORTEX-2009. For investigating the effect of snow albedo on the modeled irradiance, we used the Libradtran RT model (Mayer and Kylling, 2005), with our measurement data as model input. For the albedo simulations we utilized the SNICAR on-line version (Flanner et al., 2007), with our measured snow data as model input.

2.1 The SNORTEX experiment

The Snow Reflectance Transition Experiment (SNORTEX, 2008–2010) aimed at acquiring in situ measurements of snow and forest properties in support of the development of modeling tools, and validating coarse resolution satellite products (Roujean et al., 2009, 2010). The goal was to integrate its results into operational chains devoted to map snow properties from the MetOp satellite within the framework of the SAF (Satellite Application Facilities) Land, Climate and Hydrology activities, supported by EUMETSAT and the national meteorological services. The SNORTEX study area was located in the Finnish Lapland beyond the Arctic Circle, and benefited from existing facilities provided by the Finnish Meteorological Institute – Arctic Research Center (FMI-ARC), based in Sodankylä (67°22′ N, 26°39′ E, 179 m.a.s.l.). The SNORTEX sites consisted of (i) the Arctic Center at Sodankylä; with temporal daily data series of various parameters collected within SNORTEX, as well as operationally by FMI; and (ii) SNORTEX experiment sites in the Sodankylä region, representing different types of environment, e.g., open area, forested area, snow on the lake, etc.

2.2 Albedo measurements

For detecting snow albedo (A), we measured the upwelling $Q\uparrow$ and downwelling radiation energy $Q\downarrow$ hemispherically at 2pi:

$$A = \frac{Q\uparrow}{Q\downarrow}\,. \tag{1}$$

Three different types of simultaneous albedo measurements at Sodankylä during SNORTEX-2009 (April period) were utilized for our study (Table 1): (i) spectral measurements

Table 1. The hemispherical spectral and broadband albedo measurements used for the study.

Instrument	Spectral range	Spectral resolution	Measurement place
Bentham spectrometer	290–550 nm	10 nm spectral	FMI Sodankylä Arctic Center, open field exclusively chosen for Bentham measurements within SNORTEX, size 80 m north–south, and 50 m east–west
Solar Light SL-501 radiometer	280–400 nm	One band with erythemal weight function (280–320 nm most weighted)	FMI Sodankylä Arctic Center operative albedo field, size 16 m × 16 m
Kipp & Zonen CM-14 albedometer	310–2800 nm	One band, no weight function, the relative spectral transmittance is largest (> 0.5) at 400–900 nm	Three separate SNORTEX experiment sites: Kommattivaara (a lightly forested hill), Mantovaaranaapa (completely open aapa mire) and Korppiaapa (also completely open aapa mire)

at 290–550 nm, on an open field at the Arctic Center (primary site of the study, Fig. 1), exclusively measured within the SNORTEX campaign during the intensive melt period of 20–24 April; (ii) continuous broadband UV albedo measurements on the operative albedo field of the FMI, Arctic Center (1 min data measured every year since 2007, during spring time snow months, Fig. 1); and (iii) broadband albedometer measurements on three SNORTEX sites representing three vegetation types (Table 1). For the analysis of the in situ albedo data and the model data, we focused on data for solar zenith angle (SZA) $< 70°$ (06:00–14:00 UTC). The amount of radiation reaching the Earth is minimal at larger SZA, (UV Index < 1), increasing uncertainties in the measurements.

Fig. 1. The Bentham spectral albedo field (left), and the broadband SL-501 UV albedo field (right), at the Sodankylä Arctic Research Center.

2.2.1 Bentham spectrometer

The Bentham spectroradiometer, with a special setup of two identical entrance optics for albedo measurements, participated in the SNORTEX-2009 campaign (April period). Down-welling and up-welling spectral measurements of global irradiance (irradiance received hemispherically by a flat sensor surface) were performed at the 290–550 nm wavelength range. The measurement height was 2.5 m in order to allow the maximum distance from the spectrometer to the sensor holder (minimum loss in the optical cable length), and to be as close to the 2 m height recommendation by WMO as possible. These Bentham measurements were used to retrieve the spectral albedo $A(\lambda)$ of the snow surface for the spectral range 290–550 nm with a 10 nm wavelength step. The up and down measurement scans were made one after another. The measurement procedure and the parameter setup of these highly accurate measurements is not a trivial task. Here, a 6 min time step was used for clear sky conditions, and a 2 min step was elaborated for variable cloudiness, to optimize the measurement setup and minimize the changes in SZA and cloudiness during the measurements.

The Bentham albedo field had been protected for this particular purpose since autumn, to provide undisturbed snow. The mast and holder with the proper leveling possibility had been tailored and mounted in autumn, and the instrument was transported from FMI Helsinki for the purpose. The intensive melt period started 21 April, and the Bentham was operated from 20 to 25 April. At the end of the measurement period, the snow was practically melted from this particular field. For 21 and 23 April, the sky conditions were with variable cloudiness, resulting changes in the radiation field. 22 April was a cloudless day, and 24 April an overcast day with mainly diffuse sky conditions (Fig. 2).

The size of the open Bentham albedo field was 80 m north–south, and 50 m east–west, situated close to the Sodankylä ozone sounding station. The surface underneath the two Bentham sensors (at the height of 2.5 m from the ground) was covered with snow in a radius of more than 10 m on the south, west and east direction, and up to 3 m in the north direction.

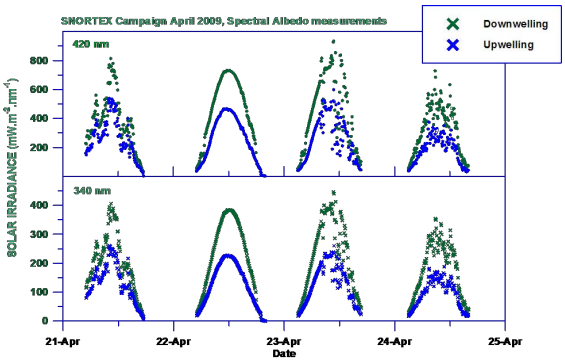

Fig. 2. Global downwelling and upwelling irradiance for 340 nm and 440 nm during the campaign.

The field of view of the sensors was mostly free. Direct Sun irradiance was blocked by trees from 03:00 to 05:00 UTC, and after 17:00 UTC. In addition, shadows of the trees were covering all or part of the snow surface underneath the instruments in the morning till 06:10 UTC, and after 15:30 UTC.

The Bentham spectroradiometer system consists of a commercially available Bentham DM-150 double monochromator with a focal length of 150 mm, and with gratings of 2400 lines mm^{-1}. The entrance and exit slit widths were chosen to yield a nearly triangular slit function, with a full width at half maximum (FWHM) resolution of 0.74 nm. The solar irradiance is sampled through a specially designed entrance optics (CMS Schreder, Model UV-J1002), connected to the port of the spectroradiometer through a quartz fiber. The fiber optic splits and leads to two identical entrance optics receivers (diffusers) that can be distinguished through an internal switch. The angular response of the two diffusers is better than 2 % for incident angles less than 70 degrees. As the instrument is designed for outdoor solar measurements, the whole spectroradiometer system, including the data-acquisition electronics, is contained in a temperature-controlled box that is stabilized to a predetermined temperature with a precision of 0.5 K. Absolute irradiance scale calibration is performed using measurements of calibrated 1000 W quartz halogen lamps. To measure at locations far from its laboratory, a portable irradiance scale was devised. It is composed of a portable lamp enclosure (calibrator), a set of 100 and 250 W tungsten halogen lamps, and a feedback system. For this particular campaign, the two entrance optics were used for measurements of the down-welling and the up-welling global solar irradiance. The calibration of the instrument was performed at the beginning and at the end of the campaign, showing deviations of less than ±1 % for the entire spectral range based on measurements of the three lamps used for the calibration procedure.

2.2.2 Broadband UV albedo

Broadband UV albedo data were provided by continuous bi-hemispherical data of two radiometers (Model SL501, Solar Light Co.) which were located 20 m away from the site of the spectroradiometric measurements. The UV albedo is detected above the FMI Sodankylä Arctic Center operational albedo field (size 16 m × 16 m, low metal fences protecting the operational field). These measurements were started in 2007 as part of the International Polar Year IPY (2007–2008) ORACLE-O3 cluster project (Ozone layer and UV radiation in a changing climate evaluated during IPY, http://www.awi-potsdam.de/atmo/ORACLE-O3, Meinander et al., 2008, 2009). Two well maintained and calibrated SL501 sensors with similar spectral and cosine responses were used (Fig. 1 of Meinander et al., 2008); one facing upwards, and the other downwards, at a height of 2 m. The data are recorded in 1 min intervals and stored in the FMI climate database. The SL501 resembles the action spectrum from erythema (Seckmeyer et al., 2005), which also has a contribution from the UVA. The SL501 measured dose of the radiant energy Q_{ery} is calculated as the temporal and spectral integral of the convolution of the global solar spectral irradiance and the erythemal response (Grainger et al., 1993), measured hemispherically at 2 pi. To gain the erythemally weighted broadband albedo A_{ery}, the ratio of the hemispherically measured up-welling (↑) to down-welling (↓) UV solar radiation is then calculated:

$$A_{\mathrm{ery}} = \frac{Q_{\mathrm{ery}}\uparrow}{Q_{\mathrm{ery}}\downarrow} \tag{2}$$

where Q_{ery} is the bi-hemispherically measured temporal (T) and spectral (λ) integral of the convolution of the solar radiance (E) and the erythemal response function (ε) is

$$Q_{\mathrm{ery}} = \int_{T1}^{T2}\int_{\lambda 1}^{\lambda 2} E(\lambda, T)\varepsilon(\lambda)\mathrm{d}\lambda\mathrm{d}T. \tag{3}$$

As the hemispherical global solar spectral irradiance is used for the calculation of the dose, the measured downwelling irradiance includes both the direct and diffuse components, and the upwelling part consists of the hemispherically reflected global spectral diffuse radiance, similarly to any non-weighted sensor used for an albedo measurement.

2.2.3 Broadband visible albedo

The broadband albedo observations from three days during SNORTEX-2009 were measured with a Kipp & Zonen CM-14 albedometer (www.kippzonen.com) at one non-weighted broadband from 310 to 2800 nm, whose accuracy may be estimated at 5–10 % relative. The general technical data of CM-11 pyranometer applies to the CM-14 albedometer, and the relative spectral transmittance is largest (> 0.5) at 400–900 nm.

The observations were made at SNORTEX sites of (a) Kommattivaara (a lightly forested hill) during 20 April, (b) Mantovaaranaapa (a completely open aapa mire) during 22 April, and (c) Korppiaapa (also a completely open aapa mire) during 23 April. The CM-14 instrument was carefully leveled on a tripod and operated without breaks during the field day. During postprocessing, the data were corrected for the shadowing effect of the tripod legs and imperfections in cosine response at high solar zenith angle conditions after Michalsky et al. (1995).

All three days were effectively clear-sky, with no significant cloud disturbances on the observed irradiance. There were no obstructions in the path of the incoming solar radiation during the measurements of 22 April or 23 April 2009. Some tree shadows disturbed the measurements on 20 April. The instrument was mounted at a height of 1.5 m, implying an observed area with a radius of 15 m. Thus, the observed albedo may be seen as representative of the areal mean of the mire (or open woodland in the case of 20 April).

2.3 Snow properties

2.3.1 Snow depth and snow liquid water content

Snow depth was measured manually with a measurement stick in the Bentham spectral albedo field. For the measurements of snow liquid content in the same field, we used the commercially available Snow Fork by Toikka Oy (www.toikkaoy.com). The sensor is a steel fork that is used as a microwave resonator. The Snow Fork measures the electrical parameters: resonant frequency, attenuation, and 3 dB bandwidth. From these measurement results, the liquid water content is calculated as described in detail in Sihvola and Tiuri (1986), and Toikka (1992). In addition to the actual snow liquid water content, the snow impurities and grain sizes, hardness and density, etc., may affect the measurement results.

2.3.2 Snow grain size, temperature and snowball-test

The measurements on snow grain size, snow temperature and the snowball test were made at the Bentham spectral albedo field, on the north side of the field where the Bentham was measuring towards the south, and thus with snow facing similar radiation conditions as those under the Bentham sensor.

The temporal changes in the snow grain sizes and shapes, according to Fierz et al. (2009), were both estimated visually with a mm-grid, and the snow grains on the grid were also macro-photographed to allow image analysis afterwards. An example of such a photo is in Meinander et al. (2008, Fig. 4).

The snow temperature was measured with a digital Printel thermometer (www.printel.fi). The thermometer was calibrated using isopropanol measured with a Fluke accuracy thermometer in the measured temperatures from $-20.72\,^{\circ}\mathrm{C}$ to $+1.218\,^{\circ}\mathrm{C}$ at 99 different temperatures. Empirical calibration was calculated and the measured snow temperatures were corrected using this calibration.

A simple "snowball-test" was also made periodically in the Bentham albedo field. The test is in regular use in all Sodankylä snow research. This practical test tells if the properties of snow are such that one succeeds in making a snowball out of the snow on the ground. Snowballs can only be made when snow properties are suitable for making them; i.e., snow contains water but is not yet too wet. With the test, for instance the start of snowmelt can be easily detected, as corresponding snow property information would be hard to determine otherwise.

2.3.3 Snow elemental carbon and organic carbon contents

At the Sodankylä Arctic Center, snow surface (first 2 cm of snow) samples have been collected from the same location for impurity analysis since 2009 on a weekly basis during snow time, the location protected with reindeer fences. Sampling and analysis follow the same general methodology developed by Forsström et al. (2009) and Aamaas et al. (2011), in which snow samples are melted in a microwave oven, then filtered through sterilized micro-quartz filters (55 mm diameter) using a hand pump attached to the filtering system to create a vacuum during filtering. The volume of meltwater is needed for concentration conversions. Dried filters are analyzed with a Thermal/Optical Carbon Aerosol Analyzer (OC/EC) (Sunset Laboratory Inc., Forest Grove, USA) for their elemental carbon (EC) and organic (OC) concentration, following the NIOSH 5040 protocol developed by Birch (2003). The thermal–optical method was created by Birch and Cary (1996), where a detailed description of the method is presented.

One of these routine snow impurity samplings took place during the intensive melt days (24 April), one right before (17 April) and one after (30 April). The data from 2009 are used in our study related to the measured albedo. The data from 2009–2011 are used for the transport analysis to study the origin of the BC in snow.

2.4 Other ancillary data

The Sodankylä automatic weather station (AWS) measures the state of the atmosphere at a height of 2 m once a minute. From these data, information on, e.g., the onset of precipitation, snow depth and cloud cover, can be gained. The Sodankylä Arctic Center measurement program includes a large variety of environmental parameters; here use was made of, e.g., the measured aerosol parameters and total ozone as input values for the RT calculations (Sect. 2.5).

2.5 RT and albedo model calculations

We used the Libradtran RT model (Mayer and Kylling, 2005) to calculate the up-welling and down-welling diffuse and

direct spectral irradiances during a cloudless day (22 April). The measured spectral albedo (Bentham spectroradiometer data), total ozone (Sodankylä ozone sounding; Brewer spectrophotometer data), and aerosol properties measured with a Precision Filter Radiometer/SunPhotometer (http://litdb.fmi.fi/) were used as main inputs for the RT calculations. Our hypothesis was the following: the measured diurnal albedo change is big enough to have an impact on the solar irradiance at the surface level. The albedo values used in the RT model were the ones measured with the spectroradiometer. Solar irradiances were calculated from the RT model using the morning albedo value and were compared with irradiances that were calculated using the albedo as measured at various times during the day. A difference in irradiance in [%] between the morning and afternoon would indicate changes in radiative forcing caused by changes in albedo due to melting snow. Only relative changes were considered when comparing measurements with the model to eliminate the effect of absolute calibration scale uncertainties of the measurement data. The absolute calibration scale should not affect the albedo measured by the Bentham spectroradiometer, as the same monochromator/light directing system is used for both the upward and downward sensors.

The edge effect on albedo (i.e., the effect of forest surrounding the open albedo field) was studied on the assumption of a Lambertian surface (Meinander and Räisänen, 2010) (see also Sect. 4.7).

We also used the Snow, Ice, and Aerosol Radiation (SNICAR) on-line version (Flanner et al., 2007) to gain simulated data on snow albedo to compare with in situ albedo data. The measured parameter values of snow depth, snow grain size and elemental carbon (BC) content were used as input values to simulate a clear sky case (day 22 April) and a diffuse sky case (24 April). In SNICAR-online, there are two types of black carbon input parameters: (1) uncoated (mimicking hydrophobic particles), with properties tuned to achieve a mass absorption cross-section of 7.5 $m^2\,g^{-1}$ at 550 nm (Bond and Bergstrom, 2006); and (2) sulfate-coated black carbon (mimicking hydrophilic black carbon), which is composed of a weakly-absorbing shell (sulfate) surrounding black carbon, resulting in an absorption enhancement (per unit mass of black carbon) of about 1.5 (Bond et al., 2006). Most of the BC in the snow at Sodankylä can be assumed to originate from longer transport, and therefore the BC in snow can be assumed to become hydrophilic. Yet, with the current snow analysis data we cannot determine that all BC would be hydrophilic. Therefore, in our simulated data, we used both these options separately to compare their effect on albedo. For melting seasonal snow in northern Finland, the averaged snow density values of 329 $kg\,m^{-3}$ for forest, and 349 $kg\,m^{-3}$ for open sites, have been reported (Kuusisto, 1984). From these we used the value reported for northern Finland.

2.6 Source identification for snow impurities

The impurities at melting snow surface can be either brought there together with the snowfall or result from dry deposition to the snow surface. To identify the sources of snow pollution at Sodankylä we have used the mixing ratio of elemental carbon in surface snow samples collected weekly in Sodankylä during 2009–2011. According to simple models of wet deposition, the concentration of a pollutant in precipitation is proportional to the column concentration in the air below a cloud layer. Thus concentrations in samples of fresh snow can be used to quantify in-air concentrations during preceeding snowfall.

A qualitative analysis of the origins of pollution in the air can be done with simple backward trajectories. For quantitative and comparatively accurate assessment in case of limited observational information, the so-called "footprint" computations can be used (e.g., Prank et al., 2010). This approach is based on solving the adjoint dispersion equation for, e.g., an isolated episode registered by a single measurement device. The resulting fields describe the sensitivity distribution of that particular measurement to a source location, e.g., the observed values can be affected only by the emission fluxes from the area where the sensitivity is nonzero.

The modeling was performed with SILAM (System for Integrated modeLing of Atmospheric coMposition) version v5_2. The system has Eulerian non-diffusive advection scheme of Galperin (2000) and the adaptive vertical diffusion algorithm of Sofiev (2002). For a more detailed description we refer to Sofiev et al. (2008) and http://silam.fmi.fi. The verification of the model has been performed within the scope of EU-GEMS project (http://www.ecmwf.int/gems) and is continued on a routine basis within the EU-MACC (http://www.gmes-atmosphere.eu).

The meteorological fields from short-term operational forecasts of the European Centre for Medium-range Weather forecasts (ECMWF) were used as a driver for SILAM. The adjoint simulations were performed with resolution 0.5×0.25 degree on a domain 10–60° E. 55–75° N (shown in Fig. 9) with 8 vertical layers of thickness from 30 m at surface to 2000 m within a height range from surface to 6 km. The footprints were taken for the layer 150–300 m, which we expect to correspond to the height of industrial emissions due to combustion.

The observational function of atmospheric concentrations corresponding to measured in-snow concentrations was taken to be uniform with height from the surface to the bottom of a cloud and weighted by snowfall intensity in time, so total sensitivity is unity. The footprints were calculated for each sample separately. To minimize the effect of dry deposition and to ensure the consistency between observed and modeled snowfalls, only the cases were selected when snowfall was reported by both the weather station at Sodankylä and the meteorological driver, reporting more than 1 mm snowfall within 24 h before the sample collection and

the amount of the precipitation agreeing within a factor of 2 between them. The volumetric content of black carbon was used as a tracer of anthropogenic pollution. With above criteria out of 70 snow samples we selected 10 "clean" (< 20 ppb of BC) and 12 "dirty" (> 30 ppb of BC) samples and calculated the average footprint for both classes. Since the size of air-borne black carbon is unknown, the footprints were calculated for passive gas with no deposition, for 1.5 µm (fine) particles and for 20 µm (coarse) particles.

3 Results

3.1 Spectral albedo

The measured Bentham albedo values were 0.5–0.7 for the ultraviolet and visible range, both under clear sky and variable cloudiness (Figs. 2 and 3). During the four days of intensive melt, the spectral Bentham albedo at 330 nm decreased from ∼ 0.65 (the morning of the first day) to 0.45 (the afternoon of the fourth day). At 450 nm, the decrease was from 0.72 to 0.53, accordingly. During each day, the albedo decreased on average by approx. 10 %. The albedo was higher in the morning than in the afternoon, i.e., the albedo was asymmetric to SZA. Also, in the mornings, the albedo signal was slightly higher than it had been the previous evening.

To understand the spectral behavior of albedo under our circumstances (i.e., intensively melting snow with big effective snow grains), we studied the measured albedo as a function of wavelength (Fig. 4). Irrespective of any possible albedo SZA symmetry or asymmetry, the snow albedo at any given time increased as a function of wavelength. During the clear sky day of 22 April, an average difference of ∼ 8 % in the calculated albedo was found when comparing UVB (at 320 nm) and visible (at 550 nm) wavelengths. Deviations up to 5 % from this spectral behavior could be seen during the day. We then calculated the mean values for UV-B (at 310 nm), UV-A (at 330–360 nm) and visible (at 450–550 nm). The regression of snow albedo A for UV-A, applying the shortest measured wavelengths of A(UV-B), were in our Bentham spectra:

$$A(\text{UV-A}) = 1.0049A(\text{UV-B}) + 0.0054, \ (R^2 = 0.9744), \quad (4)$$

$$A(\text{VIS}) = 1.1602A(\text{UV-B}) - 0.0213, \ (R^2 = 0.6012), \quad (5)$$

for SZA < 70.0 degrees, under clear sky conditions on melting snow measured at 2.5 m height.

3.2 Broadband UV and VIS albedo

The broadband erythemal SL-501 UV albedo, representing the FMI operational albedo field, decreased both within a day (from morning till afternoon), and as a function of time (days) (Fig. 5). For example, on 22 April, from 06:00 UTC to 12:00 UTC, the decline in albedo was 10 %. The UV albedo

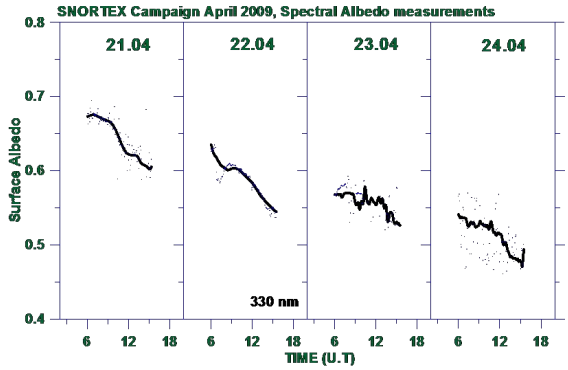

Fig. 3. Snow albedo at 330 nm, during 21–24 April, 2009. Blue dots represent 6 min period measurements, and black line time interpolated 1 min ratios.

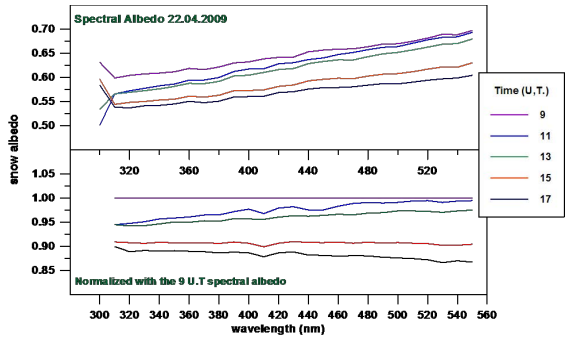

Fig. 4. The snow albedo increased as a function of wavelength. (Upper panel) Spectral snow albedo for 22 April for different periods during the day. (Lower panel) Ratio of each of the above spectral measurements to the 09:00 UTC measurement.

values (17–30 April) ranged from 0.51 to 0.38 in the morning, and from 0.48 to 0.37 in the afternoon.

The broadband CM14 albedo revealed values of ∼ 0.6–0.75 (Fig. 6). The data of three various SNORTEX sites showed that (a) the broadband albedos were significantly lower than for even aged midwinter snow (measured during other SNORTEX experiments), (b) observed albedos decrease during a single field day owing to snow metamorphism and surface melt, and (c) the level of the broadband albedos fell consistently during the four-day period as the melt season progressed. The very large albedo decrease observed on 20 April arises from a combination of snowmelt and metamorphism effects and lengthening tree trunk shadows, which both decrease the observable reflected radiation flux. The different albedo decrease rates observed on 22 and 23 April are most likely a result of several factors. The snow characteristics at the observed site were somewhat different, and also the air temperature on the night between 22–23 April was below freezing only for a few hours (not shown),

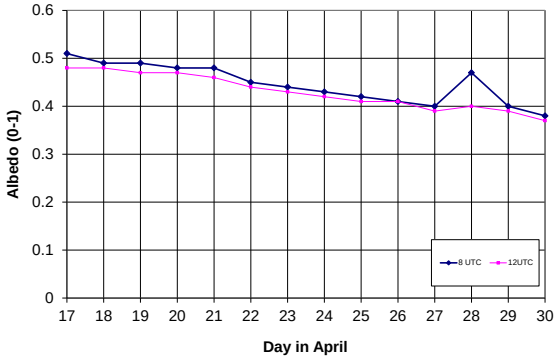

Fig. 5. The broadband erythemal UV albedo of snow from 17 April to 30 April 2009, measured with SL-501 radiometers, at the operational albedo field of the Sodankylä Arctic Research Center. The albedo declined slightly during each day: blue line for 08:00 UTC, purple line for 12:00 UTC.

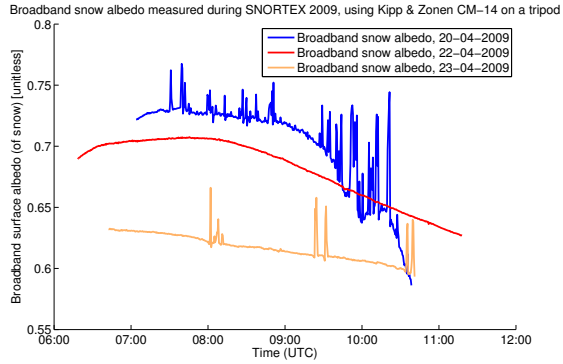

Fig. 6. The broadband VIS albedo of snow measured with CM4 at SNORTEX sites of **(a)** Kommattivaara (a lightly forested hill) during 20 April, **(b)** Mantovaaranaapa (a completely open aapa mire) during 22 April, and **(c)** Korppiaapa (also a completely open aapa mire) during 23 April.

implying that the snow surface did not have the chance to refreeze properly, leading to a lower albedo already at the start of the measurement day of 23 April.

3.3 Snow properties and AWS results

Between 20–24 April, an intensive snowmelt process took place at the open field of our Bentham spectrometer albedo (Table 2). On 20 April, there was a new snow layer on the snow surface. The snowball tests revealed that the snow was not yet melted to the extent that snowballs could be made. This was the case also the next day 21 April at 13:50 UTC. Later that day, the conditions changed. At 16:38 UTC, the snowball test was successful. After almost 2 h later, the snowball test failed again. The new snow layer could still be seen on the snow surface, although it was now wet. On 22 April, the new snow layer could no longer be separated at the surface. The snowball test was successful during the day. The melt process was under way. The snow depth (data not shown) was manually measured to change from 30 cm to totally melted in some places. The automatically measured snow height at the Sodankylä AWS measurement place declined from 48 cm to 38 cm.

The data on snow liquid water content (Fig. 7), as a function of time and snow depth, at the same field as the Bentham measurements, showed that when the first measurement was taken (at about 07:00), the highest water content was at the deepest depth (24 cm). The changes in the water content were such that the water content started to increase in the surface layer, whereafter the surface values dropped. At the same time the concentrations in the deeper layers were first lower and increased later.

The snow temperature of the same area showed both a vertical and temporal increase during the study days (Fig. 6 of Meinander et al., 2010), and the snow surface observations

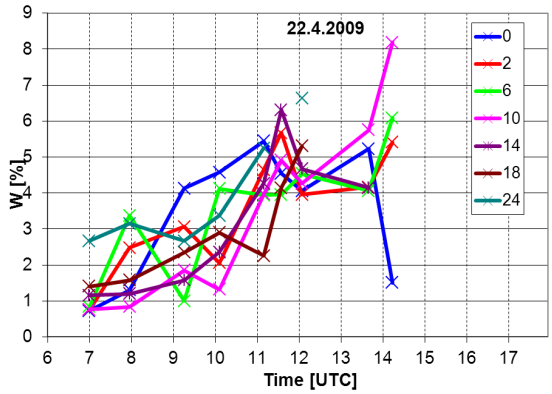

Fig. 7. The snow liquid water content on 22 April as a function of time and snow depth (0, 2, 6, 10, 14, 18, 24 cm). The data shows that the water content first increased in the surface layer. Later, the water content was higher at deeper layers.

indicated an intensive melt on 22 April, with snow grain sizes changing from 0.25 mm up to 3 millimeters (Table 2). Also, on the basis of image analysis, the snow surface grain shapes changed from 21 April to 22 April: there were first surface hoar crystals (SHsu), then rounding surface hoar (SHxr) and then later melt forms, rounded polycrystals (MFpc) (Table 2).

The AWS data showed that at 06:00 UTC the air temperatures were $< 0\,^{\circ}\mathrm{C}$ during 20–21 April, and $> 0\,^{\circ}\mathrm{C}$ on 22–24 April. During those days, the maximum air temperatures varied from -2.5 to $5.4\,^{\circ}\mathrm{C}$, and at 18:00 UTC, the air temperatures were always $> 0\,^{\circ}\mathrm{C}$, with maximum temperatures from 0.5 to $9.5\,^{\circ}\mathrm{C}$.

Table 2. Snow conditions during the time [UTC] of the spectral albedo measurements. The snow grain shapes are according to Fierz et al. (2009).

Day/Time	Snow Surface
20 April	
17:46	Snowball test: negative
21 April	
09:15	Snow surface layer 0.5 cm with surface hoar crystals (SHsu), under that a layer with melt forms, rounded polycrystals (MFpc)
13:50	Snowball test: negative, grain size 0.25 mm, new snow layer exists, icy snow
14:45	Snow surface layer 0.5 cm with rounding surface hoar (SHxr), under that a layer with melt forms, melt freeze crust (MFcr)
16:38	Snowball test: positive, 1 mm grains melted together, sunny cloudless calm weather; melting snow, new snow layer exists
17:30	Wet new snow layer exists, surface layer of 0.5 cm
18:19	Snowball test: negative
22 April	
09:35	Surface layer of 0.5 cm with melt forms, rounded polycrystals (MFpc), under that a layer with melt forms, melt freeze crust (MFcr)
12:35	No new snow layer, icy snow, 0.5 cm surface layer with grain minimum size 0.25 mm, maximum size 1 mm, all stick together; the rest of the snow is 1.5–5 mm grains and sticks together
13:00	1 mm grains, sunny weather, clear sky
13:58	2 mm grains on the surface
15:17	Snowball test: positive, 2–3 mm grains on the surface, wet snow
16:08	3 mm grains
17:12	Snowball test: positive, 3 mm grains, wet snow
20:17	Wet snow, 3 mm grains, fluffy surface

3.4 RT modeling

For the clear sky day 22 April, for SZA 55–70, the spectroradiometer measured albedo minimum was $A_{\min} = 0.54$, the maximum $A_{\max} = 0.65$ at 330 nm. The measured spectral albedo $A(\lambda)$ was dependent on the time t. These were used as input parameter values for the RT calculations. The irradiance spectra were modeled from 06:00 UTC to 14:00 UTC to produce the spectra S1(t, $A_{\min}(L)$), S2(t, $A_{\max}(L)$), and S3(t, $A(\lambda)$), where S1, S2 and S3 are the various types of modeled spectra (from 1 to 3), t is time, A is albedo, $A_{\min} = 0.54$, $A_{\max} = 0.65$, L is the Lambertian assumed reflectance, and $A(\lambda, t)$ is the actual measured spectral albedo. Instead of the Lambertian RT model assumption of an isotropic surface (independent of the direction), the actual measured spectral albedo $A(\lambda, t)$ is influenced by the forward-scattering nature of snow. A Lambertian albedo can still depend on wavelength. The values of the other measured input parameters for both types of RT calculations were as follows: Ångström parameters $\alpha = 1.253$ and $\beta = 0.038$ (for the calculation of aerosol optical thickness $\tau a = \beta\lambda^{-\alpha}$), and 347 DU for ozone. The maximum difference was observed when $A_{\max}$ was used for the model calculations, as in reality the albedo was decreasing as a function of time. For the same reason, the measured irradiance was expected to be closest to the case of $A_{\min}$, as confirmed by our modeling results (data not shown). The differences were 2.5–4.5 % for wavelengths from 320 to 400 for this one day showing the 10 % change in the albedo (Fig. 8). The difference was calculated to be up to 9 % when using the results for the 4 days of the melting snow period.

3.5 Snow impurities

Sodankylä results on the impurities in snow, in parts per billion by mass (ppb), showed that during the intensive snowmelt period (24 April), EC was 87 ppb, and OC 2894 ppb (Table 3). Prior to this, both EC (16 ppb) and OC (988 ppb) concentrations were much lower. At the very end of the melt period (30 April), EC remained at the same level as during the melt (86 ppb), but the OC was as high as 7172 ppb. The Sodankylä snow impurity results from years 2009–2011 suggest some increase of OC toward the late spring (many days with > 2000 ppb in April). The EC results showed, in addition to the increase in EC toward spring, some variability from day to day, with concentrations between 9–106 ppb.

Table 3. Results of EC and OC [ppb] in the snow samples of the Sodankylä Arctic Research Center, since the beginning of 2009 until the snowmelt in spring 2011.

	Concentration			
Date	μg L^{-1} Organic C	μg L^{-1} OC ±	μg L^{-1} Elemental C	μg L^{-1} EC ±
21.1.2009	1751.1	90.3	31.6	4.3
30.1.2009	1051.2	55.5	38.2	4.7
6.2.2009	974.5	51.4	17.3	3.6
20.2.2009	492.1	27.1	23.6	3.6
27.2.2009	816.6	43.6	19.1	3.8
6.3.2009	575.1	31.4	22.7	3.9
13.3.2009	925.6	49.0	20.6	3.8
13.3.2009	482.7	26.6	38.5	4.4
20.3.2009	1844.9	95.9	18.8	4.5
27.3.2009	1518.5	78.8	41.5	5.3
3.4.2009	2870.5	146.1	48.1	5.0
10.4.2009	3342.0	169.6	106.3	7.8
17.4.2009	988.0	51.8	15.7	3.2
24.4.2009	2894.0	147.3	87.1	6.9
30.4.2009	7171.9	361.3	85.7	6.9
4.12.2009	236.4	14.3	16.9	3.4
11.12.2009	203.6	12.8	46.3	5.0
18.12.2009	288.3	16.9	55.0	5.3
25.12.2009	850.2	45.0	36.9	4.3
1.1.2010	533.6	29.2	52.8	5.2
8.1.2010	161.1	10.5	20.4	3.6
15.1.2010	467.6	25.7	22.6	3.5
22.1.2010	2263.4	115.7	84.2	6.7
29.1.2010	2057.5	105.3	54.7	5.2
5.2.2010	415.3	23.4	16.8	3.5
12.2.2010	249.9	15.0	16.1	3.3
19.2.2010	216.9	13.4	15.7	3.3
26.2.2010	274.2	16.2	21.9	3.6
5.3.2010	3337.9	169.3	32.6	4.1
12.3.2010	1502.6	77.9	15.1	3.5
19.3.2010	787.0	41.8	24.1	3.8
26.3.2010	167.3	10.9	9.4	3.1
2.4.2010	242.5	14.6	23.2	3.6
9.4.2010	1860.1	95.7	32.3	4.3
16.4.2010	1784.6	91.8	26.7	3.4
23.4.2010	4312.0	218.2	59.3	5.5
30.4.2010	4442.1	224.6	52.9	5.1
7.5.2010	5367.5	271.0	56.8	5.5
14.5.2010	15324.4	768.7	59.7	5.5
29.10.2010	380.5	21.5	14.6	3.2
5.11.2010	378.7	21.4	37.3	4.4
12.11.2010	522.5	28.6	34.4	4.3
3.12.2010	428.1	23.9	36.6	4.3
19.11.2010	585.1	31.7	29.8	4.1
26.11.2010	520.4	28.5	35.0	4.3
10.12.2010	130.3	9.0	14.4	3.3
17.12.2010	683.1	36.6	12.4	3.2
24.12.2010	425.0	23.6	15.5	3.1
31.12.2010	121.1	8.5	20.5	3.5
7.1.2011	226.2	13.7	16.7	3.3
14.1.2011	133.4	9.1	19.1	3.4
21.1.2011	89.0	7.0	24.7	3.9
28.1.2011	556.9	30.3	15.8	3.3
4.2.2011	243.7	14.7	10.3	3.0
11.2.2011	234.7	14.3	18.8	3.4
18.2.2011	834.3	44.2	37.6	4.3
25.2.2011	1506.2	77.9	73.8	6.3
4.3.2011	294.9	17.2	9.5	2.9
11.3.2011	209.2	13.0	25.2	3.7
18.3.2011	1875.0	96.3	24.7	3.8
25.3.2011	734.3	39.2	13.1	3.1
2.4.2011	1060.9	55.5	23.6	3.6
8.4.2011	949.9	50.0	60.2	5.4
15.4.2011	5078.3	256.4	79.9	6.5
22.4.2011	4245.7	214.8	90.4	7.0
29.4.2011	2185.7	111.8	51.5	5.1
6.5.2011	1912.8	98.2	42.1	4.7

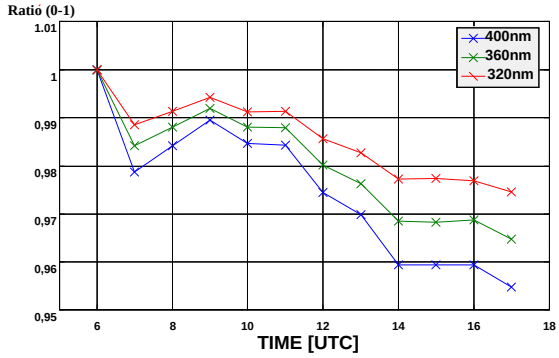

Fig. 8. The ratios (0–1) of modeled irradiances using maximum measured albedo A_{max} for 22 April, and measured albedo A for the same day.

3.6 Snow albedo simulations

The simulated albedo data were calculated using the SNICAR-online version with our measurement results as input data for clear sky (22 April, intensive melting) and diffuse sky (24 April, snow almost melted). To simulate the lowest possible albedo due to the effect of SZA, the value of SZA = 55 degrees was used, as it was the SZA minimum value for midday on 22 April, at one degree accuracy. We used the following realistic input values (otherwise model default values applied): (a) clear sky case – snow depth of 10 cm, snow grain size radius 1.5 mm, hydrophobic or hydrophilic black carbon of 87 ppb; (b) diffuse sky case – snow depth 5, snow

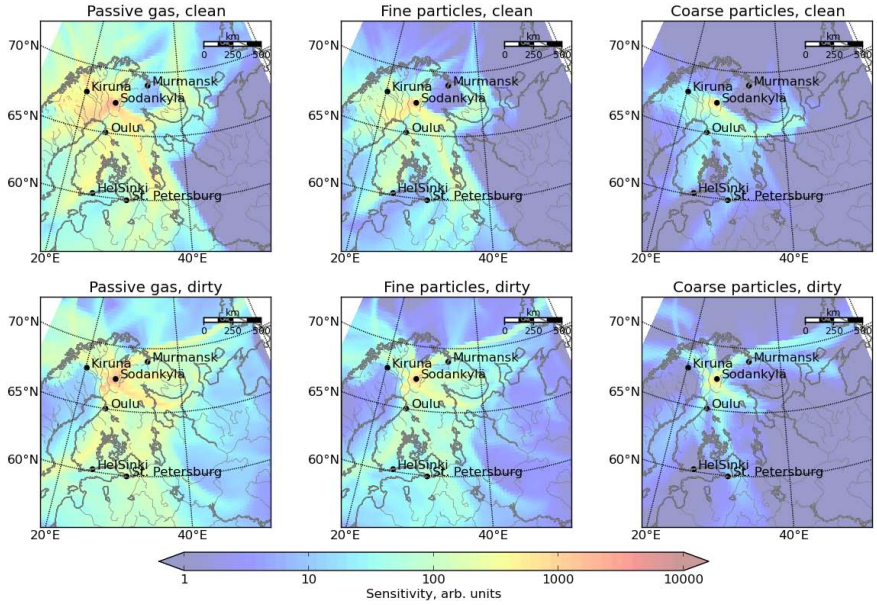

Fig. 9. The footprints for "clean" (upper panels) and "dirty" snowfall (lower panels), on the basis of measured BC mixing ratio in surface-snow samples, for (i) passive gas (no deposition, decay, etc., left), (ii) fine aerosol (middle), and (iii) coarse aerosol (right).

grain radius 1.5 mm, hydrophobic or hydrophilic black carbon black carbon of 87 ppb. A snow density value of 350 $\mathrm{g\,m^{-3}}$ was used, following Kuusisto (1984).

From these, the clear sky simulated albedo (Fig. 10) with 10 cm snow depth and 350 $\mathrm{g\,m^{-3}}$ snow density, produced broadband $A = 0.58$ (for both the hydrophobic and hydrophilic BC). The spectral albedo values for wavelengths 300–400 nm were $A < 0.77$ and $A < 0.76$, accordingly. In turn, for diffuse sky with 5 cm snow and 350 $\mathrm{g\,m^{-3}}$ density, the broadband albedo was $A = 0.58$ (for both the hydrophobic and hydrophilic BC). The spectral albedo values for wavelengths 300–400 nm were $A < 0.69$, and $A < 0.68$, accordingly. These albedo values were based on the snow analysis result of EC = 87 ppb, determined by the thermo–optical method (discussed further in Sect. 4.4).

3.7 Origins of snow impurities

The attribution of impurities at the surface of melting snow can hardly be done without detailed information on wet and dry deposition and on dynamics of the melting process. However, a general picture on the origins of snow pollution due to long-range transport can be obtained from footprint modeling. Figure 9 shows average footprints for "clean" and "dirty" snow for (i) passive gas, i.e., substance with no deposition, decay, etc.); (ii) fine aerosol that has little deposition; and (iii) coarse aerosol that is subject to intensive wet and dry deposition. The deposition rate controls the extent of a footprint for each species.

The comparison of "clean" and "dirty" patterns clearly reveals a sensitivity area at Kola Peninsula for "dirty" footprint that corresponds to a gap in sensitivity for "clean samples". The gap is most pronounced for fine aerosol particles (middle panels), which are likely to be responsible for the snow pollution. The pattern also agrees with the location of main air pollution sources in the region (Prank et al., 2010): mining and refining industries located at Kola Peninsula.

4 Discussion

We have presented spectral and broadband UV and VIS albedo results on seasonal intensively melting snow at Sodankylä, beyond the Arctic Circle. Prior published measurements of albedo for clean snow in this spectral range are 0.97–0.98 (Fig. 4 of Grenfell et al., 1994) and 0.98–0.99 (Fig. 6 of Hudson et al., 2006); consistent with the extremely small absorption coefficient of ice in this spectral region (Wiscombe and Warren, 1980; Warren et al., 2006; Warren and Brandt, 2008). On the contrary, our albedo results reveal spectral albedo for UV and visible, at wavelengths of 300–560 nm, for SZA 55–70 degrees, and for clear sky and cloudy sky, to be in the range $\sim$ 0.5–0.7. These low albedo results are supported by three simultaneous independent albedo measurement setups (one Bentham spectrometer, one SL-501 filter radiometer, one CM-14 albedometer) measuring during the same days at slightly different locations at Sodankylä, as well as by simulated albedo data using SNICAR-online

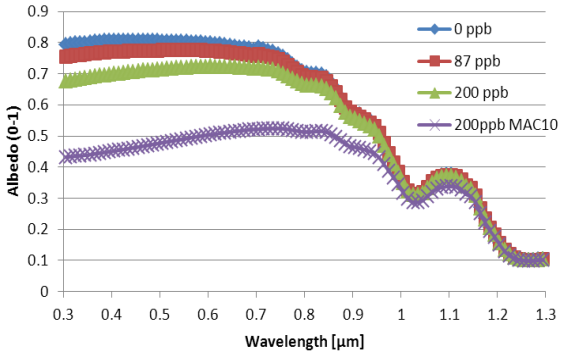

Fig. 10. The SNICAR online simulated snow albedo spectra at 0.3–1.3 µ m (clear sky at SZA = 55 degrees, grain radius 1.5 mm, snow depth 10 cm, snow density 350 kg m^{-3}) demonstrate that the absorption caused by impurities in snow is greater the shorter the wavelength, compared to clean snow (blue). The EC in snow determined by the thermo–optical method was 87 ppb (red). The snow BC concentration was assumed to be approx. double the EC concentration determined by the thermo–optical method (green). Introducing a mass absorption coefficient MAC = 10 produced albedo values close to the lowest measured albedo of ∼ 0.4–0.5 at UV (purple).

(Flanner et al., 2007) with realistic large snow grains (3 mm diameter) and black carbon (87 ppb). We have also measured previously UV albedos of 0.5–0.7 for melting snow at Sodankylä (Meinander et al., 2008). Here, a plausible explanation for our low albedo results is given and discussed.

4.1 Melting snow and albedo

First of all, our measurements represent albedo of intensively melting seasonal Arctic snow at Sodankylä, beyond the Arctic Circle. In the beginning of our spectral measurement period (21 April 2009), the melting period had already started. Hence, the albedo values of our work do not represent the albedo values of the snow accumulation period, or new snow cases, when higher albedo values would be expected. Secondly, the maximum grain size diameter was reported to be 3 mm. During the SNORTEX-2009 campaign, the snow grains of various snow pits in Sodankylä have been recorded and stored by macro photography. An example of such a photo is in Meinander et al. (2008, Fig. 4). We have also evidenced the meltwater to increase in the snow surface layer of the spectral albedo field. When snow melts, the effective grain size increases as water surrounds the snow grains. From this it follows that the effective grain size may be even bigger than the observed grain size, already up to several millimeters. Our albedo results on the melting Arctic snow showed a rapid decrease in the albedo as a function of time. Thus, our data showed some indication of possible SZA asymmetric albedo. SZA asymmetry in albedo could also be due to surface features like sastrugi, but in our case the changes in albedo were caused by melting snow, as the forward scattering nature of snow was detected by our measurements with the Sun shining from the southern direction. Hence, the albedo decline was found to dominate over the SZA-dependent albedo signal. The main driver of albedo was intensively melting snow.

4.2 Supporting measured low albedo

The low albedo values and the diurnal decrease in albedo, first detected by the spectral data, were supported by the simultaneous broadband measurements. Bentham showed albedo values of ∼ 0.5–0.7, SL-501 of ∼ 0.4–0.5, and CM14 of ∼ 0.6–0.75. The operational field erythemal SL-501 albedo was most often smaller than the albedo values of the primary Bentham field, or of the CM14 at the various SNORTEX sites. However, on 24 April, the spectral values ($A = 0.45$ at 330 nm and $A = 0.53$ at 450 nm) and the erythemal UV albedo ($A =\sim 0.42$–0.43) were close to each other. The decrease in erythemal UV albedo within a day was of ∼ 10 %, i.e., the same as for the spectral data. Earlier, we have also reported, for the same Sodankylä operational albedo field, erythemally weighted SL-501 radiometer snow UV albedo values of ∼ 0.45–0.69 during the melt period in 2007 (Table 3 of Meinander et al., 2008). After the melt period, the intensive melt period took place until the ground under snow became visible. During that period the albedos were lower than 0.5 (Fig. 10 of Meinander et al., 2008). Hence, the melt stage (accumulation, melt, intensive melt) of the measurement field affects the measured albedo values. If the various open snowfields are under different stages of melt, it is possible that the snow height and albedo values differ spatially even at close-by locations. Therefore, it is important to have the ancillary data on snow from the same place as the albedo measurement.

The independent broadband CM14 albedo data showed that (a) the broadband albedos were lower than for even aged midwinter snow (measured during SNORTEX experiments), implying that the melt was well under way; (b) the drop in observed albedos during a single field day suggests that snow metamorphism was also very active during this time; and (c) the level of the broadband albedos falled consistently during the four-day period. This behavior is consistent with an increase in effective grain size as the melt enlarges the grain size of the snowpack, and also the thinning snowpack brings more impurities closer to the surface layer where they have a greater effect on the albedo.

4.3 Optically thin snowpack

A melting snowpack can become optically thin due to the large grain size, with the result that the low-albedo ground underneath the snow can be “seen”. For instance, in Wiscombe and Warren (1980), the 1000 micron grain size would

correspond to a liquid-equivalent depth, for which the snowpack becomes semi-infinite, to be 50 cm of old melting snow. In SNICAR-online (Flanner et al., 2007), the underlying ground albedo influences the reflectance of a relatively thin snowpack, but density and effective grain size also determine the influence of underlying ground. In the Arola et al. (2003) work on satellite respectivity versus snow depth (Fig. 1 in their paper), the respectivity of a 0.02 m (2 cm) snow depth is marginally different from a 0.1 m thick snowpack. This gives rise to the question of the importance of the surface layer compared with the layer beneath, when melting snow is considered. Here, the liquid water content of the surface layer (0 cm) was very low in the afternoon, while the lower layers were more wet. Further, melting leads to radiation entering deeper into the snowpack, where radiation may become effectively trapped if snow is polluted. In our data, UV is relatively more attenuated than visible from 09:00 to 11:00 UTC (Fig. 4), which could indicate absorptive extinction.

4.4 Impurities in snow

Moreover, our Sodankylä Arctic Center data in 2009 (Table 3), showed that the EC and OC amounts in snow were 87 ppb and 2894 ppb, respectively, at the time of the albedo measurements. These impurities have the potential to absorb radiation and thus reduce snow albedo (Warren and Wiscombe, 1980). Yet, according to our experience, as far as snow OC concentrations are concerned, the results may sometimes suffer from contamination by tree debris. On the other hand, however, the results from M. Wang et al. (2013) indicate that in the thermal–optical measurement of EC and OC, elemental carbon and dust generally mix as agglomerates. The agglomerate structure will contribute to an underestimation of EC and OC during OC/EC-analysis. This underestimation has been shown to be dependent on the analysis protocol used during OC/EC-analysis (Aamaas et al., 2011; Chow et al., 2001; Reisinger et al., 2008). The NIOSH 5040 protocol has been argued to underestimate the EC content by a factor of two. As a result, we simulated new SNICAR on-line (Flanner et al., 2007) albedo spectra with 200 ppb, i.e., approx. double the BC amount that was measured using the thermal–optical method. For the clear sky case with 10 cm snow, and with realistic 200 ppb of hydrophilic BC (Fig. 10) and other parameter values kept the same, the broadband albedo $A = 0.55$ and spectral albedo $A(300–400\,\text{nm}) = 0.68–0.70$ were gained. For the diffuse sky with 5 cm snow, the broadband albedo was now $A = 0.56$, and the spectral albedo $A(300–400\,\text{nm})$ was approx. 0.64.

The mass absorption coefficient (MAC) default value in SNICAR is MAC = 1. The MAC of BC is a measure of how much sunlight BC particles can absorb. According to Bond et al. (2013), the measured values for freshly generated BC fall within a relatively narrow range of $7.5 \pm 1.2\ \text{m}^2\,\text{g}^{-1}$ at 550 nm, and the MAC of BC increases by approximately 50 % as BC becomes internally mixed with other aerosol chemical components. In Hadley and Kirchstetter (2012), their upper limit of simulated spectral albedo corresponds to a BC MAC equal to $7.5\,\text{m}^2\,\text{g}^{-1}$ at 550 nm, indicated as an appropriate value for freshly emitted BC. Their lower limit corresponds to snow contaminated with BC that is twice as absorbing (MAC $= 15\,\text{m}^2\,\text{g}^{-1}$), indicated as an appropriate value for atmospherically aged BC. Using MAC = 10 $\text{m}^2\,\text{g}^{-1}$ together with the 200 ppb hydrophobic BC as input values for the SNICAR simulated albedo, we could match the lowest measured albedos of approx. 0.4 (Fig. 10). For the clear sky case with 10 cm snow, we then gained albedo values $A = 0.43–0.45$ for 300–400 nm, and $A = 0.4$ for broadband. Comparing the 87 ppb and the 200 ppb albedo spectra with MAC = 1 or MAC = 10 (Fig. 10), it is obvious that the absorbance due to increased BC is greater the shorter the wavelength at UV. The effect of absorbing substances on snow albedo has been stated to be the most pronounced: the shorter the wavelength, the bigger the snow grain (Hadley and Kirchtetter, 2012). The same is also true for atmospheric absorbtion by BC (Fig. 9, Voisin et al., 2012).

Black carbon values measured elsewhere in Arctic Scandinavia (Tromsø, Norway) are only ~ 20 ppb in April, although the surface concentration can increase to 60 ppb in late May because of concentration during melting (Table 8 of Doherty et al., 2010). According to our results, the Sodankylä snow samples contained higher impurity concentrations than those in the study by Doherty et al. (2010), and there is a similar increase in impurity concentrations toward the spring. Recently collected snow samples in Arctic Scandinacia show spatial variability in impurities in the snow (Svensson et al., 2013, unpublished data).

Figure 9 shows that the average footprint over cases of clean snow have a very pronounced gap around Murmansk, i.e., a major source of BC in snow is located in the eastern half of the Kola Peninsula, which agrees quite well with the location of the industrial activities. Hence, our high concentrations of BC in snow may be due to air masses originating from the Kola Peninsula, Russia, where there are mining and concentrated industry (e.g., Rigina, 2002).

The scientific understanding of the snow organic carbon absorption has started to develop only recently (e.g., McNeill et al., 2012; X. Wang et al., 2013). The main sources of organic carbon to the atmosphere and to snowpack are anthropogenic activities and biomass burning (e.g., Hegg et al., 2010). Hagler et al. (2007) found snow to have a much higher OC to EC ratio (205 : 1) than air (10 : 1), suggesting that snow is additionally influenced by watersoluble gasphase compounds. France et al. (2012) demonstrated that black carbon alone could not account for all the absorption seen in the Barrow snowpacks, and an additional absorption by Humic Like Substances (HULIS), part of brown carbon, and other chromophores was necessary to explain variation. Voisin et al. (2012) measured HULIS optical properties and reported them to be consistent with aged biomass burning or a possible marine source. McNeill et al. (2012) discussed

the adsorption and desorption of organic species to and from snow and ice surfaces, and how these processes influence the transport of organic trace gases through snowpack. Moreover, according to Bond et al. (2013), a large fraction of particulate light absorption in Arctic snow (about 30 to 50 %) is due to non-BC constituents and most of the absorption would be due to light-absorbing organic carbon from biofuel and agricultural or boreal forest burning.

4.5 About spectral albedo

The spectral albedo results in Fig. 4 show the decrease of albedo as a function of time (upper panel), and the relative wavelength dependent change (lower panel). From the upper panel we can see the chronological order from highest albedo to lowest albedo (from 09:00 to 17:00 UTC). This decrease in albedo as a function of time is according to the snow grain size (Table 2), changing from 0.25 mm to 3 mm diameter grains as a function of time. These results agree with the Wiscombe and Warren (1980) paper, where albedo is expected to decrease with increasing grain size.

The lower panel shows that the spectral change (compared to the 09:00 UTC albedo) is greater the shorter the wavelength (the 11:00 and 13:00 UTC values). This is consistent with the theoretical results of Warren and Wiscombe (1980), which show that absorption due to impurities in snow increases with decreasing wavelength. At 15:00 UTC this spectral behavior seems to disappear and the albedo values are 90 % of those in the morning regardless the wavelength. The SZA is then $\sim 70°$. At 17:00 UTC, with SZA $= 83°$, the spectral behavior turns slightly toward the opposite, the difference from the morning values is larger for VIS than UV. At large zenith angles, the proportion of diffuse radiation is increased as a direct effect, then drastically decreases (e.g., Fig. 8 of Gardner and Sharp, 2010), and the snow albedo is known to decrease as a function of wavelength as the diffuse-to-direct radiation ratio increases (Fig. 12 of Wiscombe and Warren, 1980).

4.6 On the importance of albedo estimates

A variety of climatological studies including radiative forcing of the planet are dependent on snow albedo assumptions at given seasons. For melting snow seasons these assumptions have to be very carefully implemented in various modeling codes. Also, during snowmelt, the effective surface UV albedo distributions (like those presented in Tanskanen and Manninen, 2007, and Robinson and Kukla, 1984) are expected to move toward smaller values. We may expect that snow height-dependent parameterizations (like in Arola et al., 2003), in turn, might function well during melt time. Winther (1993) has presented the progress of snow albedo for a Norwegian research site, where the albedo decreased as the snow went under a process of metamorphosis. Snow albedo was first determined as a function of temperature index alone. An improved accuracy of 2–6 % in estimated snow albedo was obtained when solar radiation was included. In several models, such as CAM 3.0 (Collins et al., 2004), ECHAM5 (Roeckner et al., 2003; Roesch and Roeckner, 2006), and in the ECWMF model (ECWMF, 2010), snow albedo decreases with temperature (either linearly or exponentially). The basic parameterizations have the potential to be improved. According to Pedersen and Winther (2005), snow depth-dependent parameterizations perform better during the snowmelt period than temperature-dependent parameterizations. In the paper by Cheng et al. (2006) it has been shown, that in the case that the albedo parameterization is too sensitive to surface temperature, errors in the surface energy and mass balance grow rapidly due to the strong positive feedback between albedo and temperature errors. Furthermore, according to Pirazzini (2008), the representation of the snow and ice albedo for climate and numerical weather prediction models may be one of the most serious oversimplifications, and this may cause large errors in weather prediction and climate simulations. Pirazzini (2008) has presented a simulation experiment with the two-dimensional mesoscale model of the University of Helsinki, Finland, where the old snow albedo of 0.7 was used instead the measured albedo of 0.83 (fresh snow). They concluded that in the case of fresh snow, the use of old snow albedo and thermodynamic values alone caused a delay in the surface cooling and about 3 °C of error in the surface temperature. Therefore, we might expect that the differences in snow albedo during melt with variation from approx. 0.8 to 0.4 in our results might cause a significant effect, too.

The spectral behavior in snow albedo needs to be considered, especially in cases of wavelength-dependent absorbtance of impurities in the snow. A simple empirical regression converting UVA, UVB, and VIS albedo from one to another may serve as a tool for any application where the albedo is measured at one wavelength range, but the interest lies in another. In our data, when calculating albedo in the visible from albedo at 310 nm, R^2 was only 0.6, indicating that in these data (snow with large snow grains and containing impurities) a linear model was not as good a method as for UVA conversion from UVB ($R^2 = 0.97$). Earlier, Li and Trishchenko (1999) made a study on the development and validation of narrow band to broadband conversion models. According to them, a linear regression (a basic conversion model) between shortwave (SW) albedo (α_{sw}) and VIS albedo (α_{vis}): $\alpha_{\mathrm{sw}} = a_0 + b_0\alpha_{vis}$ that does not require any auxiliary information, has been most widely used. For snow and ice, they gave $a_0 = 10.802$ and $b_0 = 0.725$.

We also found that the albedo of melting snow also decreased by ~ 10 % as a function of time within a single day, asymmetrically to SZA. In the mornings, the albedo signal was slightly higher than it had been the previous evening, possibly due to frost conditions during the night. Here, the bottom surface (24 cm) had liquid water, and a temperature profile close to melting conditions (0 °C), suggesting that water vapour from the ground could possibly enter the snow

surface layer, forming ice crust. The ice crust could then affect the albedo by increasing albedo when icy, and decreasing albedo when melting from the surface. The RT calculations showed that if this 10 % daily melt time asymmetry effect is ignored, an error of ∼2–4 % in the calculated clear sky downward irradiance is made for one day. This would mean, e.g., that if using daily satellite-based albedo data for radiative transfer applications, even if satellite and ground albedo were to match perfectly, there would be a remaining error of the mentioned percentages caused by diurnal snow melting.

4.7 On the error sources

Finally, the possible error sources in albedo measurements need to be addressed. There are several sources for measurement errors when measuring the solar irradiance. However, many of these errors are eliminated in the albedo results when the division of upward radiation signal to downward radiation signal is performed. This is the case when one properly leveled sensor is used, or when the up and down facing sensors have similar cosine and spectral responses. The error and uncertainty analysis of Bernhard and Seckmeyer (1999) has been our reference in use, in addition to the guidelines of the World Meteorological Organization (WMO). All the FMI-owned irradiance measuring instruments are regularly checked for their angular, spectral and radiometric responses, and the required calibration procedures are carefully performed to produce reliable measurements to fulfill the WMO requirements.

The error caused by the fact that the size of the snow patch used for the spectral measurements extended only 3 m from the radiometer in one direction has been evaluated in Meinander and Räisänen (2010). According to these calculations, e.g., if the true snow albedo were $Asnow = 0.7$ and the environmental albedo $Aenv = 0.1$, the measured albedo would be 0.629, with an error of −0.071, assuming that the surface is a Lambertian reflector. While this is a significant error, it is not large enough to explain the difference between our albedo results and those measured in, e.g., Grenfell et al. (1994) and Hudson et al. (2006). Moreover, the error estimate provided above is most probably too pessimistic due to the assumption of Lambertian surface. Scattering by snow has a strong forward-scattering component. As the measurements were made for solar azimuths between about 110 and 250° (south being 180°), the Lambertian assumption most probably overestimates the contribution that the area north of the snow patch makes to the measured upwelling irradiance. These calculations have assumed that the surface is flat, and that there are no objects protruding upwards from the surface, so that the downwelling irradiance is horizontally uniform. This is not strictly true, as the snow patch was surrounded by forest. The data analysis was restricted to periods when the sun was high enough (> 20°) so that direct sunlight could reach the sensor and the surrounding surface (at least the nearest 10 m around the sensor) without being blocked by trees. It is, however, possible that some of the diffuse (scattered) radiation was blocked by the trees. This violates the above assumption that the downwelling irradiance $F\downarrow$ is independent of location. Specifically, as the sensor is located 2.5 m above the surface, the sensor probably experiences slightly less shadowing than the surrounding surface, which means that $F\downarrow$ reaching the sensor may be slightly larger than $F\downarrow$ reaching the surface. This would cause a slight negative bias in the measured albedo, in addition to the negative bias associated with the north edge of the snow patch.

The results presented here are not meant to be representative for the whole melt period, for longer time periods and also not for larger areas, as such. Our major aim with this work was to investigate the spectral behavior of intensively melting snow, and not to repeat the work of Meinander et al. (2008), which deals with issues that require longer-term measurements.

Here, the albedo values detected by the various setups differed slightly from each other. We have evaluated the uncertainty of our SL-501 albedo results (when studying the SZA asymmetry) to be around 2 % (Meinander et al., 2008). The effect of the equipment setup and operator footprints on the CM-14 snow albedo of the observed area have been experimentally confirmed to be no more than 0.02 during the SNORTEX campaigns (A. Riihelä, unpublished data). We explain these differences to be due the fact that the melting phase at a certain time may vary slightly at different places, as evidenced here by the snow height data, too.

If simultaneous albedo values of various close-by open snowfields are at different stages of melt due to local environmental conditions (differences in size of the open area, snow height, etc.), then relative changes in albedo values (e.g., in % from day to day or morning to afternoon) may offer better information on the changes in albedo during melt than the albedo values alone. This is also supported by the fact that in addition to the snowmelt stage, size of the open field, and snow height, the detected albedo may also be affected by the actual measurement height. Some effect may be also due to small-scale spatial variability of absorbing impurties in the snow (Svensson, 2011). In addition, the calibration factor of the broadband SL-instruments could be improved (as described earlier in Meinander et al., 2008), and different distributions of up- and down-welling radiance might even require different cosine corrections of the two meters. Yet, the most important fact of our results remains: all these measurement results showed albedo values lower than those presented in the literature for clean snow.

5 Conclusions

We have measured spectral albedo, as well as ancillary parameters, of seasonal intensively melting snow at boreal region in Sodankylä, Finland (67°22′ N, 26°39′ E) beyond the

Arctic Circle. Our spectral measurements revealed albedo values of ∼ 0.5–0.7 for ultraviolet and visible range, both under clear sky and variable cloudiness. Our low albedo values were supported by three independent simultaneous albedo measurement setups and simulated albedo data, as well as previous continuous long-term UV albedo data since 2007. During the most intensive snowmelt period of four days, albedo decreased from 0.65 to 0.45 at 330 nm, and from 0.72 to 0.53 at 450 nm. In the literature, the UV and VIS albedo for clean snow are ∼ 0.97–0.99, consistent with the extremely small absorption coefficient of ice in this spectral region.

We explain the low albedo values to be due to (i) large snow grain sizes up to ∼ 3 mm in diameter; (ii) meltwater surrounding the grains and increasing the effective grain size; and (iii) absorption caused by impurities in the snow, with concentration of elemental carbon (black carbon) in snow of 87 ppb, and organic carbon 2894 ppb, at the time of albedo measurements. Due to the thermal–optical method used, the real BC concentrations could be expected to be approximately double the amounts reported here. Even as such, i.e., without correcting the results, Sodankylä snow samples contained higher impurity concentrations than measured elsewhere in Arctic Scandinavia (Doherty et al., 2010). So far, during the years 2009–2011, the snow EC concentration results have varied between 9–106 ppb, with an average value of 36 ppb. When dividing these into clean (snow EC < 20 ppb) and dirty (EC > 30 ppb) cases, the high concentrations of carbon were observed due to air masses originating from Kola Peninsula, Russia, where mining and refining industries are located.

Acknowledgements. We highly appreciate the comments given by Stephen G. Warren and Thomas C. Grenfell (University of Washington, Seattle, WA, USA) during the open discussion of our manuscript. On the basis of their comments, as well as the valuable comments by the three anonymous referees, our manuscript has been greatly improved. The work was supported by the Academy of Finland (projects SAARA and A4). The Sodankylä snow UV albedo and snow impurity studies are included in the Nordic Centre of Excellency Project CRAICC (Cryosphere–Atmosphere Interactions in a Changing Arctic Climate).

Edited by: V.-M. Kerminen

References

Aamaas, B., Bøggild, C. E., Stordal, F., Berntsen, T., Holmén K., and Ström, J.: Elemental carbon deposition to Svalbard snow from Norwegian settlements and long-range transport, Tellus, 63B, 340–351, doi:10.1111/j.1600-0889.2011.00531.x, 2011.

Arola, A., Kaurola, J., Koskinen, L., Tanskanen, A., Tikkanen, T., Taalas, P., Herman, J. R., Krotkov, N., and Fioletov, V.: A new approach to estimating the albedo for snow-covered surfaces in the satellite UV method, J. Geophys. Res., 108, 4531, doi:10.1029/2003JD003492, 2003.

Bernhard, G. and Seckmeyer, G.: Uncertainty of measurements of spectral solar UV irradiance, J. Geophys. Res., 104, 14321–14345, 1999.

Bernhard, G., Booth, C. R., Ehramjian, J. C., Stone, R., and Dutton, E. G.: Ultraviolet and visible radiation at Barrow, Alaska: Climatology and influencing factors on the basis of version 2 National Science Foundation network data, J. Geophys. Res., 112, D09101, doi:10.1029/2006JD007865, 2007.

Birch, M. E.: Diesel Particulate Matter (as Elemental carbon) Method 5040, in NIOSH Manual of Analytical Methods, National Institute of Occupational Safety and Health, Cincinnati, Ohio, 2003.

Birch, M. E. and Cary, R. A.: Elemental carbon-based method for monitoring occupational exposures to particulate diesel exhaust, Aerosol Sci. Technol., 25, 221–241, 1996.

Blumthaler, M. and Ambach, W.: Solar UVB-Albedo of various Surfaces, Photochem. Photobiol., 48, 85–88, 1988.

Bond, T. C. and Bergstrom, R. W.: Light absorption by carbonaceous particles: An investigative review, Aerosol Sci. Technol., 40, 27–67, doi:10.1080/02786820500421521, 2006.

Bond, T. C., Habib, G., and Bergstrom, R. W.: Limitations in the enhancement of visible light absorption due to mixing state, J. Geophys. Res., 111, D20211, doi:10.1029/2006JD007315, 2006.

Bond, T. C., Doherty, S. J., Fahey, D. W., Forster, P. M., Berntsen, T., DeAngelo, B. J., Flanner, M. G., Ghan, S., Kärcher, B., Koch, D., Kinne, S., Kondo, Y., Quinn, P. K., Sarofim, M. C., Schultz, M. G., Schulz, M., Venkataraman, C., Zhang, H., Zhang, S., Bellouin, N., Guttikunda, S. K., Hopke, P. K., Jacobson, M. Z., Kaiser, J. W., Klimont, Z., Lohmann, U., Schwarz, J. P., Shindell, D., Storelvmo, T., Warren, S. G., and Zender, C. S.: Bounding the role of black carbon in the climate system: A scientific assessment, J. Geophys. Res., doi: 10.1002/jgrd.50171, 2013.

Cheng, B., Vihma, T., Pirazzini, R., and Granskog, M. A.: Modelling of superimposed ice formation during the spring snowmelt period in the Baltic Sea, Ann. Glaciol., 44, 139–146, 2006.

Chow, J. C., Watson, J. G., Crow, D., Lowenthal, D. H., and Merrifield, T.: Comparison of IMPROVE and NIOSH Carbon Measurements. Aerosol Sci. Technol., 34, 23–34, 2001.

Collins, W. D., Rasch, P. J., Boville, B. A., Hack, J. J., McCaa, J. R., Williamson, D. L., Kiehl, J., Briegleb, B., Bitz, C., Lin, S.-J., Zhang, M., and Dai, Y.: Description of the NCAR Community Atmosphere Model (CAM 3.0), NCAR/TN-464+STR NCAR TECHNICAL NOTE June 2004, http://www.cesm.ucar.edu/models/atm-cam/docs/description/node35.html, 2004.

Doherty, S. J., Warren, S. G., Grenfell, T. C., Clarke, A. D., and Brandt, R. E.: Light-absorbing impurities in Arctic snow, Atmos. Chem. Phys., 10, 11647–11680, doi:10.5194/acp-10-11647-2010, 2010.

Domine, F., Taillandier, A.-S., and Simpson, W. R.: A parameterization of the specific surface area of snow in models of snowpack evolution, based on 345 measurements, J. Geophys. Res., 112, F02031, doi:10.1029/2006JF000512, 2007.

ECWMF: The European Centre for Medium-Range Weather Forecasts, The ECMWF Integrated Forecast System (IFS), IFS documentation CY25r1, operational on 9 April 2002, Eq. 7.29 at http://www.ecmwf.int/research/ifsdocs/CY25r1/Physics/Physics-08-05.htm, 2010.

Fierz, C., Armstrong, R. L., Durand, Y., Etchevers, P., Greene, E., McClung, D. M., Nishimura, K., Satyawali, P. K., and Sokratov, S. A.: The International Classification for Seasonal Snow on the Ground. IHP-VII Technical Documents in Hydrology, no. 83, IACS Contribution no. 1, UNESCO-IHP, Paris, http://unesdoc.unesco.org/images/0018/001864/186462e.pdf, 2009.

Flanner, M. G., Zender, C. S., Randerson, J. T., and Rasch, P. T.: Present day climate forcing and response from black carbon in snow, J. Geophys. Res., 112, D11202, doi:10.1029/2006JD008003, 2007.

Forsström, S., Ström, J., Pedersen C. A., Isaksson, E., and Gerland, S.: Elemental carbon distribution in Svalbard snow, J. Geophys. Res., 114, D19112, doi:10.1029/2008JD011480, 2009.

France, J. L., Reay, H. J., King, M. D., Voisin, D., Jacobi, H., Beine, H. J., Anastasio, C., MacArthur, A., and Lee-Taylor, J.: Hydroxyl radical and NO_x production rates, black carbon concentrations and light-absorbing impurities in snow from field measurements of light penetration and nadir reflectivity of on-shore and off-shore coastal Alaskan snow, J. Geophys. Res., 117, D00R12, doi:10.1029/2011JD016639, 2012.

Galperin, M.: The approaches to correct computation of airborne pollution advection, in: Problems of ecological Monitoring and Ecosystem Modelling, Gidrometeoizdat, 54–68, 2000.

Gardner, A. S. and Sharp, M. J.: A review of snow and ice albedo and the development of a new physically based broadband albedo parameterization, J. Geophys. Res., 115, F01009, doi:10.1029/2009JF001444, 2010.

Grainger, R. G., Basher, R. E., and McKenzie, R. L.: UV-B Robertson-Berger meter characterization and field calibration, Appl. Optics, 32, 343–349, 1993.

Grenfell, T. C., Warren, S. G., and Mullen, P. C.: Reflection of solar radiation by the Antarctic snow surface at ultraviolet, visible, and near-infrared wavelengths, J. Geophys. Res., 99, 18669–18684, 1994.

Hadley, O. L. and Kirchstetter, T. W.: Black carbon snow albedo reduction, Nature Climate. Change, 2, 437–440, doi:10.1038/nclimate1433, 2012.

Hagler, G. S. W., Bergin, M. H., Smith, E. A., and Dibb, J. E.: A summer time series of particulate carbon in the air and snow at Summit, Greenland, J. Geophys. Res., 112, D21309, doi:10.1029/2007JD008993, 2007.

Hegg, D. A., Warren, S. G., Grenfell, T. C., Doherty, S. J., and Clarke, A. D.: Sources of light-absorbing aerosol in arctic snow and their seasonal variation, Atmos. Chem. Phys., 10, 10923–10938, doi:10.5194/acp-10-10923-2010, 2010.

Hudson, S. R., Warren, S. G., Brandt, R. E., Grenfell, T. C., and Six, D.: Spectral bidirectional reflectance of Antarctic snow: Measurements and parameterization, J. Geophys. Res., 111, D18106, doi:10.1029/2006JD007290, 2006.

Kuusisto, E.: Snow accumulation and snowmelt in Finland. Publications of the Water Research Institute, National Board of Waters, Finland, No. 55, 149 pp., 1984.

Kylling, A., Persen, T., Mayer, B., and Svenøe, T.: Determination of an effective spectral surface albedo from ground-based global and direct UV irradiance measurements, J. Geophys. Res., 105, 4949–4959, 2000.

Li, Z. and Trishchenko, A.: A Study toward an Improved Understanding of the Relationship between Visible and Shortwave Measurements, J. Atmos. Ocean. Tech., 16, 347–360, 1999.

Mayer, B. and Kylling, A.: Technical note: The libRadtran software package for radiative transfer calculations – description and examples of use, Atmos. Chem. Phys., 5, 1855–1877, doi:10.5194/acp-5-1855-2005, 2005.

McNeill, V. F., Grannas, A. M., Abbatt, J. P. D., Ammann, M., Ariya, P., Bartels-Rausch, T., Domine, F., Donaldson, D. J., Guzman, M. I., Heger, D., Kahan, T. F., Klán, P., Masclin, S., Toubin, C., and Voisin, D.: Organics in environmental ices: sources, chemistry, and impacts, Atmos. Chem. Phys., 12, 9653–9678, doi:10.5194/acp-12-9653-2012, 2012.

Meinander, O. and Räisänen, P.: Authors' reply to the Anonymous Referee #1 General Comment #1: A first estimate for the albedo error associated with the edge, Atmos. Chem. Phys. Discuss., 10, C11474–C11474, http://www.atmos-chem-phys-discuss.net/10/C11474/2010/acpd-10-C11474-2010-supplement.pdf, 2010.

Meinander, O., Kontu, A., Lakkala, K., Heikkilä, A., Ylianttila, L., and Toikka, M.: Diurnal variations in the UV albedo of arctic snow, Atmos. Chem. Phys., 8, 6551–6563, doi:10.5194/acp-8-6551-2008, 2008.

Meinander, O., Wuttke, S., Seckmeyer, G., Kazadzis, S., Lindfors, A., and Kyrö, E.: Solar zenith angle asymmetry cases in polar snow UV albedo, Geophysica, 45, 1–2, 2009.

Meinander, O., Kazadzis, S., Arola, A., Kivi, R., Kontu, A., Suokanerva, H., Aaltonen, V., Manninen, T., Roujean, J.-L., and Hautecoeur, O.: Spectral albedo of arctic snow during intensive melt period, Atmos. Chem. Phys. Discuss., 10, 27075–27098, doi:10.5194/acpd-10-27075-2010, 2010.

Michalsky, J. J., Harrison, L. C., and Berkheiser III, W. E.: Cosine Response Characteristics of Some Radiometric and Photometric Sensors, Solar Energy, 54, 397–402, 1995.

Pedersen, C. A. and Winther, J.-G.: Intercomparison and validation of snow albedo parameterization schemes in climate models, Clim. Dyn., 25, 351–362, 2005.

Pirazzini, R.: Factors controlling the surface energy budget over snow and ice. PhD Thesis. 141 p. Finnish Meteorological Institute Contributions 73, available at: https://oa.doria.fi/bitstream/handle/10024/42713/factorsc.pdf?sequence=1, 2008.

Prank, M., Sofiev, M., Denier van der Gon, H. A. C., Kaasik, M., Ruuskanen, T. M., and Kukkonen, J.: A refinement of the emission data for Kola Peninsula based on inverse dispersion modelling, Atmos. Chem. Phys., 10, 10849–10865, doi:10.5194/acp-10-10849-2010, 2010.

Reisinger, P., Wonashütz, A., Hitzenberger, P., Petzold, A., Bauer, H., Jankowski, N., Puxbaum, H., Chi, X., and Maenhaut, W.: Intercomparison of measurement techniques for black or elemental carbon under urban background conditions in wintertime: Influence of Biomass Combustion, Environ. Sci. Technol., 42, 884–889, 2008.

Rigina, O.: Environmental impact assessment of the mining and concentration activities in the Kola Peninsula, Russia by multidate remote sensing, Environ Monit Assess., 75, 11–31, 2002.

Robinson, D. A. and Kukla, G.: Maximum surface albedo of seasonally snow-covered lands in the Northern Hemisphere, J. Clim. Appl. Meteorol., 24, 402–411, 1984.

Roeckner, E., Bäuml, G., Bonaventura, L., Brokopf, R., Esch, M., Giorgetta, M., Hagemann, S., Kirchner, I., Kornblueh, L., Manzini, E., Rhodin, A., U. Schlese, U., Schulzweida U., and Tompkins, A.: The atmospheric general circulation model ECHAM5 , Part I, Model description, Report

349, Max Planck Institute for Meteorology, ISSN 0937 – 1060, http://www.mpimet.mpg.de/fileadmin/models/echam/mpi_report_349.pdf, 2003.

Roesch, A. and Roeckner, E.: Assessment of Snow Cover and Surface Albedo in the ECHAM5 General Circulation Model, J. Climate, 19, 3828–3843, 2006.

Roujean, J.-L., Manninen, T., Kontu, A., Peltoniemi, J., Hautecoeur, O., Riihelä, A., Lahtinen, P., Siljamo, N., Suokanerva, H., Sukuvaara, T., Kaasalainen, S., Aulamo, O., Aaltonen, V., Thölix, L., Karhu, J., Suomalainen, J., Hakala, T., and Kaartinen, H.: SNORTEX (Snow Reflectance Transition Experiment): Remote sensing measurement of the dynamic properties of the boreal snow-forest in support to climate and weather forecast: report of IOP-2008, 2009 IEEE International Geoscience & Remote Sensing Symposium, 12–17 July, Cape Town, South Africa (Paper 1167), 2009.

Roujean, J.-L., Manninen, T., Sukuvaara, T., Peltoniemi, J., Kaasalainen, S., Hautecoeur, O., Lahtinen, P., Riihelä, A., Siljamo, N., Lötjönen, M., Karjalainen, T., Kontu, A., Suokanerva, H., Aulamo, O., Lemmetyinen, J., Suomalainen, J., Hakala, T., Kaartinen, H., Thölix, L., Meinander, O., and Karhu, J.: SNORTEX: Remote sensing measurement of snowmelt in European boreal forest, iLEAPS Newsletter Issue No. 9, April 2010, http://www.ileaps.org/index.php?option=com_phocadownload\&view=category\&id=3:\&Itemid=81, 2010.

Seckmeyer, G., Bais, A., Bernhard, G., Blumthaler, M., Booth, R.,S. Lantz, K., and McKenzie, R. L.: Instruments to measure solar ultraviolet radiation, part II: Broadband instruments measuring erythemally weighted solar irradiance, WOM-GAW report, 2005.

Sihvola, A. and Tiuri, M.: Snow Fork for Field Determination of the Density and Wetness Profiles of a Snow Pack, IEEE Transactions on Geoscience and Remote Sensing, 24, 717–721, 1986.

Sofiev, M.: Extended resistance analogy for construction of the vertical diffusion scheme for dispersion models, J. Geophys. Res. Atmos., 107, 4159, doi:10.1029/2001JD001233, 2002.

Sofiev, M., Galperin, M., and Genikhovich, E.: Construction and evaluation of Eulerian dynamic core for the air quality and emergency modeling system SILAM, in: NATO Science for piece and security Serties C: Environmental Security, Air pollution modelling and its application, XIX, edited by: Borrego, C. and Miranda, A. I., Springer, 699–701, 2008.

Svensson, J.: Horizontal meter scale variability of elemental carbon in surface snow, Master's thesis, Dept. of Quaternary Geology and Physical Geography, Stockholm Uni, Stockholm, Sweden, 2011.

Tanskanen, A. and Manninen, T.: Effective UV surface albedo of seasonally snow-covered lands, Atmos. Chem. Phys., 7, 2759–2764, doi:10.5194/acp-7-2759-2007, 2007.

Toikka, M.: Field tests with the Snow fork in determining the density and wetness profiles of a snow pack, Microwave Signature-92, IGLS-Innsbruck, Austria, 1–3 July 1992.

Voisin, D., Jaffrezo, J.-L., Houdier, S., Barret, M., Cozic, J., King, M. D., France, J. L., Reay, H. J., Grannas, A., Kos, G., Ariya, P. A., Beine, H. J., and Domine F.: Carbonaceous species and HUmic LIke Substances (HULIS) in Arctic snowpack during OASIS field campaign in Barrow, J. Geophys. Res., 117, D00R19, doi:10.1029/2011JD016612, 2012.

Wang, M., Xu, B., Zhao, H., Cao, J., Joswiak, D., Wu, G., and Lin, S.: The Influence of Dust on Quantitative Measurements of Black Carbon in Ice and Snow when Using a Thermal Optical Method, Aerosol Sci. Tech., 46, 60–69, doi:10.1080/02786826.2011.605815, 2012.

Wang, X., Doherty, S. J., and Huang, J.: Black carbon and other light-absorbing impurities in snow across Northern China, J. Geophys. Res., doi:10.1029/2012JD018291, in press, 2013.

Warren, S. G. and Brandt, R. E.: Optical constants of ice from the ultraviolet to the microwave: A revised compilation, J. Geophys. Res., 113, D14220, doi:10.1029/2007JD009744, 2008.

Warren, S. G. and Wiscombe, W. J.: A model for the spectral albedo of snow. II: Snow containing atmospheric aerosols, J. Atmos. Sci., 37, 2734–2745, 1980.

Warren, S. G., Brandt, R. E., and Grenfell, T. C.: Visible and near-ultraviolet absorptionspectrum of ice from transmission of solar radiation into snow, Appl. Optics, 45, 5320–5334, 2006.

Weller, G.: The tundra microclimate during snow-melt at Barrow, Alaska, Arctic, 25, 291–299, 1972.

Winther, J.-G.: Short- and longterm variability of snow albedo, Nordic Hydrology, 24, 199–212, 1993.

Wiscombe, W. J. and Warren, S. G.: A model for the spectral albedo of snow. I: Pure snow, J. Atmos. Sci., 37, 2712–2733, 1980.

WMO Guide to Meteorological Instruments and methods of Observation, WMO-No. 8 (Seventh Edition,6 August 2008), http://www.wmo.int/pages/prog/www/IMOP/publications/CIMO-Guide/CIMO_Guide-7th_Edition-2008.html, 2008.

Reprinted from
The Cryosphere, 8, 991– 995,
doi: 10.5194/tc-8-991-2014

III

The Cryosphere, 8, 991–995, 2014
www.the-cryosphere.net/8/991/2014/
doi:10.5194/tc-8-991-2014

The Cryosphere Open Access

Brief communication: Light-absorbing impurities can reduce the density of melting snow

O. Meinander[1], A. Kontu[2], A. Virkkula[1], A. Arola[3], L. Backman[1], P. Dagsson-Waldhauserová[4,5], O. Järvinen[6], T. Manninen[1], J. Svensson[1], G. de Leeuw[1,6], and M. Leppäranta[6]

[1]Finnish Meteorological Institute, Helsinki, Finland
[2]Arctic Research Center, Finnish Meteorological Institute, Sodankylä, Finland
[3]Kuopio Unit, Finnish Meteorological Institute, Kuopio, Finland
[4]University of Iceland, Department of Physics, Reykjavik, Iceland
[5]Agricultural University of Iceland, Faculty of Environment, Hvanneyri, Iceland
[6]Department of Physics, University of Helsinki, Helsinki, Finland

Correspondence to: O. Meinander (outi.meinander@fmi.fi)

Received: 20 November 2013 – Published in The Cryosphere Discuss.: 10 January 2014
Revised: 10 April 2014 – Accepted: 14 April 2014 – Published: 26 May 2014

Abstract. Climatic effects of black carbon (BC) deposition on snow have been proposed to result from reduced snow albedo and increased melt due to light-absorbing particles. In this study, we hypothesize that BC may decrease the liquid-water retention capacity of melting snow, and present our first data, where both the snow density and elemental carbon content were measured. In our experiments, artificially added light-absorbing impurities decreased the density of seasonally melting natural snow. No relationship was found in case of natural non-melting snow. We also suggest three possible processes that might lead to lower snow density.

1 Introduction

For seasonal snow, snow melting is an important part of the natural annual hydrological cycle. It is forced by atmospheric sensible heat flux and solar radiation, where the albedo is a critical factor due to its large variability. Snow albedo depends primarily on the grain size, wetness, impurities in the near-surface snow layer, and directional distribution of the down-welling irradiance. Deposition of anthropogenic emissions to snow cover potentially causes albedo changes. In terms of its climate forcing, black carbon (also known as light-absorbing aerosol) has been hypothesized to be the second most important human emission, and only carbon dioxide is estimated to have a greater forcing (Bond et al., 2013). The climatic effects of black carbon (BC) in snow are due to reduced snow albedo caused by absorption of solar radiation, and induced melt of darker snow, which again lowers the albedo via the albedo feedback mechanism (e.g. Warren and Wiscombe, 1980; Doherty et al., 2010).

Snow melt starts when snow temperature reaches the melting point. Then, if the heating continues, the volume of liquid water increases until the holding capacity or the saturation point of liquid water is reached. This capacity is 3–5 % on a mass basis and depends on snow grain structure and packing (DeWalle and Rango, 2008). When the flow of melt water begins, the impurities may either be washed down through the snow with the flow, or remain in the snow. It has been shown that BC is less likely to be washed down through the snow with melt water (Conway et al., 1996; Doherty et al., 2013).

Hence, if we consider natural snow with anthropogenic BC, we can assume this impurity to remain in the melting snowpack, not to be washed down, and to potentially cause changes in the snow properties and structure, as compared to clean snow. Therefore, we hypothesize that BC in snow might affect the liquid-water retention capacity of melting snow. To test this hypothesis, we use our data of cold and melting snow, where both the snow density and BC content were measured.

2 Materials

All our snow density and BC data have been obtained for natural seasonally melting snow in Sodankylä (67°25′ N, 26°35′ E), Finland, north of the Arctic Circle. By natural snow we refer to a snow pack that has formed from snowfall (i.e. has not been produced by a snow cannon, and has not been affected by human activity, e.g. snow clearing). The data contain cases of cold and melting snow, both with and without experimentally added impurities (Table 1).

The cold snow samples were snow on a lake (17 March 2009), various sites around the Sodankylä area (13 and 19 March 2009 and 23–24 March 2010), and a fenced experimental field (6 and 10 April 2013). The melting snow data were from the experimental field only (17–18 April 2013 before and after rain).

The data originate from three campaigns: the Soot on Snow experiment in 2013 (SoS-2013); the Snow Reflectance Transition Experiment (SNORTEX 2008–2010, see Meinander et al., 2013 for more details); and the SnowRadiance-campaign (SR-2009). The SoS-2013 campaign was carried out at the Sodankylä airport to study the effects of deposition of impurities on surface reflectance, albedo and melt of seasonal snow. The experimental area was a large, flat, fenced open space, and the gravel ground was not covered with concrete or asphalt (Fig. 1). Different amounts of impurities were deposited to snow on different spots, each with diameter of 4 m, and thereafter the spots were monitored until the snow had melted. The sites were left to develop naturally, introducing as little disturbance as possible. Here we used data from three experimental spots with chimney soot, one spot with Icelandic volcanic sand from Ólafur Arnalds (Agricultural University of Iceland) and Haraldur Olafsson (University of Iceland), and one reference spot.

The SnowRadiance (SR) was an ESA-funded project aiming at determining snow properties from optical satellite measurements. The BC samples were collected from the snow over ice on Lake Orajärvi. The lake is frequently used in the winter, e.g. for snowmobiling.

During the SoS-2013, the SNORTEX-2009, and the SR-2009 campaigns, surface snow samples were collected for analysis of their elemental carbon (EC) and organic carbon (OC) concentrations using the filter-based thermal-optical method, described and used in, for example, Forsström et al. (2009). The EC is used as a proxy of BC, due to the measurement technique used. In the SNORTEX-2010 campaign, the sampling, filtering, and laboratory spectrometer analysis followed the procedures presented in Doherty et al. (2010). Several samples were collected from each location.

The snow densities (weight per volume) were measured manually, for either the whole snowpack vertical column (snow tube for SR and SNORTEX data), or for separate horizontal snow layers (density cutter for SoS data to measure the density of the visually dirty surface snow). One density measurement for each location was made. To estimate the standard deviation of the density measurement, an earlier data set of FMI was applied. Sampling of wet snow for density measurements may be difficult since liquid water easily escapes from the sampling box. Here the SoS data for melting snow was obtained for two subsequent days (Table 1), before and after rainfall. The snow was then wet, but not dripping wet, and no water escape from sampling was detected.

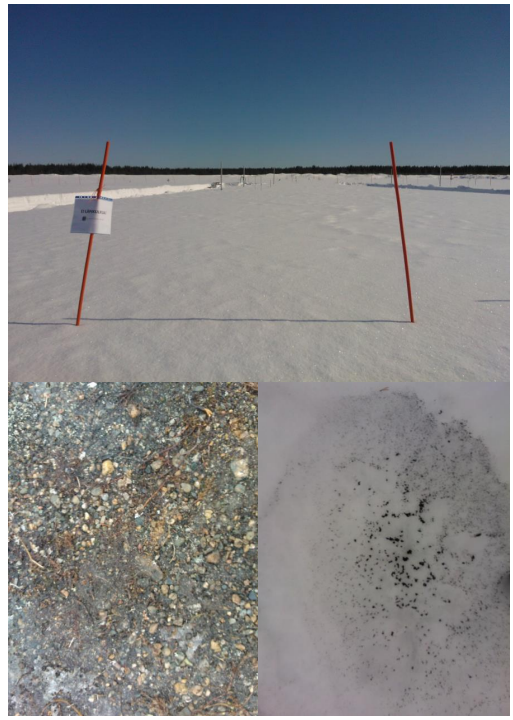

Figure 1. The SoS-2013 experiment. **(a)** Top: the flat and open experimental field with the seasonal snow pack; **(b)** bottom left: the ground under the snow, i.e. a natural gravel surface, not covered by concrete or asphalt, offered an uniform surface for the snow cover; **(c)** bottom right: previously added impurities were visible on the surface of the melting snow, here volcanic sand.

In the SoS-2013 data, snow hardness, grain sizes, and grain shapes were estimated and classified according to the International Classification for Seasonal Snow on the Ground (Fierz et al., 2009).

3 Results

In our data for non-melting natural snow from the SR-2009, SNORTEX-2009, SNORTEX-2010 and SoS-2013 campaigns, the BC concentrations varied between 8 and 126 ppb, and snow densities were 200–264 kg m^{-3}. The density did not depend on the BC content (Fig. 2a, the dots inside the circle).

Table 1. The origin of our Sodankylä snow density data coupled with BC analysis results. The campaigns are explained in the text.

Year	Date	Data origin	Location	Snow	Artificial impurities	BC analysis
2009	17 Mar	SR campaign	Snow on lake Orajärvi	Cold snow	No	Thermal-optical
2009	13, 19 Mar	SNORTEX	Sodankylä area	Cold snow	No	Thermal-optical
2010	23, 24 Mar	SNORTEX	Sodankylä area	Cold snow	No	Spectrometer (Doherty et al., 2010)
2013	6, 10 Apr	SoS-2013	Sodankylä airport	Cold snow	Yes	Thermal-optical
2013	17 Apr	SoS-2013	Sodankylä airport	Melting, before rain	Yes	Thermal-optical
2013	18 Apr	SoS-2013	Sodankylä airport	Melting, after rain	Yes	Thermal-optical

However, in our SoS-experiment data of 6 April 2013, the snow with the BC maximum of 1465 ppb (Fig. 2a, one data point for wood burning soot), had the lowest density of all our data, 168 kg m^{-3}. MFcr-grains (melt–freeze crust, as a result of melting and freezing) were 0.25–1.5 mm in diameter, the surface hardness value was 4 (hard snow) and the snow depth was 56 cm. For comparison, with the reference non-sooted natural snow at that time (10 April 2013) on the same experimental field: the Ppir-grains (Precipitation particles) were irregular crystals, of 0.25–0.75 mm in diameter. The BC concentration was 126 ppb, the density was 210 kg m^{-3}, the hardness value was 1 (very soft snow), and the snow depth was 65 cm.

Our experimental data show that for the seasonally melting natural Arctic snow, with and without artificially added soot or volcanic ash, there was a correlation between the density and the BC content of snow (Fig. 2b). This was the case both prior to a rain period, and the next day after the rain. The densities and the corresponding BC contents were measured separately for the top 5 cm of the snow, not for the whole snow pack, and the impurities of volcanic sand, soot from oil burner and wood burning soot were visually observed to remain on the snow surface, too (Fig. 1). All the grains of the surface layer were melt–freeze crust (MFcr).

The BC concentrations in individual snow samples varied from 9 to 730 ppb. From these, the averages for each experimental spot were calculated (92–310 ppb), and plotted in Fig. 2b. The standard deviation (σ) for the clean reference snow samples (no added impurities) was 34 ppb ($n = 7$), and most often σ was larger for spots with added impurities, dependent on the number of samples (from 1 to 5) and the spot properties; e.g. for one spot with added soot, it was $\sigma = 28$ ppb ($n = 5$). The Eq. (1) shows the relation between the snow density ρ_s [kg m^{-3}], and the BC content C_{BC} [ppb] for the melting snow derived from the SoS-2013 data ($R^2 = 0.66$):

$$\rho_s = -0.27 C_{BC} + 440.6, \quad (1)$$

where $C_{BC} = [92{,}310]$ ppb. The 95 % confidence interval of the slope of the Eq. (1) is from -0.46 to -0.08, that is, we are 95 % confident that the true slope of this equation is in the range defined by -0.27 ± 0.19.

For the snow density, we had one measurement for each location. Therefore, using a previous FMI Sodankylä snow density data set (unpublished data), the average standard deviation was determined, providing a value of 17 kg m^{-3} ($n = 79$ pairwise measurements, $n_{tot} = 158$, $\rho_s = [104{,}408]$ kg m^{-3}) for the Sodankylä data.

4 Discussion and conclusions

All our data of cold snow and melting snow represent the natural seasonal snow cover in Sodankylä, north of the Arctic Circle. For the cold snow, the density was 200–264 kg m^{-3} with BC 8–126 ppb. Our experimental results for an excessive (1465 ppb) amount of added BC (wood-burning soot) show a reduction of the cold snow density. This result is based on comparison of one sooted vs. one reference spot only; more data are needed to confirm this result. Earlier, Meinander et al. (2013) reported on a larger data set (their Table 3), where the snow BC content, in Sodankylä snow cover in 2009–2011, varied in one sampling location between 9 and 106 ppb in the natural snow cover. Thus, our cold snow data presented here represents well the natural BC variability in Sodankylä.

Artificially added impurities in our experiments on natural snow decreased the snow density of melting snow (Fig. 2, Eq. 1). Moreover, the densities were measured both prior to and after rainfall (4.9 mm water in 3 h), which occurred between two subsequent measurement days. In both cases, the larger the BC content, the smaller the density. Thus the rain did not change this order, which further supported our hypothesis that the impurities may affect the water retention capacity. Furthermore, according to our recent laboratory experiment (unpublished data), we found that snow with artificially added soot released melt water sooner than snow without added soot. For this experiment, we added a known amount of soot to a snow sample, mixed the soot and snow, and let the snow melt indoors, while measuring the melt water on a drip pan as a function of time. The results showed

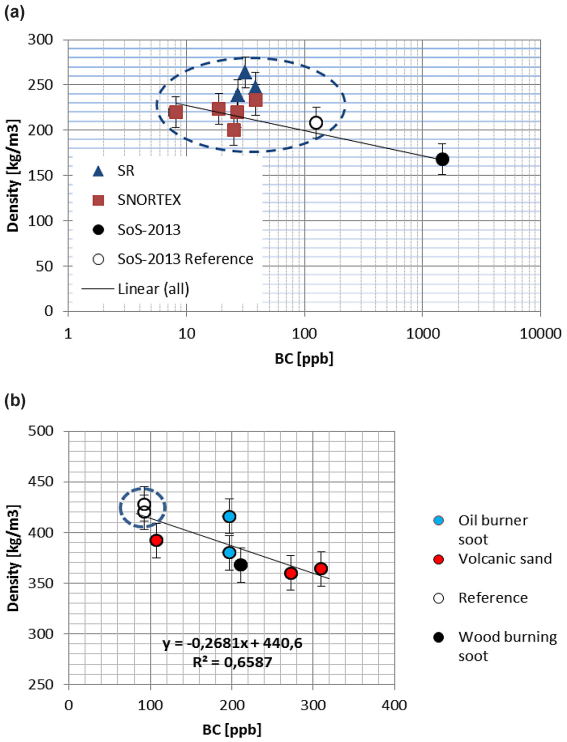

Figure 2. The black carbon (BC) content [ppb] vs. density [kg m^{-3}] for the natural seasonal snow cover in Sodankylä, north of the Arctic Circle with and without artificially added impurities. The line is the least squares linear fit through all the points. **(a)** Cold snowpack: for natural snow without added impurities, BC concentrations were 8–126 ppb, and snow densities were 200–264 kg m^{-3} and for the reference SoS-2013 spot BC was 126 ppb and the snow density was 210 kg m^{-3} (within the circle); when wood-burning soot was artificially deposited to this SoS-spot, BC in snow was measured to be 1465 ppb, and snow density decreased to 168 kg m^{-3} (outside the circle). **(b)** Melting snow: SoS-2013 data for reference spots (within the circle), and spots with artificially added impurities of volcanic sand, soot from oil burner and wood burning soot (outside the circle). The densities and corresponding carbon contents were measured separately for the specified surface layers, not for the entire snow pack.

that while the control snow started to release melt water after 40 min, the snow with added soot released melt water already after 12 min. When cold water was added on snow, the control snow released water after 29 min, while the same amount of water in sooted snow caused water to release already after 7 min. All the snow samples were of the same size (same weight and volume) representing the same natural snow, and mechanically treated the same way whether soot was added or not, for example, the control snow was also mixed although no soot was added. Hence, these new experimental data were found to support our hypothesis that BC may decrease the liquid-water retention capacity of melting snow.

As a summary, according to our experience and observations, we suggest three possible processes that might lead to the lower snow density:

1. *A semi-direct effect of absorbing impurities*. Absorbing impurities would cause melt and/or evaporation from the liquid phase and sublimation from the solid phase of the surrounding snow, resulting in air pockets around the impurities, and thus lower snow density. We have empirical observations, where impurities (both organic and inorganic) in the snow have been surrounded by air pockets.

2. *BC effect on the adhesion between liquid water and snow grains*. If BC reduces adhesion, the liquid-water holding capacity decreases. For linear warming the influence on the density of wet snow is then max 5 % (at this level water flow starts in natural snow). However, with daily cycles, warm days and cold nights, the weaker adhesion may push liquid water down more day-by-day and then the influence to the density would be larger. This way also melt–freeze metamorphosis would produce less dense snow.

3. *BC effect on the snow grain size.* Absorbing impurities would increase the melting and metamorphosis processes, resulting in larger snow grains, which would lower the water retention capacity. Earlier, Yamaguchi et al. (2010) have suggested that the water retention curve of snow could be described as a function of grain size using soil physics models. Here our data showed some slight indication for the possibility of soot in snow to result in larger snow grain sizes via increased melt and metamorphosis, and our data did not show clear evidence against this possibility.

Volcanic sand is assumed not to contain BC (Dadic et al., 2013, Fig. 12a). This assumption is further supported by our own EC analysis of volcanic sand samples with the thermal – optical method showing hardly any EC. Instead, the BC in our volcanic sand spot can be assumed to originate either from long-range transport, or from our other experimental spots with added soot; carbonaceous material in volcanic aerosols has also been proposed to be due to tropospheric air that is entrained into the volcanic jet and plume (Andersson et al., 2013). Our observations and measurements indicate that for a visually darker snow surface, the analyzed BC content is larger and the measured snow density is smaller, regardless of whether soot or volcanic sand had been added to the spot.

The significance of our results on reduction of snow density, and possibly also decreasing water holding capacity due to the black carbon, may be due to the fact that (i) snow density is an important snow parameter that has been found to

correlate with several factors affecting the snow melt, such as snow age and liquid-water holding capacity (Kuusisto, 1984); (ii) snow density multiplied by snow depth equals the important climate model parameter of snow water equivalent (SWE); and (iii) our results may have potential in reducing the uncertainties (IPCC, 2013) related to the effect of black carbon on snow melt and climate change.

In nature, the low density of new dry snow increases due to gravitational settling, wind packing, sintering, and melt–freeze events. These processes depend on the grain size, shape and organization, and snow temperature. The density of snow is also affected by water vapour diffusion in the snow pack, as well as by the temperature and the vegetation under the snow. In our experimental data, we can assume similar environmental conditions with only the impurity contents in snow being the varying factor; our results are for natural snow on natural ground, and we did not have data for drainage of melt water in the snowpack. Here we reported our first results, and more data are needed to further study the effect of light-absorbing impurities on density and water retention capacity of melting snow.

Acknowledgements. The authors thank all the participants of the campaigns of SoS-2013, SNORTEX-2010, SNORTEX-2009 and SR-2009, especially Antti Aarva. Filters from the 2010 snow samples were analyzed for BC by S. Doherty. We gratefully acknowledge support from the Academy of Finland (A4-project), and the Nordic Center of Excellence (NCoE), Nordic Top Research Initiative "Cryosphere-atmosphere interactions in a changing Arctic climate" (CRAICC), and the EU Life+ project Mitigation of Arctic warming by controlling European black carbon emissions, MACEB (project no. LIFE09 ENV/FI/000572).

Edited by: M. Boy

References

Andersson, S. M., Martinsson, B. G., Friberg, J., Brenninkmeijer, C. A. M., Rauthe-Schöch, A., Hermann, M., van Velthoven, P. F. J., and Zahn, A.: Composition and evolution of volcanic aerosol from eruptions of Kasatochi, Sarychev and Eyjafjallajökull in 2008–2010 based on CARIBIC observations, Atmos. Chem. Phys., 13, 1781–1796, doi:10.5194/acp-13-1781-2013, 2013.

Bond, T. C., Doherty, S. J., Fahey, D. W., Forster, P. M., Berntsen, T., DeAngelo, B. J., Flanner, M. G., Ghan, S., Kärcher, B., Koch, D., Kinne, S., Kondo, Y., Quinn, P. K., Sarofim, M. C., Schultz, M. G., Schulz, M., Venkataraman, C., Zhang, H., Zhang, S., Bellouin, N., Guttikunda, S. K., Hopke, P. K., Jacobson, M. Z., Kaiser, J. W., Klimont, Z., Lohmann, U., Schwarz, J. P., Shindell, D., Storelvmo, T., Warren, S. G. and Zender, C. S.: Bounding the role of black carbon in the climate system: A scientific assessment, J. Geophys. Res.-Atmos., 118, 5380–5552, doi:10.1002/jgrd.50171, 2013.

Conway, H., Gades, A., and Raymond, C. F.: Albedo of dirty snow during conditions of melt, Water Resour. Res., 32, 1713–1718, 1996.

Dadic, R., Mullen, P. C., Schneebeli, M., Brandt, R. E., and Warren, S. G.: Effects of bubbles, cracks, and volcanic tephra on the spectral albedo of bare ice near the Transantarctic Mountains: Implications for sea glaciers on Snowball Earth, J. Geophys. Res.-Earth, 118, 1658–1676, doi:10.1002/jgrf.20098, 2013.

DeWalle, D. R. and Rango, A.: Principles of snow hydrology, Cambridge University Press, Cambridge, UK, 2008.

Doherty, S. J., Warren, S. G., Grenfell, T. C., Clarke, A. D., and Brandt, R. E.: Light-absorbing impurities in Arctic snow, Atmos. Chem. Phys., 10, 11647–11680, doi:10.5194/acp-10-11647-2010, 2010.

Doherty, S. J., Grenfell, T. C., Forsström,S., Hegg, D. L., Brandt, R. E., and Warren, S. G.: Observed vertical redistribution of black carbon and other insoluble light-absorbing particles in melting snow, J. Geophys. Res.-Atmos., 118, 5553–5569, 2013.

Fierz, C., Armstrong, R. L., Durand, Y., Etchevers, P., Greene, E., McClung, D. M., Nishimura, K., Satyawali, P. K. and Sokratov, S. A.: The International Classification for Seasonal Snow on the Ground, IHP-VII Technical Documents in Hydrology No. 83, IACS Contribution No. 1, UNESCO-IHP, Paris, 2009.

Forsström, S., Ström, J., Pedersen C. A., Isaksson, E., and Gerland, S.: Elemental carbon distribution in Svalbard snow, J. Geophys. Res., 114, D19112, doi:10.1029/2008JD011480, 2009.

IPCC, "Climate Change 2013: The Physical Science Basis. Working Group I Contribution to the IPCC 5th Assessment Report – Changes to the Underlying Scientific/Technical Assessment" (IPCC-XXVI/Doc.4), http://www.ipcc.ch/report/ar5/wg1/ (last access: 22 May 2014), 2013.

Kuusisto, E.: Snow accumulation and snowmelt in Finland. Publications of the Water Research Institute, National Board of Waters, Finland, No. 55, 149 pp., 1984.

Meinander, O., Kazadzis, S., Arola, A., Riihelä, A., Räisänen, P., Kivi, R., Kontu, A., Kouznetsov, R., Sofiev, M., Svensson, J., Suokanerva, H., Aaltonen, V., Manninen, T., Roujean, J.-L., and Hautecoeur, O.: Spectral albedo of seasonal snow during intensive melt period at Sodankylä, beyond the Arctic Circle, Atmos. Chem. Phys., 13, 3793–3810, doi:10.5194/acp-13-3793-2013, 2013.

Warren, S. G. and Wiscombe, W. J.: A model for the spectral albedo of snow. II: Snow containing atmospheric aerosols, J. Atmos. Sci., 37, 2734–2745, 1980.

Yamaguchi, S. Katsushima, T., Sato, A., and Kumakura, T.: Water retention curve of snow with different grain sizes, Cold Reg. Sci. Technol., 64, 87–93, doi:10.1016/j.coldregions.2010.05.008, 2010.

Reprinted from
The Arabian Journal of Geosciences, 9: 126,
doi:10.1007/s12517-015-2224-6

IV

Arab J Geosci (2016) 9: 126
DOI 10.1007/s12517-015-2224-6

ORIGINAL PAPER

Insulation effects of Icelandic dust and volcanic ash on snow and ice

Monika Dragosics[1] · **Outi Meinander**[2] · **Tinna Jónsdóttír**[1] · **Tobias Dürig**[1] · **Gerrit De Leeuw**[2,3] · **Finnur Pálsson**[1] · **Pavla Dagsson-Waldhauserová**[1,4,5,6] · **Throstur Thorsteinsson**[1]

Received: 28 July 2015 / Accepted: 20 October 2015 / Published online: 24 February 2016

Abstract In the Arctic region, Iceland is an important source of dust due to ash production from volcanic eruptions. In addition, dust is resuspended from the surface into the atmosphere as several dust storms occur each year. During volcanic eruptions and dust storms, material is deposited on the glaciers where it influences their energy balance. The effects of deposited volcanic ash on ice and snow melt were examined using laboratory and outdoor experiments. These experiments were made during the snow melt period using two different ash grain sizes (1 ϕ and 3.5 ϕ) from the Eyjafjallajökull 2010 eruption, collected on the glacier. Different amounts of ash were deposited on snow or ice, after which the snow properties and melt were measured. The results show that a thin ash layer increases the snow and ice melt but an ash layer exceeding a certain critical thickness caused insulation. Ash with 1 ϕ in grain size insulated the ice below at a thickness of 9–15 mm. For the 3.5 ϕ grain size, the insulation thickness is 13 mm. The maximum melt occurred at a thickness of 1 mm for the 1 ϕ and only 1–2 mm for 3.5 ϕ ash. A map of dust concentrations on Vatnajökull that represents the dust deposition during the summer of 2013 is presented with concentrations ranging from 0.2 up to 16.6 g m^{-2}.

Keywords Iceland · Insulation · Ash · Dust · Snow · Albedo

This article is part of the Topical Collection on *DUST*

✉ Monika Dragosics
mod3@hi.is

[1] Institute of Earth Sciences, University of Iceland, Reykjavik, Iceland

[2] Finnish Meteorological Institute, Helsinki, Finland

[3] Department of Physics, University of Helsinki, Helsinki, Finland

[4] Faculty of Environmental Sciences, Agricultural University of Iceland, Hvanneyri, Iceland

[5] Faculty of Physical Sciences, University of Iceland, Reykjavík, Iceland

[6] Faculty of Environmental Sciences, Department of Ecology, Czech University of Life Sciences Prague, Prague, Czech Republic

Introduction

The physical and optical properties of snow are influenced by the presence of impurities, in particular by absorbing material such as aerosol particles deposited on the snow surface (e.g., Doherty et al. 2010 and Painter et al. 2012). Effects of aerosol particles on, for instance, snow melt and albedo (e.g., Meinander et al. 2013) and bidirectional reflection (Peltoniemi et al. 2009) have been studied for natural snow and during campaigns where impurities were deposited on snow in different quantities (e.g., Meinander et al. 2014). Commonly, the effects of impurities, such as black carbon, are studied, which are transported from their source regions to the snow-covered northern latitudes. The properties of snow and ice on the surface of glaciers in Iceland are influenced by the deposition of dust (Arnalds et al. 2014) and, during volcanic eruptions, by volcanic ash. The 2010 eruption of Eyjafjallajökull (Thorsteinsson et al. 2012) not only influenced the whole global air traffic by tephra release into the atmosphere up to 10 km a.s.l. reaching as far as the southern parts of Europe (e.g., Bonadonna et al. 2011; Bursik et al. 2012; Gudmundsson et al. 2012a) but also drastically influenced the albedo of glaciers in Iceland (Gudmundsson et al. 2012b and Pálsson

et al. 2013). The majority of Icelandic tephra is basaltic in origin resulting from the mid ocean ridge basalt, but the chemical composition of tephra varies between different volcanic systems and even eruptions. Phreatomagmatic basaltic eruptions are typical in Iceland and occur from subglacial, subaerial, and submarine volcanoes (Thordarson and Larsen 2007). Therefore, Icelandic ash and dust is mainly basaltic volcanic glass which is deposited in Iceland's sandy deserts which cover an area over 22.000 km^2. Deserts of this composition are globally unique (Arnalds 2010). The ash from Eyjafjallajökull 2010 was of andesitic composition, slowly progressing from benmorite to thrachyte as the eruption proceeded with a silicic content ranging from ~58–69 % SiO_2. (Gislason et al. 2011 and Gudmundsson et al. 2012a)

Several dust storms occur in Iceland every year with deposition of dust or ash on the ice caps (Arnalds et al. 2014) with varying amounts at different altitudes which influence their melting behaviour. These dust storms are as well volcanic in origin (Arnalds et al. 2013) but redistributed and deposited in the glacier forefield where it is mixing with glacial till. From the forefield, it can be resuspended into the air by the action of wind and carried onto the glacier. After the 2010 eruption, the entire Eyjafjallajökull ice cap and most of the neighbouring Mýrdalsjökull were covered with a thick tephra layer, insulating the glacier surface whereas a thin tephra layer on Vatnajökull, Hofsjökull and Langjökull significantly increased the absorption of shortwave radiation and therefore enhanced melting (Gudmundsson et al. 2012b and Pálsson et al. 2013). In this paper, effective and critical thicknesses for Eyjafjallajökull (2010) ash are studied and compared with the help of outdoor and laboratory experiments. The effective thickness is the thickness when the material-covered ablation is maximized The critical thickness is the thickness of the material covering the ice or snow where the ablation rate of the material-covered ice or snow equals that of clean snow or ice; more material will start to insulate. (Brock et al. 2007).

The aim was to study the influence of ash layers of variable thickness, as would result from dust storms or eruptions and how they influence glacier surface mass balance, whether they insulate the ice or enhance melting. The thickness of dust layers in dust storms is rather thin and is expected to enhance melting, whereas during eruptions layers can be very thick. In Gudmundsson et al. (2012a), it was reported that the maximum thickness of the ash layer from the Eyjafjallajökull 2010 eruption exceeded 30 m close to the vent and 1 m thickness 2 km away from the vent, whereas on SW Vatnajökull it was reported to be a 0.1 mm thick tephra layer covering the ice. In the 2011 eruption of Grímsvötn, observations showed ash thicknesses on Tungnaárjökull (W-Vatnajökull) in a cm to mm scale.

Effective and critical thicknesses for Mt St Helens (1980) tephra are 3 and 24 mm, respectively (Driedger 1981). For the Icelandic volcano Hekla (1947), where tephra was covering ice at Gígjökull, these values were 2 and 5.5 mm, respectively (Kirkbride and Dugmore 2003). For rock debris effective and critical thicknesses are much thicker than for tephra (usually ~10 and ~15–50 mm, respectively) due to its low thermal conductivity. Because of the typically darker colour of tephra, small concentrations can dramatically reduce snow or ice albedo and increase ablation rates (Driedger 1981).

No previous scientific papers were found on the insulation effect of the tephra from the 2010 Eyjafjallajökull eruption, and only one previous paper on insulation effect of Icelandic tephra was found (Kirkbride and Dugmore 2003). Our results were compared with earlier works as described in Table 1.

Table 1 Effective and critical thickness for different materials such as tephra, rock debris and dust

Material	Effective thickness (mm)	Critical thickness (mm)
Mt St Helens (1980) ash[a]	3	24
Hekla (1947) tephra[b]	2	5.5
Rock debris[b]	~10	~15–50
Villarrica tephra (lapilli)[c]	–	<5
Dust (largely organic matter)[d]	–	1.33
Eyjafjallajökull ash (2010, 1 ϕ)	1	9–15
Eyjafjallajökull ash (2010, 3.5 ϕ)	≤1–2	13

[a] Driedger (1981)

[b] Kirkbride and Dugmore (2003)

[c] Brock et al. (2007)

[d] Adhikary et al. (2000)

Materials and methods

Four outdoor and laboratory experiments have been carried out at the Finnish Meteorological Institute (FMI) at Kumpula Kampus in Helsinki, Finland. These experiments contribute to a better understanding of insulation characteristics of ash and dust deposition on Icelandic glaciers. The modalities of different experiments are related to natural conditions, which are described below.

Dust distribution 2013 on Vatnajökull

Dagsson-Waldhauserova et al. (2014) suggest that about half of all dust storms in south Iceland each year occur at temperatures at or below 0 °C; therefore, dust can be mixed together with snow. The deposition of dust on snow or ice has an important climatic effect due to influence on surface albedo reduction and enhanced melt.

Arnalds et al. (2014) calculated the total deposition of dust on the Icelandic glaciers to be 4.5 million tons per year with a mean deposition of 400 g m^{-2} $years^{-1}$. To compare this number with in situ measurements, snow samples from 16 locations on the surface of Vatnajökull (Fig. 1) were sampled in October 2013. Vatnajökull is Iceland's biggest ice cap with an area of more than 8.000 km^2 (Björnsson and Pálsson 2008). These samples represent dust that was deposited during one summer on the glacier surface. The top 8 cm of the snow surface (about 1–2 kg of snow) was collected from an area of approx. 57.2×10^{-3} m^2 for each sample. The 16 snow samples were brought back frozen in plastic bags to the laboratory in Reykjavík where they were melted, evaporated and the mass of the dust was weighed.

Origin and properties of ash used in the experiments

Material used for experiments at FMI was ash from the 2010 Eyjafjallajökull eruption in Iceland. The material was collected on Eyjafjallajökull (sample site in Fig. 1) at 1420 m a.s.l., about 3 km east of the vent. It was collected just after the eruption ended in late May 2010.

The transport distance of different grain sizes depends on wind speed. The smaller the grain size the easier it is transported over long distances. Because of reconstruction of the main mode of the Eyjafjallajökull tephra fall out (Bonadonna et al. 2011 and Folch et al. 2012), ash has been used in the grain sizes 1 ϕ (500 μm) and 3.5 ϕ (90 μm) in the experiments. The bulk density for the 1 ϕ ash was measured as 2.57 g cm^{-3} and for 3.5 ϕ 2.46 g cm^{-3}. The particles of both grain sizes were investigated by SEM analysis. The ash

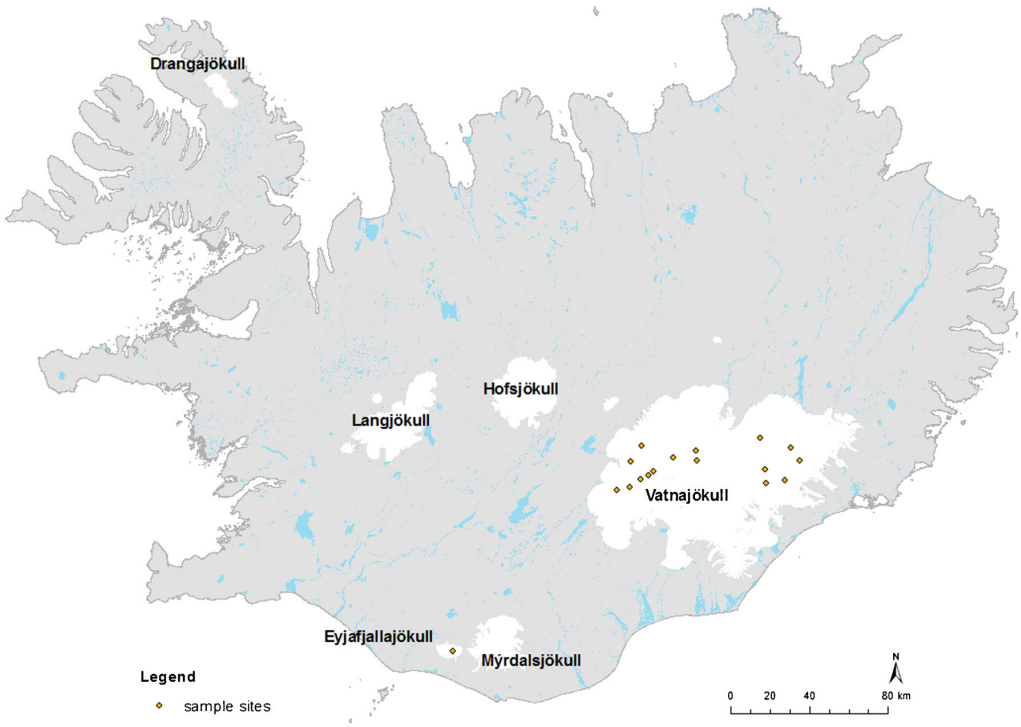

Fig. 1 Iceland with glacier outlines and sample sites on Vatnajökull and Eyjafjallajökull (base map by Landmælingar Íslands, 1993)

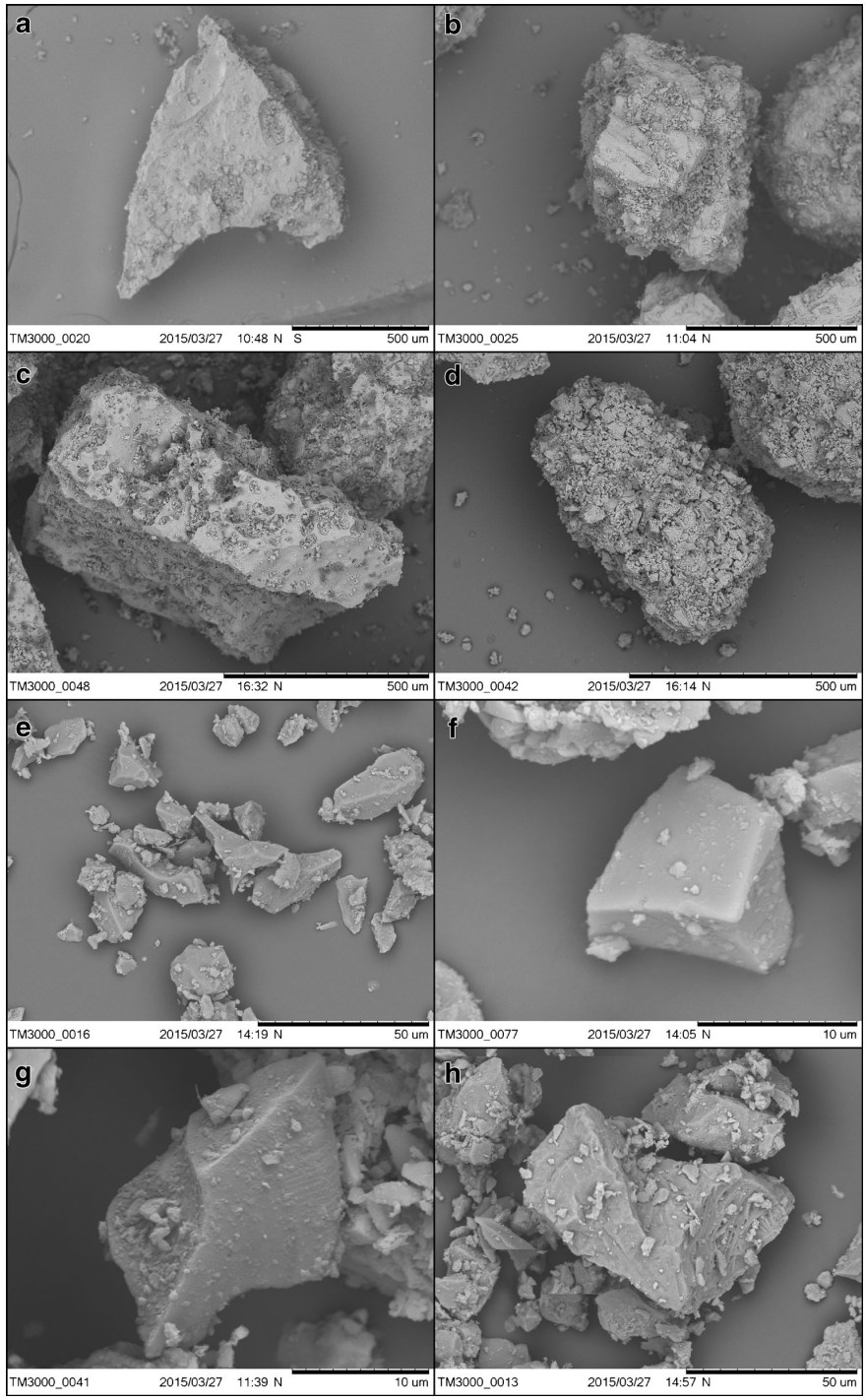

Fig. 2 SEM images of representative ash particles. **a** Particles of the fraction 1 ϕ are of blocky shape with angular or **b** stepped surfaces, **c** partly featuring indications of high vesicularity. **d** The surfaces of these coarse grains are mostly covered by adhesive ash particles of the smaller fractions which considerably affect their overall shape. **e** A blocky shape is also the key characteristic of the particles from the 3.5 ϕ fraction. **d-g** Both, angular and **h** stepped surface features can be identified

population is dominantly characterized by blocky shaped particles with stepped features and blocky angular particles with clustered clasts with smaller adhesive particles (Fig. 2) and is in agreement with former investigations of the ash (Dellino et al. 2012). However, this research includes as well proximal samples of the vent that have not been yet investigated before.

Experiments

Four outdoor (AoS-2015, Roof 2015 and AiC-2015) and laboratory (AoI-2015) experiments were carried out using snow (AoS-2015), ice (AoI-2015, Roof 2015) and snow over ice (AiC-2015). Ash of 1 ϕ grain size was used for the AoS-2015, AoI-2015 and AiC-2015 experiments, whereas ash of 1 and 3.5 ϕ was used for Roof 2015 experiment. Layer thicknesses were measured above 1 mm and in dry condition of the ash.

AoS-2015

The Ash on Snow (AoS-2015) experiment is an outdoor experiment on the effect of ash on snow in natural conditions. The experiments started on 6 February 2015 using natural snow in a fenced area, i.e., unperturbed by direct human interference. There are some impurities due to deposition of atmospheric aerosol particles from the air, with an unknown concentration; however, their concentration is negligible compared to the ash applied to the surface. Three different amounts of ash, 15 g (166 g m^{-2}), 85 g (944 g m^{-2}) and 425 g (4722 g m^{-2}, 15 mm layer thickness) with grain size 1 ϕ, were deposited on an area of 0.3 × 0.3 m^2 on a snow surface (Fig. 3) with a snow density of 280 kgm^{-3}.

Snow depth and temperature were then monitored for 17 days when the snow was melted naturally.

AoI-2015

A controlled experiment with ash on ice was made both indoors (AoI-2015) and outdoors (Roof-2015), to identify and separate the effects of temperature and solar irradiance.

Ash on Ice (AoI-2015) were laboratory experiments to examine the effect of ash layer thickness on ice melting, in a temperature-stabilized environment kept at +24 °C. For these experiments, small, transparent plastic boxes (Fig. 4) were filled with 200 ml of tap water and frozen (surface area 84 cm^2). This resulted in an ice layer with a depth of 25–28 mm. To find the insulating threshold of ash on ice, four different amounts of the 1 ϕ impurity were deposited: 3 g (1.3 ml, 366 g m^{-2}), 35 g (15 ml, 4219 g m^{-2}, 1 mm layer thickness), 71 g (30 ml, 8437 g m^{-2}, 3 mm layer thickness) and 283 g (120 ml, 33,749 g m^{-2}, 9–13-mm layer thickness). After deposition of material, the ice was transferred into white pots with holes in the bottom to measure the meltwater runoff.

Roof 2015 experiment

The laboratory experiments were repeated outside on the roof of the FMI building in sunny conditions to study effects of solar irradiance in addition to that of temperature above zero. The experiment was repeated with the same volume of impurities, but using two different grain sizes of the Eyjafjallajökull 2010 ash: 1 ϕ (samples A) and 3.5 ϕ (samples B). The concentrations for the 3.5 ϕ B-samples were: 2.46 g (1 ml, 292 g m^{-2}); 36.8 g (15 ml, 4385 g m^{-2}, 1-mm layer thickness), 73.7 g (30 ml, 3–5-mm layer thickness, 8772 g m^{-2}) and 294.7 g (120 ml, 35,086 g m^{-2}, 9–13-mm layer thickness). The concentrations for the 1 ϕ ash were the same as used in AoI-2015.

AiC-2015

The Ash in Container (AiC) experiment was performed in a cold container where ash was deposited on snow over ice. This experiment should evaluate to see if the ash starts insulating as in the outdoor experiments even with a slight different setup of snow over ice. This setup shows more realistically the surface of a glacier with ice below and therefore cooling from above and melting temperatures only from the surface.

A big pot, inside a cold container, was filled at the bottom with a thick ice layer and on top of that an 8.5-cm thick layer of snow was deposited (Fig. 5). Two different amounts of impurities were used as in the outdoor experiments (Fig. 5): 15 g (166 g m^{-2}) and 425 g (4722 g m^{-2}, 15 mm thickness) of 1 ϕ Eyjafjallajökull ash on a 0.3 × 0.3 m^2 area. The experiment started at a temperature of −10 °C inside the container; then, the cooling system was shut down, and it adapted to outdoor temperatures up to +4 °C. Snow depth and behaviour of the ash were monitored.

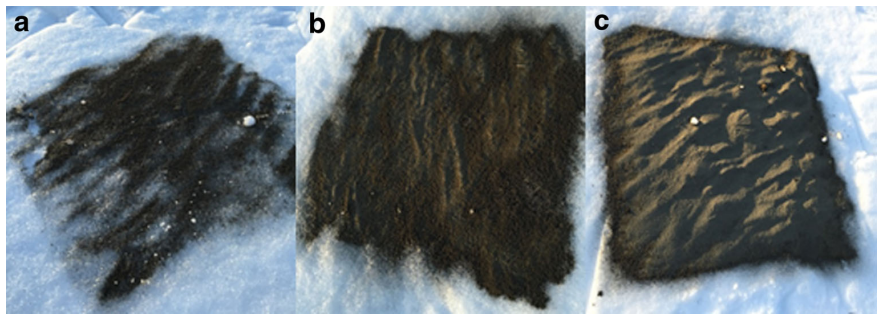

Fig. 3 During the AoS-2015 experiment, different amounts of ash were deposited on a 0.3 × 0.3-m^2 snow surface. **a** 15 g (166 g m^{-2}), **b** 85 g (944 g m^{-2}) and **c** 425 g (4722 g m^{-2}, 15-mm layer thickness)

Fig. 4 During the AoI-2015 experiment, different ash concentrations were applied to ice indoors

Results

Results from the outdoor and indoor snow experiments with Icelandic ash at FMI are presented in this chapter as well as in situ measurements on Vatnajökull depicted in the dust distribution map (Fig. 6). Experiments have helped to understand impacts of deposited amounts on glaciers as in the example of the dust distribution map.

Dust distribution map 2013

Figure 6 shows a map representing the spatial distribution of dust concentration deposited in the summer 2013 on Vatnajökull, a year without volcanic eruptions. This should show that very small amounts of dust or ash are getting deposited on the glacier. The map in Fig. 6 shows the location points (called *stations*) where dust samples were collected, and the colours show the spatial distribution of the dust concentration obtained by interpolation of the measured values (interpolation with the geostatistical analyst method Inverse Distance Weighting (IDW) in ArcMap). Topography was not taken into account in the interpolation. The point locations are not evenly distributed over the glacier area, and the southern part of Vatnajökull was not included in the interpolation due to too large distance from the measurement stations. The southern part of Vatnajökull was left out mainly due to the course of watersheds and snow line at Breiðamerkurjökull.

More dust was deposited in the western part of Vatnajökull than in the north eastern part (Fig. 6). The highest concentration, 16.6 g m^{-2}, was found at station T05 on Tungnaárjökull (SW Vatnajökull). Much lower amounts were found on the upper part of the ice cap, namely at D09, Br7 and BB0. As observed in nature, the highest amounts of dust do not necessary have to be at the lowest altitudes of the glacier (closest to the dust source). Whether the material stays on the surface or is accumulated at a certain spot depends on the local topography, the exposure to wind, the material properties, local weather and melt conditions.

Fig. 5 During the Ash in Container (AiC-2015) experiment, two different amounts of ash were deposited on snow over of ice. Bottom 15 g (166 g m^{-2}) and top 425 g (4722 g m^{-2}, 15 mm layer thickness) of 1 ϕ ash

AoS 2015

The Ash on Snow (AoS-2015) outdoor experiments were started on 6 February (day 0) and lasted for 17 days, until all the snow had melted.

The effective thickness was reached at the medium concentration (turquoise curve, Fig. 7) of ash (85 g), where the snow depth was the lowest, which means that melt was maximized. The ash is absorbing solar irradiance and warming up the snow. The medium concentration seems to be able to absorb more heat than the small concentration (15 g). However, the snow with the two thinnest layers of ash had melted completely in 14 days below the ash, so also faster than the control snow. The snow with the thickest layer of ash (425 g; 15 mm layer thickness) was still 2 cm deep after 14 days and it took 3 more days (day 17) before it had completely melted. Therefore, critical thickness was achieved with the largest deposition of 15 mm layer thickness (7 mm layer thickness in wet conditions at the end of the experiment remained) since the control snow took as long to melt as the large deposition. This observation supports the hypothesis that ash starts insulating the snow when its thickness exceeds a certain limit.

AoI-2015

During AoI-2015, the indoor ice experiment, melting started after 43 min. The clean ice and the two smallest impurities

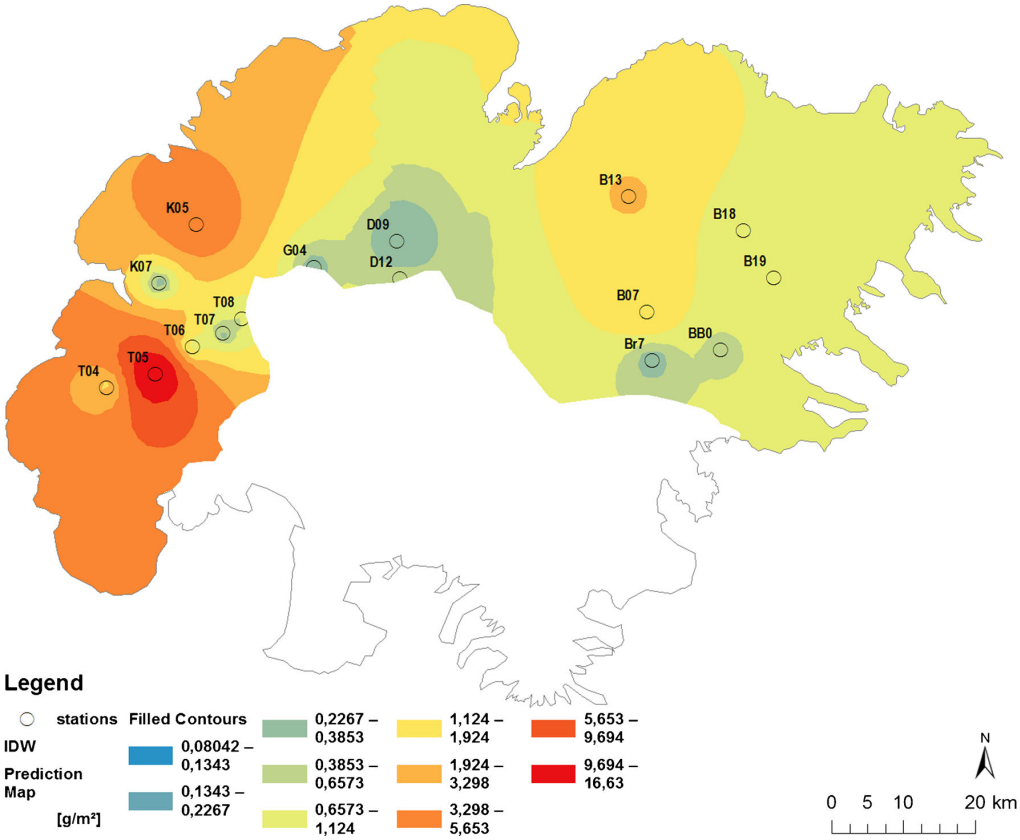

Fig. 6 Inferred dust distribution on Vatnajökull in 2013. The *circles* are the stations where surface snow was collected and the results from these point samples were used for interpolation over the wider area

showed very similar melt behaviour. The onset of the 8437 g m^{-2} (3 mm layer thickness) and 33,749 g m^{-2} (9–13 mm layer thickness) melt took longer; 75 min passed until runoff started at the 8437 g m^{-2} deposition and 125 min for the 33,749 g m^{-2}. The data in Fig. 8 show that once melt had started, the melt rate was similar for all samples. Until saturation at 95 min for the 33,749 g m^{-2} ash, all the melt water was absorbed by the ash, after that it drains as melt water. Also, at the largest deposition, the ice had completely melted after 365 min, earlier then at the other depositions, because the large amount of ash was down wasting the ice and absorbed all the meltwater.

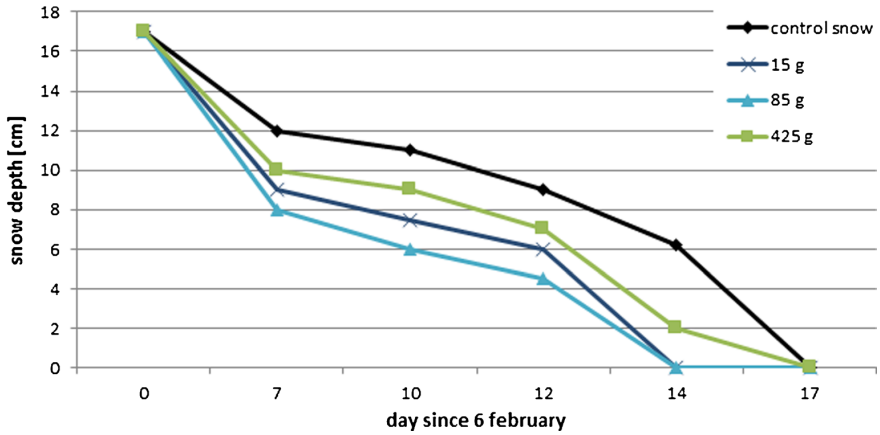

Fig. 7 Outdoor experiment (AoS-2015) with ash concentrations with three different amounts, 15 g (166 g m^{-2}), 85 g (944 g m^{-2}) and 425 g (4722 g m^{-2}, 15-mm layer thickness) in the size of 1 ϕ of impurities on natural snow on the ground

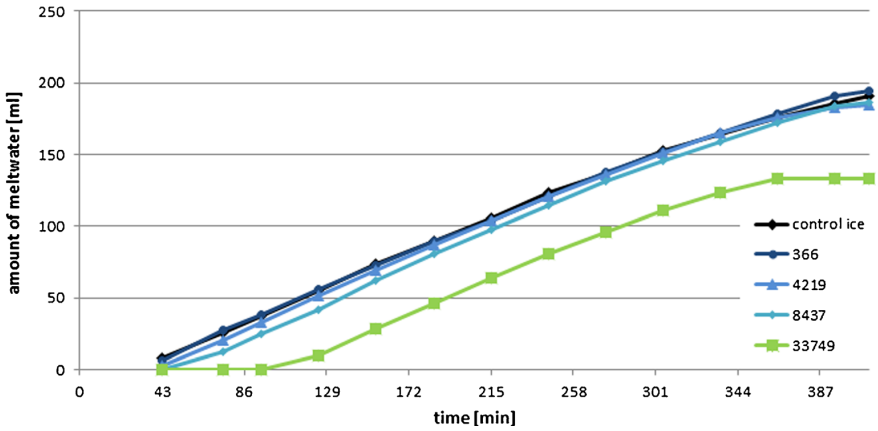

Fig. 8 Experiment with Ash on Ice (AoI) at indoor temperatures of +24 °C with four different concentrations. The amounts in g m^{-2} are indicated by different *colours* as indicated in the legend

Roof-2015

The indoor ice experiment was repeated outside in sunny conditions to study the insulating properties of ash with solar radiation. The results are presented in Fig. 9, which shows the measured amount of meltwater as a function of time for 10 different experiments. Two of these, A1 and B1, are reference measurements with clean reference ice: A1 was left in the shadow where the influence of radiation on temperature and melt is minimized, and B1 was the clean reference sample in the sun.

The highest concentrations A5 and B5 (9 and 13-mm layer thickness) were exceeding the critical thickness because they were starting to melt later (after 170 min) than the reference sample B1 in the sun. A3 with the deposition of 4219 g m^{-2} was achieving the effective thickness, with 1-mm thick layer, visible in the steepest curve and maximum melt rate. The two grain sizes showed different behaviours. After saturation of the fine B-material (87 min), it slipped off the ice (B5 in Fig. 10b) whilst the A-material stayed on the surface. Samples A2 (Fig. 10a) and B2 were forming cryoconite holes where the ash was collecting and melting into the ice.

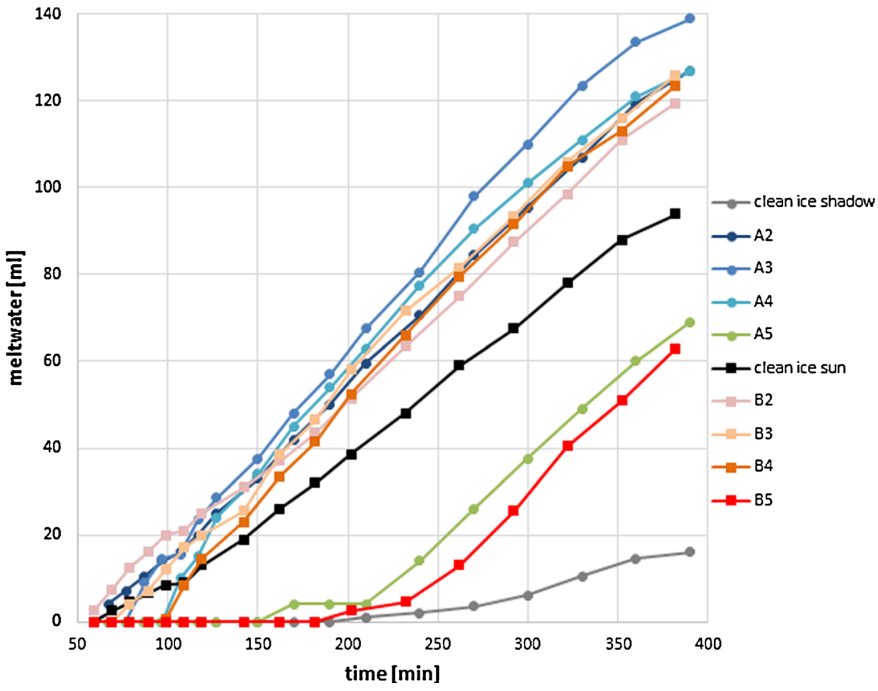

Fig. 9 Experiment with melt behaviour of different amounts of ash deposited on ice (Roof-2015 experiment) including the influence solar radiation. A-samples with 1 ϕ tephra grain sizes, B-samples with 3.5 ϕ grain sizes. A1 and B1 reference measurement (A1 in the shadow, B1 in the sun); A2 366 g m^{-2}; A3: 4219 g m^{-2}, 1-mm layer thickness; A4 8437 g m^{-2}, 3–5-mm layer thickness; A5 33,749 g m^{-2}, 9 mm layer thickness; B2 292 g m^{-2}; B3 4385 g m^{-2}; B4 8772 g m^{-2}, 1–2 mm layer thickness; B5 35,086 g m^{-2}, 13 mm layer thickness

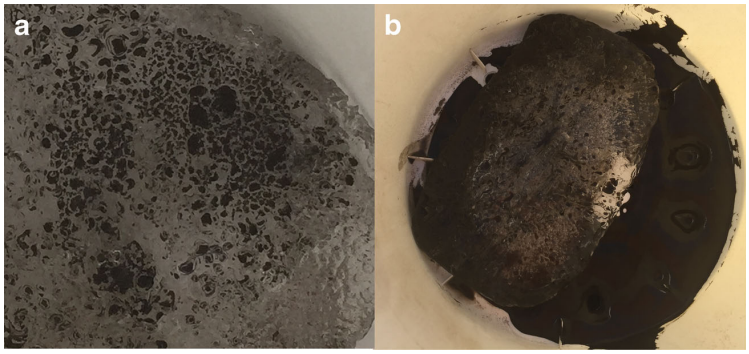

Fig. 10 An example of the ice surface at **a** sample A2 (after 360 min) where ash was melting in cryoconite holes. **b** Sample B5 (after 430 min) where the finer ash slipped off the ice

AiC-2015

The snow on top of the ice had melted inside the container after 1 week. When the control snow was in some parts totally melted, only snow spots of 5 mm thickness were left. In contrast, below the large impurity (425 g) snow of 15 mm thickness with a 5 mm ash layer (wet condition) on top remained. Therefore, the high concentration ash layer supported our assumption to insulate the snow from melt even with temperature influence only. The difference to the other ash on ice experiments was that there was ice beneath the snow so it was cooling from below and the container temperature influenced from above on the snow.

Discussion and conclusions

Our findings suggest that if the ash concentration on snow or ice is small, so the layer thickness is very thin, it has the potential to increase snow melt, but after a threshold the insulation effect begins, and the snow melt is decreased compared to clean ice.

In Table 1, critical and effective thickness of different materials is shown in comparison with the results of our experiments. The two grain sizes of the Eyjafjallajökull 2010 ash behave differently in terms of insulation. The Eyjafjallajökull ash has similar values for effective thickness to the thicknesses of the Icelandic volcano Hekla, it is in the range of 1–2 mm thickness. The critical thicknesses are comparable and visible in all our experiments: in the experiments AoS (at the large deposition with 425 g and 15 mm layer thickness), in the AoI experiment (deposition of 283 g, 120 ml, 33,749 g m^{-2} and 9–13 mm layer thickness), in the Roof 2015 experiment (A5 with 33,749 g m^{-2} and 9 mm layer thickness) as well as in the AiC experiment (425 g deposition and 15 mm layer thickness). The effective thickness was reached at Hekla tephra at 2 mm and at Eyjafjallajökull ash at 1 mm, in the Roof experiment (at A3 with a deposition of 4219 g m^{-2}). The 3.5 ϕ grain size needs a thickness of 13 mm to start insulating as observed in the Roof experiment (B5 with a deposition of 35,086 g m^{-2}). The Roof 2015 experiment shows as well that only 1–2 mm (B4) or smaller (B3, too thin layer to measure) are enough to enhance melt to a maximum for a grain size of 3.5 ϕ.

Different redistribution behaviours of the two grain sizes at the AoI-2015 experiments were observed. The smaller ash particle fraction of 3.5 ϕ slipped off the ice, whilst the layer of 1 ϕ ash stayed on the ice in-tact. It is suggested that the reason for this difference is to be found in the different surface morphologies. Due to the considerable clustering with fine adhesive particles (see e.g., Fig. 2b and d), the coarser material shows a larger specific surface area than 3.5 ϕ particles which feature smooth surfaces (see Fig. 2f and g). Hence, it is likely that the coarse grains are characterized by a larger coefficient of friction than the finer particles. This effect is even increased by the fact that 1 ϕ grains often feature a high vesicularity (Fig. 2c), which facilitates the absorption of water and is expected to enhance static friction. The majority of 3.5 ϕ particles however is blocky and shows no vesicles (see Fig. 2e). Furthermore, the 1 ϕ grains often feature vesicles, which facilitate the absorption of water. This is not the case for the blocky 3.5 ϕ particles characterized by smooth surfaces. This finding implies that finer, smooth particles, are washed away easier by melt streams on the glacier surface than coarser grains with a rough, irregular surface and high vesicularity. Hence, coarser material could have a much greater effect on the albedo.

The highest concentration of dust deposited on Vatnajökull was 16.6 g m^{-2}, which represents dust collection over the summer of 2013. This value is much lower than the mean deposition of 400 g m^{-2} $years^{-1}$ suggested by Arnalds et al. (2014). As the results of the Roof 2015 experiments show for both grain sizes that very small amounts (1–2 mm or smaller) of ash (or dust) deposition are enough to enhance melt, it is possible that the small amounts of dust or ash deposited on Vatnajökull have a comparable melt effect. Similar experiments with volcanic particles of different origins would help to clarify.

Acknowledgments The study described in this manuscript was supported by NordForsk as part of the Nordic Centre of Excellence within the framework of Cryosphere-atmosphere interactions in a changing Arctic climate (CRAICC), which is a part of the Top-level Research Initiative (TRI); Part of this work was supported by the Centre of Excellence in Atmospheric Science funded by the Finnish Academy of Sciences Excellence (project no. 272041), by the Finnish Academy of Sciences project A4 (contract 254195). Gratefully acknowledged are Matti Leppäranta for using his cold laboratory for experiments, the glaciology group of the University of Iceland as well as the Icelandic Glaciological Society for fieldwork support and the Earth Science Institute of the University of Iceland for providing the Eyjafjallajökull tephra. We thank the reviewer and editors for their constructive support.

References

Adhikary S, Nakawo M, Seko K, Shakya B (2000) Dust influence on the melting process of glacier ice: experimental results from Lirung Glacier, Nepal Himalayas. IAHS Publ. 264

Arnalds O (2010) Dust sources and deposition of aeolian materials in Iceland. Icel Agric Sci 23:3–21

Arnalds O, Thorarinsdottir EF, Thorsson J, Waldhauserova PD, Agustsdottir AM (2013) An extreme wind erosion event of the fresh Eyjafjallajokull 2010 volcanic ash. Sci Rep 3

Arnalds O, Olafsson H, Dagsson-Waldhauserova P (2014) Quantification of iron-rich volcanogenic dust emissions and deposition over the ocean from Icelandic dust sources. Biogeosciences 11(23):6623–6632

Björnsson H, Pálsson F (2008) Icelandic glaciers. Jökull 58:365–386

Bonadonna C, Genco R, Gouhier M, Pistolesi M, Cioni R, Alfano F et al (2011) Tephra sedimentation during the 2010 Eyjafjallajökull eruption (Iceland) from deposit, radar, and satellite observations. J Geophys Res Solid Earth (1978–2012), 116(B12)

Brock B, Rivera A, Casassa G, Bown F, Acuñn C (2007) The surface energy balance of an active ice-covered volcano: Villarrica volcano, southern Chile. Ann Glaciol 45(1):104–114

Bursik M, Jones M, Carn S, Dean K, Patra A, Pavolonis M et al (2012) Estimation and propagation of volcanic source parameter uncertainty in an ash transport and dispersal model: application to the Eyjafjallajokull plume of 14–16 April 2010. Bull Volcanol 74(10): 2321–2338

Dagsson-Waldhauserova P, Arnalds O, Olafsson H (2014) Long-term variability of dust events in Iceland. Atmos Chem Phys Discuss 14:17331–17358. doi:10.5194/acpd-14-17331-2014

Dellino P, Gudmundsson MT, Larsen G, Mele D, Stevenson JA, Thordarson T, Zimanowski B (2012) Ash from the Eyjafjallajökull eruption (Iceland): fragmentation processes and aerodynamic behavior. J Geophys Res Solid Earth (1978–2012), 117(B9)

Doherty SJ, Warren SG, Grenfell TC, Clarke AD, Brandt RE (2010) Light-absorbing impurities in arctic snow. Atmos Chem Phys 10(23):11647–11680

Driedger CL (1981) Effect of ash thickness on snow ablation. In: Lipman P, Mullineaux DR (eds) The 1980 eruptions of Mount St Helens. USGS Professional Paper, 1250, 757–760

Folch A, Costa A, Basart S (2012) Validation of the FALL3D ash dispersion model using observations of the 2010 Eyjafjallajökull volcanic ash clouds. Atmos Environ 48:165–183

Gislason SR, Hassenkam T, Nedel S, Bovet N, Eiriksdottir ES, Alfredsson HA et al (2011) Characterization of Eyjafjallajökull volcanic ash particles and a protocol for rapid risk assessment. Proc Natl Acad Sci 108(18):7307–7312

Gudmundsson MT, Thordarson T, Höskuldsson Á, Larsen G, Björnsson H, Prata FJ, et al (2012) Ash generation and distribution from the April-May 2010 eruption of Eyjafjallajökull, Iceland. Sci Rep 2

Gudmundsson S, Pálsson F, Björnsson H, Magnússon E, Thorsteinsson T, Haraldsson HH (2012) The impact of volcanic aerosols on the energy-and mass balance of Langjökull ice cap, SW-Iceland. In AGU Fall Meeting Abstracts (Vol. 1, p. 0659)

Kirkbride MP, Dugmore AJ (2003) Glaciological response to distal Tephra fallout from the 1947 eruption of Hekla, south Iceland. J Glaciol 49(166):420–428

Meinander O, Kazadzis S, Arola A, Riihelä A, Räisänen P, Kivi R et al (2013) Spectral albedo of seasonal snow during intensive melt period at Sodankylä, beyond the Arctic circle. Atmos Chem Phys 13(7): 3793–3810

Meinander O, Kontu A, Virkkula A, Arola A, Backman L, Dagsson-Waldhauserová P et al (2014) Brief communication: light-absorbing impurities can reduce the density of melting snow. Cryosphere 8(3):991–995

Painter TH, Skiles SM, Deems JS, Bryant AC, Landry C (2012) Dust radiative forcing in snow of the upper Colorado River basin: part I. A 6 year record of energy balance, radiation, and dust concentrations. Water Resour Res. doi:10.1029/2012WR011985

Pálsson F, Björnsson H, Guðmundsson S, Haraldsson H (2013) Vatnajökull: mass balance, meltwater drainage and surface velocity of the glacial year 2010-11. Institute of Earth Sciences, University of Iceland and National Power Company, December 2013, RH-24-2013

Peltoniemi J, Hakala T, Suomalainen J, Puttonen E (2009) Polarised bidirectional reflectance factor measurements from soil, stones, and snow. J Quant Spectrosc Radiat Transf 110(17):1940–1953

Thordarson T, Larsen G (2007) Volcanism in Iceland in historical time: volcano types, eruption styles and eruptive history. J Geodyn 43(1): 118–152

Thorsteinsson T, Jóhannsson T, Stohl A, Kristiansen NI (2012) High levels of particulate matter in Iceland due to direct ash emissions by the Eyjafjallajökull eruption and resuspension of deposited ash. J Geophys Res Solid Earth (1978–2012), 117(B9)

Reprinted from
Polar Research, 35, 31313,
doi: 10.3402/polar.v35.31313

Polar Research

LETTER TO THE EDITOR

Icelandic volcanic dust can have a significant influence on the cryosphere in Greenland and elsewhere

Outi Meinander,[1] Pavla Dagsson-Waldhauserova[2,3,4,5] & Olafur Arnalds[2]

[1] Finnish Meteorological Institute, Research and Development, Climate Research, Erik Palmenin aukio 1, FI-00560 Helsinki, Finland
[2] Faculty of Environmental Sciences, Agricultural University of Iceland, Hvanneyri, IS-311 Borgarnes, Iceland
[3] Institute of Earth Sciences, University of Iceland, Saemundargata 2, IS-101 Reykjavik, Iceland
[4] Faculty of Environmental Sciences, Czech University of Life Sciences Prague, Kamycka 961/129, CZ-165 21 Praha 6-Suchdol, Czech Republic
[5] Faculty of Physical Sciences, University of Iceland, Saemundargata 2, IS-101 Reykjavik, Iceland

The melting and darkening of Greenland Ice Sheet (GrIS) has recently been of major concern (Benning et al. 2014; Dumont et al. 2014; Polashenski 2015; Tedesco et al. 2015). Dumont et al. (2014) suggested that the spring-time darkening of the GrIS, which has been observed since 2009, is due to an increased load of light-absorbing impurities (LAIs) in snow that consist of soot or dust and, potentially, microorganisms. Benning et al. (2014) argued that microorganisms, such as the pigmented algae that reside in snow and ice, can cause a substantial reduction in albedo. They also hypothesized that as the climate warms and melt seasons become longer, biological habitats could expand and increasingly contribute to the darkening. Tedesco et al. (2015) stated that despite the crucial impact of albedo in energy balance, the roles of the different processes driving it have yet to be identified. They pointed out that cryoconite (a mixture of dust, pebbles, soot and microbes) and pigmented algae can reduce albedo. Early observations of cryoconite in Greenland snow and ice were made by the Finnish explorer Adolf Erik Nordenskiöld (1883).

More recently, Polashenski et al. (2015) showed that satellite data analysis of Moderate Resolution Imaging Spectrometer (MODIS) surface reflectance from uncorrected Terra sensor degradation has important contributions for detecting Greenland's dry snow zone albedo decline. They did not find that enhanced deposition of LAIs caused significant dry snow albedo reduction or melt events, but they acknowledged prior work on GrIS, wherein the impact of MODIS Terra degradation had been concluded as insignificant. Polashenski et al. (2015) agreed that part of the dry snow zone albedo decline could be real.

We argue that the transport and deposit of light-absorbing Icelandic volcanic dust can have a significant influence in the cryosphere, in Greenland and elsewhere, and that this effect must be addressed in order to constrain glacier and ice cap melt rates and confront the causes of deglaciation.

Iceland is the most important Arctic dust source and the largest of the Arctic deserts (Arnalds et al. 2016). Icelandic volcanic dust can be transported over the North Atlantic to Europe and Greenland (Prospero et al. 2012). Icelandic dust-storm frequency has been estimated to be up to 135 dust days per year. About half of the annual dust events in the southern part of Iceland take place in winter at sub-zero temperatures, when dust mixes with snow (Dagsson-Waldhauserova et al. 2015). The fertilizing effect of dust (Arnalds et al. 2014) can offer an important nutrient source that enables microorganisms to grow. Other living organisms present in Icelandic dust can also be intercontinentally transported. The particle–cryosphere interaction is controlled by the particle properties, which vary according to the origin from the seven major Icelandic dust sources (Arnalds et al. 2016). While hydrophilic particles can be washed down with melt water (Doherty et al. 2013), hydrophobic particles can concentrate on the surface, and play a role in creating environmental conditions within snow/ice that favour the existence of microorganisms.

Assessments of the effect of Icelandic volcanic dust on snow/ice surface darkening and melt in the Greenland cryosphere—and elsewhere—are lacking. We hypothesize that, in the Arctic, Icelandic dust may have a comparable or even larger effect on the cryosphere than soot (Bond et al. 2013). Observations of, and modelling results bearing on, Icelandic dust and cryosphere interactions for the past, present and future are urgently needed.

Correspondence
Outi Meinander, Finnish Meteorological Institute, Research and Development, Climate Research, Erik Palmenin aukio 1, FI-00560 Helsinki, Finland.
E-mail: Outi.Meinander@fmi.fi

References

Arnalds O., Dagsson-Waldhauserova P. & Olafsson H. 2016. The Icelandic volcanic aeolian environment: processes and impacts—a review. *Aeolian Research 20,* 176–195.

Arnalds O., Olafsson H. & Dagsson-Waldhauserova P. 2014. Quantification of iron-rich volcanogenic dust emissions and

Citation: *Polar Research* 2016, *35*, 31313, http://dx.doi.org/10.3402/polar.v35.31313

deposition over the ocean from Icelandic dust sources. *Biogeosciences 11*, 6623–6632.

Benning L.G., Anesio A.M., Lutz S. & Tranter M. 2014. Biological impact on Greenland's albedo. *Nature Geoscience 7*, 691.

Bond T.C., Doherty S.J., Fahey D.W., Forster P.M., Berntsen T., DeAngelo B.J., Flanner M.G., Ghan S., Kärcher B., Koch D., Kinne S., Kondo Y., Quinn P.K., Sarofim M.C., Schultz M.G., Schulz M., Venkataraman C., Zhang H., Zhang S., Bellouin N., Guttikunda S.K., Hopke P.K., Jacobson M.Z., Kaiser J.W., Klimont Z., Lohmann U., Schwarz J.P., Shindell D., Storelvmo T., Warren S.G. & Zender C.S. 2013. Bounding the role of black carbon in the climate system: a scientific assessment. *Journal of Geophysical Research—Atmospheres 118*, 5380–5552.

Dagsson-Waldhauserova P., Arnalds O., Olafsson H., Hladil J., Skala R., Navratil T., Chadimova L. & Meinander O. 2015. Snow-dust storm: unique case study from Iceland, 6–7 March 2013. *Aeolian Research 16*, 69–74.

Doherty S.J., Grenfell T.C., Forsström S., Hegg D.L., Brandt R.E. & Warren S.G. 2013. Observed vertical redistribution of black carbon and other insoluble light-absorbing particles in melting snow. *Journal of Geophysical Research—Atmospheres 118*, 5553–5569.

Dumont M., Brun E., Picard G., Michou M., Libois Q., Petit J.-R., Geyer M., Morin S. & Josse B. 2014. Contribution of light-absorbing impurities in snow to Greenland's darkening since 2009. *Nature Geoscience 7*, 509–512.

Nordenskiöld A.E. 1883. Nordenskiöld on the inland ice of Greenland. *Science 2*(44), 732–738.

Polashenski C.M., Dibb J.E., Flanner M.G., Chen J.Y., Courville Z.R., Lai A.M., Schauer J.J., Shafer M.M. & Bergin M. 2015. Neither dust nor black carbon causing apparent albedo decline in Greenland's dry snow zone: implications for MODIS C5 surface reflectance. *Geophysical Research Letters 42*, 9319–9327.

Prospero J.M., Bullard J.E. & Hodgkins R. 2012. High-latitude dust over the North Atlantic: inputs from Icelandic proglacial dust storms. *Science 335*, 1078–1082.

Tedesco M., Doherty S., Warren W., Tranter M., Stroeve J., Fettweis X. & Alexander P. 2015. What darkens the Greenland Ice Sheet? *Eos, Transactions of the American Geophysical Union 96*, doi: http://dx.doi.org/10.1029/2015EO035773

Citation: *Polar Research* 2016, *35*, 31313, http://dx.doi.org/10.3402/polar.v35.31313

FINNISH METEOROLOGICAL INSTITUTE
Erik Palménin aukio 1
P.O.Box 503
FI-00101 HELSINKI
tel. +358 29 539 1000
WWW.FMI.FI

FINNISH METEOROLOGICAL INSTITUTE
CONTRIBUTIONS No. 125
ISBN 978-951-697-895-9 (paperback)
ISSN 0782-6117
Erweko
Helsinki 2016

ISBN 978-951-697-896-6 (pdf)
Helsinki 2016